# *Pd(II) Coordination Sphere Engineering: Pyridine Cages, Quinoline Bowls and Heteroleptic Pills Binding One or Two Fullerenes*

Bin Chen,[†] Julian J. Holstein,[†] Shinnosuke Horiuchi,[†,‡] Wolf G. Hiller[†] and Guido H. Clever*[,†]

† Faculty of Chemistry and Chemical Biology, TU Dortmund University, Otto-Hahn Straße 6, 44227, Dortmund, Germany

‡ Division of Chemistry and Materials Science, Graduate School of Engineering, Nagasaki University, Bunkyo-machi, Nagasaki 852-8521, Japan

*email: guido.clever@tu-dortmund.de

## Contents:

# 1 Materials and methods

All chemicals were obtained from commercial sources and used without further purification. Fullerenes $C_{60}$ and $C_{70}$ were purchased from ABCR with a purity of 99.95% and Sigma-Aldrich with a purity of 98%, respectively.

Gel permeation chromatography (GPC) purification of ligands was performed on a JASCO LC-9210 II NEXT running with $CHCl_3$ (HPLC grade) containing 0.5% (v/v) triethylamine. NMR measurements were all conducted at 298 K on Avance-500 and Avance-600 instruments from Bruker and an INOVA 500 MHz machine from Varian. Chemical shifts for $^1H$ and $^{13}C$ are reported in ppm on the $\delta$ scale; $^1H$ and $^{13}C$ signals were referenced to the residual solvent peak: acetonitrile (1.94 ppm, 1.32 ppm); chloroform (7.26 ppm, 77.16 ppm). The following abbreviations are used to describe signal multiplicity for $^1H$ NMR spectra: s: singlet, d: doublet, t: triplet, dd: doublet of doublets; dt: doublet of triplets; m: multiplet, br: broad. All proton signals of supramolecular cage or bowl compounds were assigned with the aid of 2D NMR spectra. High resolution

electrospray ionization mass spectrometry (ESI HRMS) was performed on Bruker Apex IV ESI-FTICR and Bruker ESI timsTOF mass spectrometers. The samples were diluted with spectrum-grade $CH_3CN$ (1:10) and then recorded mass spectra. UV-Vis spectra were recorded on an Agilent DAD HP-8453 UV-Vis spectrophotometer using quartz cuvettes with an optical path length of 1 mm. The photos of crystals are taken by using Leica DM2500LED polarization microscope equipped with a camera.

# 2 Synthesis of ligands $L^1$ and $L^2$

Ligands **$L^1$** and **$L^2$** were prepared from reported bis-anhydride (9,10-dimethyl-9,10-dihydro-9,10-ethanoanthracene-2,3,6,7-dianhydride) and the corresponding powdered aromatic amines under nitrogen atmosphere as described below.

## 2.1 Synthesis of ligand $L^1$

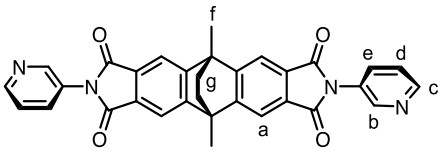


**$L^1$**

Under a nitrogen atmosphere, bis-pyridyl ligand **$L^1$** was prepared from reported bis-anhydride (9,10-dimethyl-9,10-dihydro-9,10-ethanoanthracene-2,3,6,7-dianhydride) (149.7 mg, 0.40 mmol, 1 eq.) and powdered 3-aminopyridine (753.0 mg, 8.0 mmol, 20 eq.) by heating the mixture of solids without solvent in a preheated oil bath to 165 °C for 10 min. After the black melt cooled to room temperature, it was taken up into 5 mL chloroform, sonificated and the suspension was immediately subjected to flash column chromatography on silica gel (0–2 % MeOH in $CHCl_3$) to give the crude product. This was further purified via recycling gel permeation chromatography and the solvent was removed under reduced pressure to yield the desired product as a colorless powder (139.0 mg, 66 %).

**$^1$H NMR** (500 MHz, 298 K, $CD_3CN$): $\delta$ (ppm) = 8.65 (d, J = 2.4 Hz, 2H), 8.59 (dd, J = 4.8, 1.6 Hz, 2H), 7.91 (s, 4H), 7.83 (ddd, J = 8.2, 2.5, 1.6 Hz, 2H), 7.50 (dd, J = 8.2, 4.8 Hz, 2H), 2.19 (s, 6H), 1.77 (s, 4H).

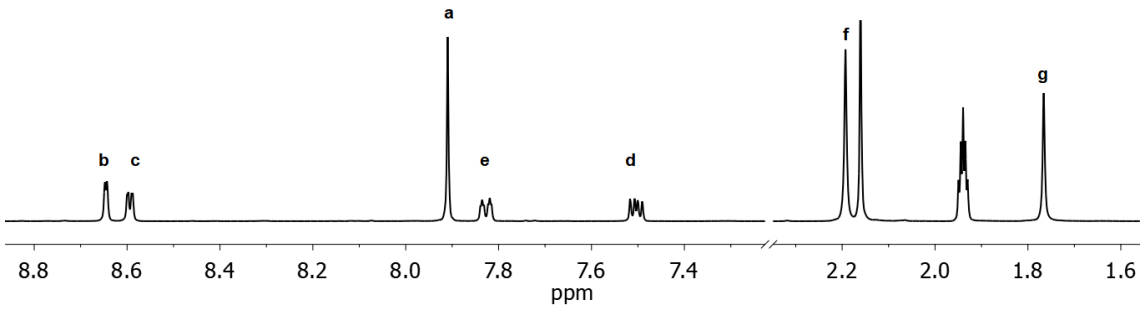


**Figure S1** $^1$H NMR spectrum (500 MHz, 298 K, $CD_3CN$) of **$L^1$**.

**$^{13}$C NMR** (126 MHz, 298 K, $CD_3CN$): $\delta$ (ppm) = 168.02, 153.68, 149.68, 148.57, 135.07, 131.01, 130.03, 124.64, 117.32, 45.09, 35.30, 18.62.

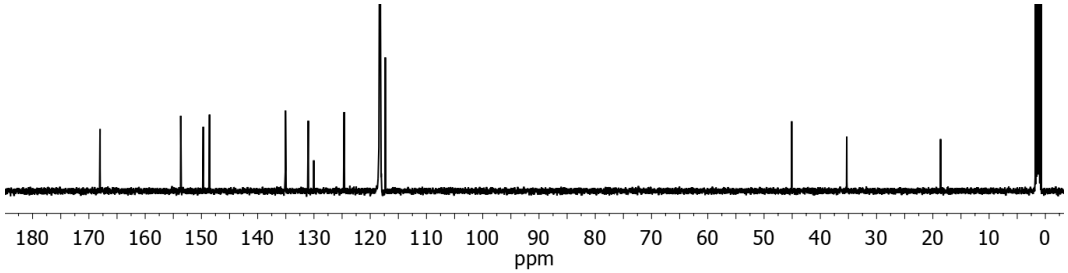


**Figure S2** $^{13}$C NMR spectrum (126 MHz, 298 K, $CD_3CN$) of **L¹**.

**ESI HRMS** ($C_{32}H_{22}N_4O_4$): $[M + H]^+$ calcd. for $C_{32}H_{23}N_4O_4$ 527.1710; found 527.1708; $[M + 2H]^{2+}$ calcd. for $C_{32}H_{24}N_4O_4$ 264.0894; found 264.0894.

## 2.2 Synthesis of ligand L²

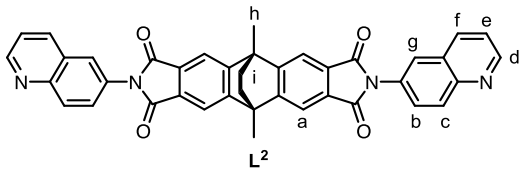


**L²**

Under a nitrogen atmosphere, ligand **L²** was prepared from reported bis-anhydride (9,10-dimethyl-9,10-dihydro-9,10-ethanoanthracene-2,3,6,7-dianhydride) (198.4 mg, 0.53 mmol, 1 eq.) and powdered 6-aminoquinoline (1540.0 mg, 10.7 mmol, 20 eq.) by heating the mixture of solids without solvent in a preheated oil bath to 165 °C for 10 min. After the black melt cooled to room temperature, it was taken up into 20 ml acetonitrile, sonificated and the suspension was filtered to afford a colorless precipitate. Then it was dissolved in $CHCl_3$ and further purified via recycling gel permeation chromatography and the solvent was removed under reduced pressure to yield the desired product as a colorless powder (196.2 mg, 59 %).

**$^1$H NMR** (500 MHz, 298 K, $CDCl_3$): $\delta$ (ppm) = 8.95 (dd, J = 4.4, 1.6 Hz, 2H), 8.21 (m, 4H), 7.95 (s, 4H), 7.92 (d, J = 2.2 Hz, 2H), 7.78 (dd, J = 9.0, 2.3 Hz, 2H), 7.44 (dd, J = 8.4, 4.2 Hz, 2H), 2.19 (s, 6H), 1.78 (s, 4H).

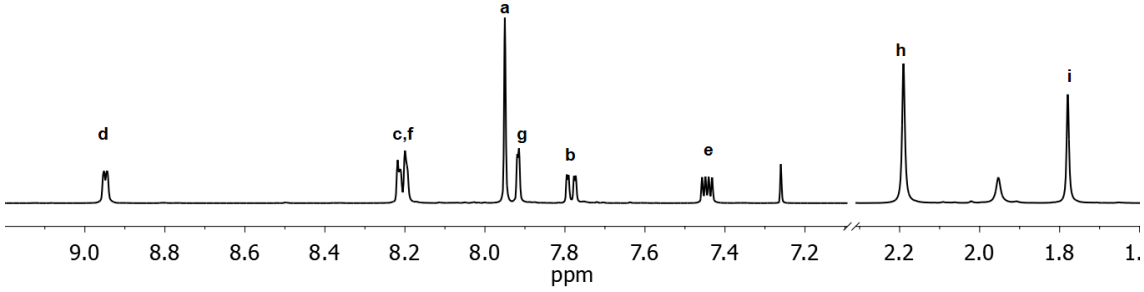


**Figure S3** $^1$H NMR spectrum (500 MHz, 298 K, $CDCl_3$) of **L²**.

**$^{13}$C NMR** (126 MHz, 298 K, $CDCl_3$): $\delta$ (ppm) = 167.47, 152.67, 151.25, 147.20, 136.40, 130.65, 130.08, 129.86, 128.22, 127.75, 125.07, 121.81, 116.80, 44.29, 34.94, 18.82.

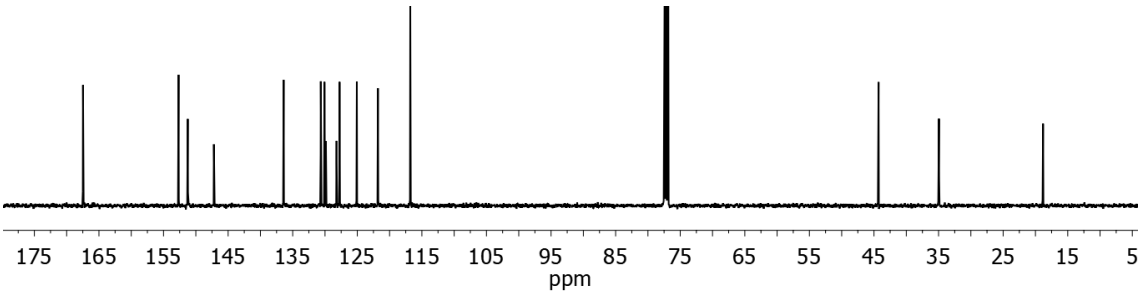


**Figure S4** $^{13}$C NMR spectrum (126 MHz, 298 K, $CDCl_3$) of **L²**.

**ESI HRMS** ($C_{40}H_{26}N_4O_4$): $[M + H]^+$ calcd. for $C_{40}H_{27}N_4O_4$ 627.2027; found 627.2026; $[M + 2H]^{2+}$ calcd. for $C_{40}H_{28}N_4O_4$ 314.1051; found 314.1051.

# 3 Formation and characterization of metallosupramolecular assemblies

## 3.1 Formation and characterization of cage $[Pd_2L^1_4]^{4+}$

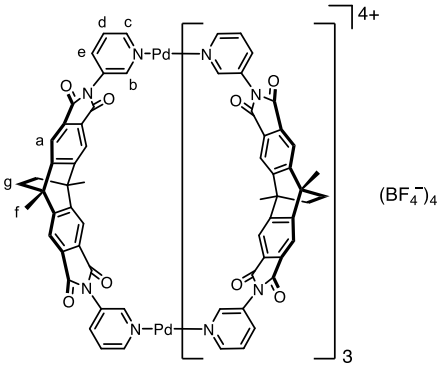


$[Pd_2\mathbf{L^1}_4]^{4+}$

A solution of $[Pd(MeCN)_4](BF_4)_2$ (233.8 µL, 15 mM/$CD_3CN$, 3.51 µmol, 1 eq.) was combined with ligand **L¹** (3.7 mg, 7.01 µmol, 2 eq.) in $CD_3CN$ (2505 µL) and heated at 70 °C for 1 d to give a 0.64 mM solution of cage $[Pd_2\mathbf{L^1}_4]^{4+}$.

**$^1$H NMR** (600 MHz, 298 K, $CD_3CN$): $\delta$ (ppm) = 9.14 (d, J = 2.2 Hz, 8H), 8.78 (dd, J = 5.8, 1.2 Hz, 8H), 8.21 (dt, J = 8.5, 1.6 Hz, 8H), 7.79 (s, 16H), 7.71 (dd, J = 8.4, 5.7 Hz, 8H), 2.13 (s, mixed with water peak in $CD_3CN$), 1.79 (s, 16H).

A signal at 2.13 ppm overlapping with the solvent residual peak in the aliphatic region could be assigned via 2D NMR spectroscopy.

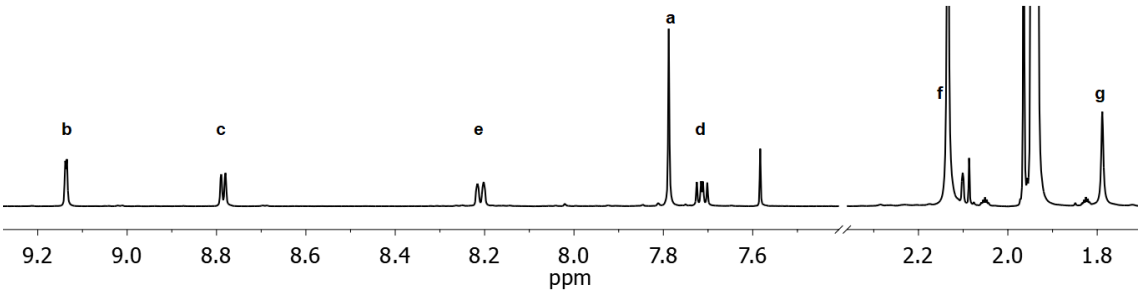


**Figure S5** $^{1}$H NMR spectrum (600 MHz, 298 K, $CD_3CN$) of $[Pd_2\mathbf{L^1}_4]^{4+}$.

**$^{13}$C NMR** (151 MHz, 298 K, $CD_3CN$): $\delta$ (ppm) = 166.49, 154.35, 150.36, 149.08, 138.41, 132.74, 130.34, 128.39, 117.71, 45.22, 35.00, 18.61.

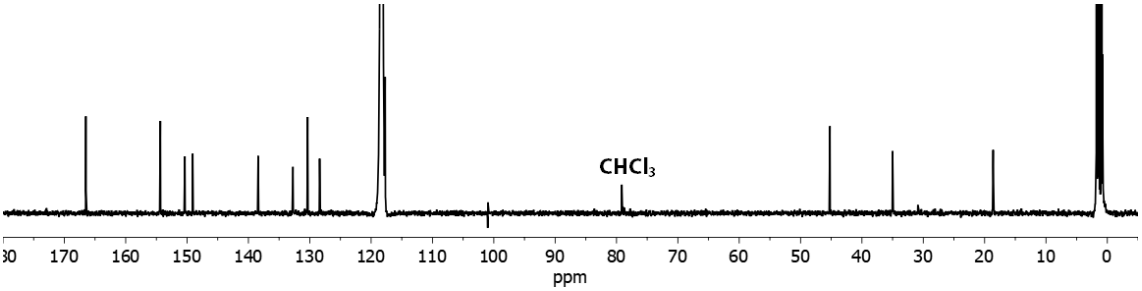


**Figure S6** $^{13}$C NMR spectrum (151 MHz, 298 K, $CD_3CN$) of $[Pd_2\mathbf{L^1}_4]^{4+}$.

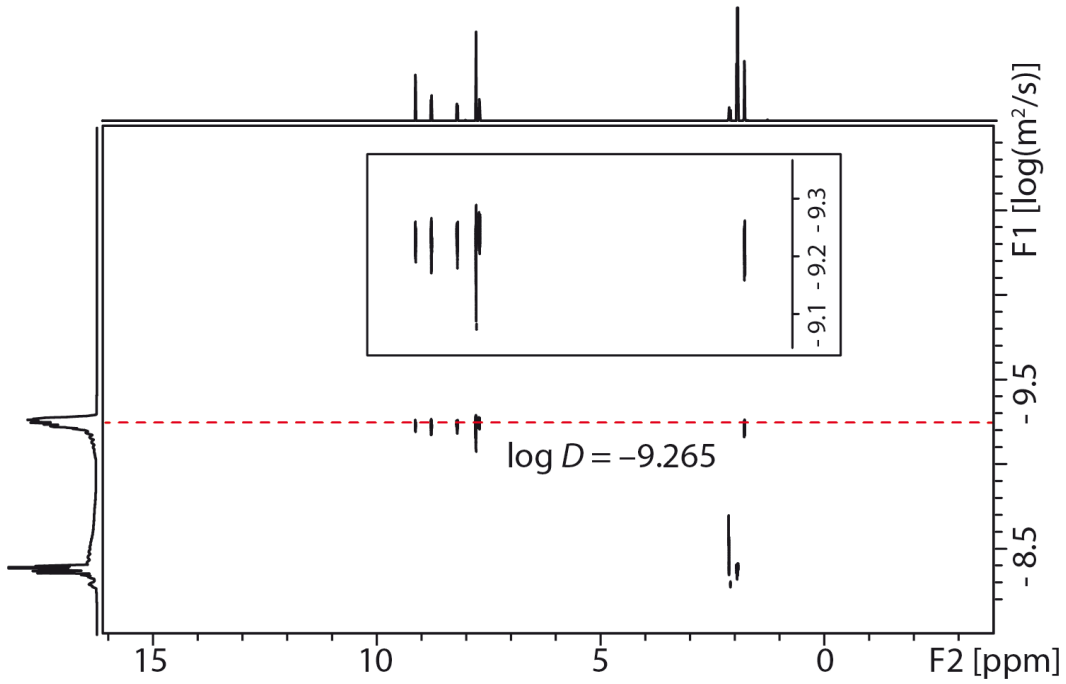


**Figure S7** DOSY spectrum (500 MHz, 298 K, $CD_3CN$) of $[Pd_2\mathbf{L^1}_4]^{4+}$: diffusion coefficient = 5.4 x $10^{-10}$ $m^2s^{-1}$, log $D$ = –9.26, r = 11.7 Å.

**ESI HRMS** ($C_{128}H_{88}N_{16}O_{16}Pd_2B_4F_{16}$): $[Pd_2\mathbf{L^1}_4]^{4+}$ calcd. for $C_{128}H_{88}N_{16}O_{16}Pd_2$ 579.6166; found 579.6176; $[Pd_2\mathbf{L^1}_4+BF_4]^{3+}$ calcd. for $C_{128}H_{88}N_{16}O_{16}Pd_2BF_4$ 801.8236; found 801.8256; $[Pd_2\mathbf{L^1}_4+2BF_4]^{2+}$ calcd. for $C_{128}H_{88}N_{16}O_{16}Pd_2B_2F_8$ 1246.2376; found 1246.2416.

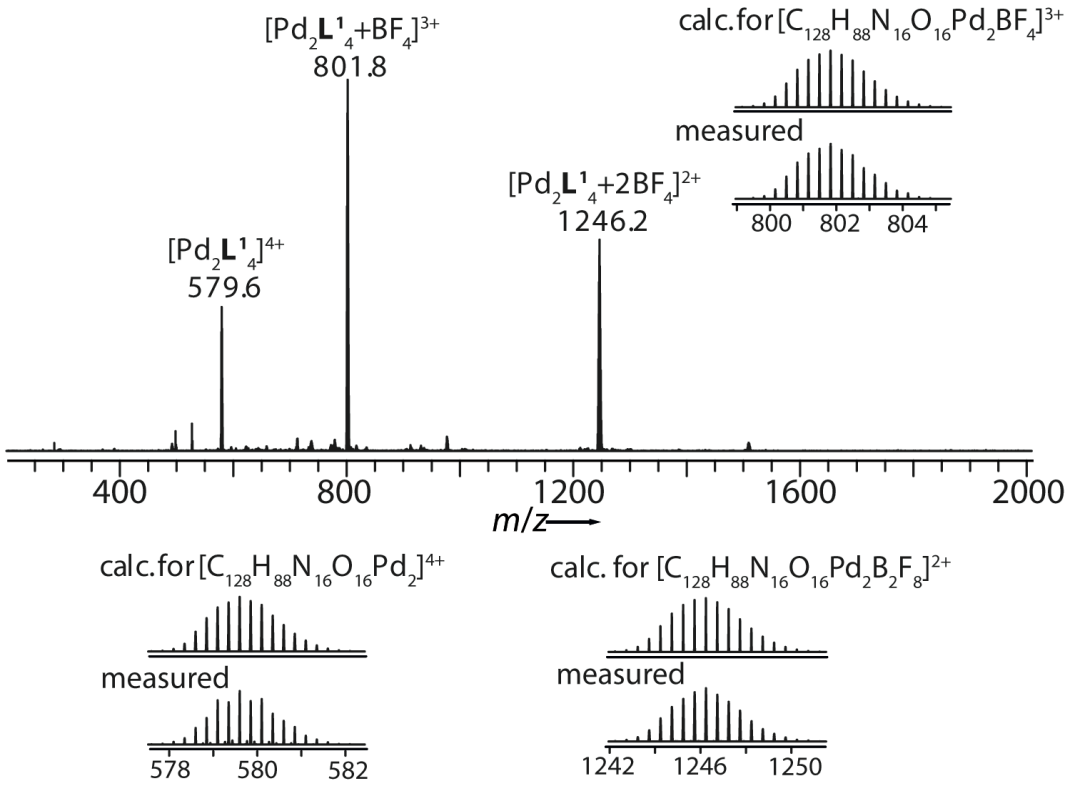


**Figure S8** ESI mass spectrum of $[Pd_2\mathbf{L^1}_4]^{4+}$.

## 3.2 Formation and characterization of cage $[C_{60}@Pd_2\mathbf{L^1}_4]^{4+}$

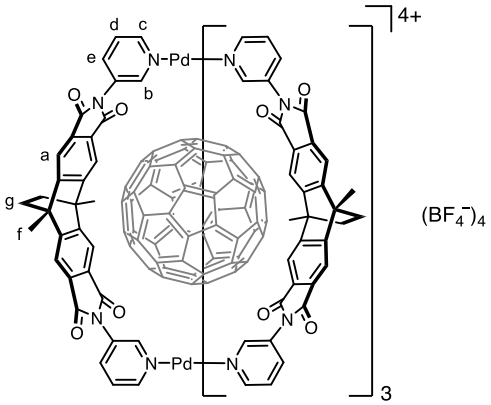


$[C_{60}@Pd_2\mathbf{L^1}_4]^{4+}$

A solution of $[Pd(MeCN)_4](BF_4)_2$ (226.8 µL, 15 mM/$CD_3CN$, 3.40 µmol, 1 eq.) was combined with ligand $\mathbf{L^1}$ (3.6 mg, 6.80 µmol, 2 eq.) and $C_{60}$ (3.7 mg, 5.11 µmol, 1.5 eq.) in $CD_3CN$ (2505 µL) and heated at 70 °C for 1 d. Excess $C_{60}$ solid was removed by filtration to give a 0.64 mM pale purple solution of host-guest complex $[C_{60}@Pd_2\mathbf{L^1}_4]^{4+}$.

**$^1$H NMR** (600 MHz, 298 K, $CD_3CN$): $\delta$ (ppm) = 8.54 – 8.52 (m, 8H), 8.41 (ddd, J = 8.4, 2.2, 1.2 Hz, 8H), 7.87 (dd, J = 8.5, 5.8 Hz, 8H), 7.85 (s, 16H), 7.59 (d, J = 2.2 Hz, 8H), 2.22 (s, 24H), 1.82 (s, 16H).

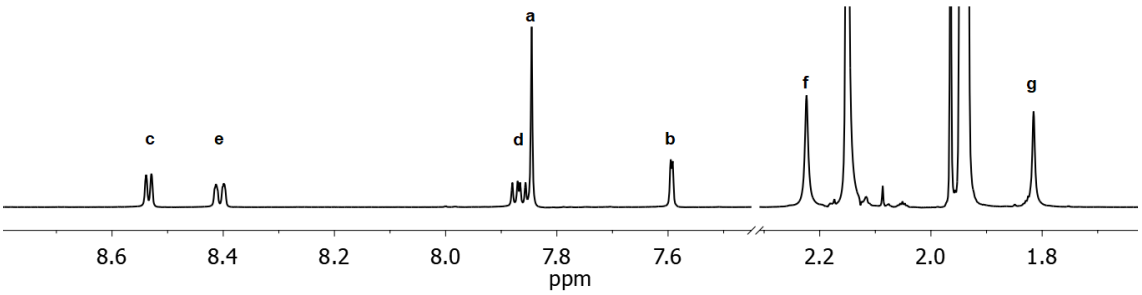


**Figure S9** $^{1}$H NMR spectrum (600 MHz, 298 K, $CD_3CN$) of $[C_{60}@Pd_2\mathbf{L^1}_4]^{4+}$.

**$^{13}$C NMR** (151 MHz, 298 K, $CD_3CN$): $\delta$ (ppm) = 166.14, 154.73, 152.32, 147.64, 141.83 ($C_{60}$), 140.46, 132.71, 130.80, 129.54, 118.60, 45.44, 34.87, 18.52.

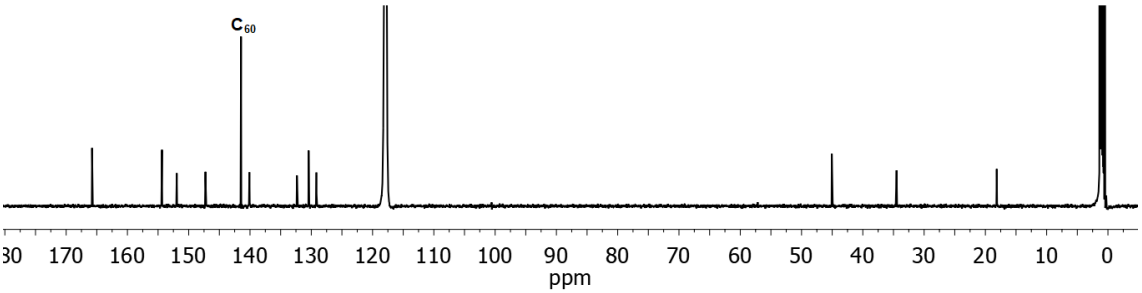


**Figure S10** $^{13}$C NMR spectrum (151 MHz, 298 K, $CD_3CN$) of $[C_{60}@Pd_2\mathbf{L^1}_4]^{4+}$. A single signal at 141.83 ppm corresponds to the encapsulated $C_{60}$.

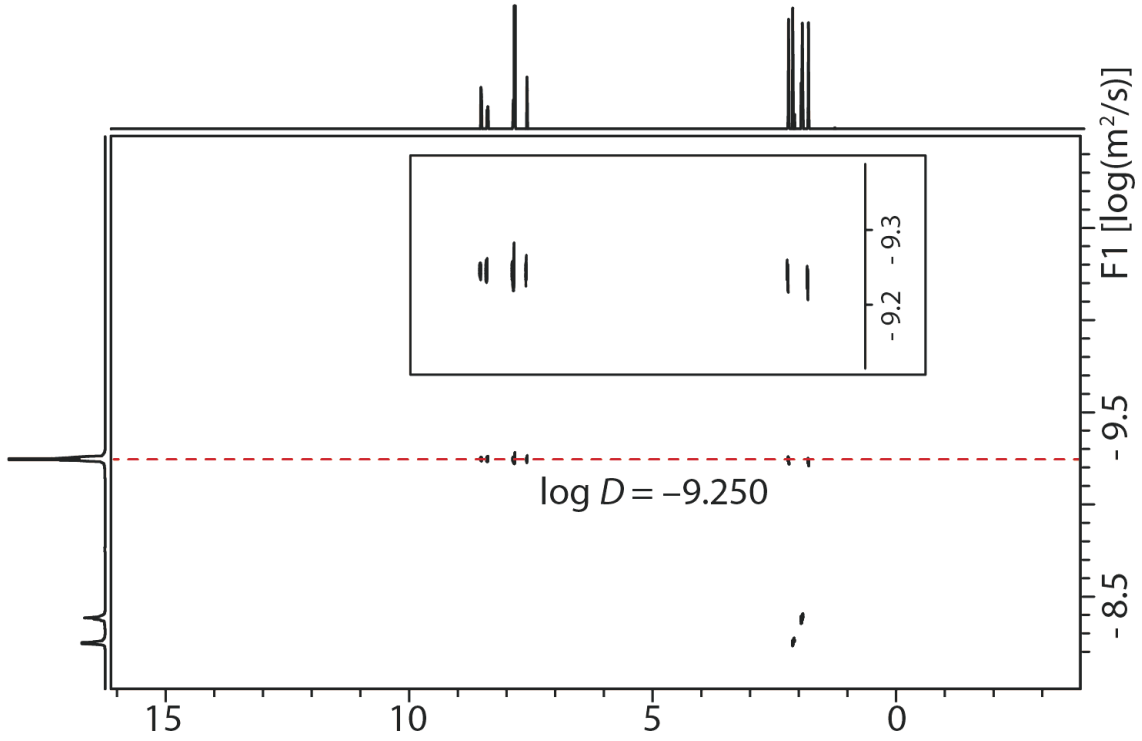


**Figure S11** DOSY spectrum (500 MHz, 298 K, $CD_3CN$) of $[C_{60}@Pd_2\mathbf{L^1}_4]^{4+}$: diffusion coefficient = 5.6 x $10^{-10}$ $m^2s^{-1}$, log *D* = –9.25, r = 11.3 Å.

**ESI HRMS** ($C_{188}H_{88}N_{16}O_{16}Pd_2B_4F_{16}$): $[C_{60}@Pd_2\mathbf{L^1}_4]^{4+}$ calcd. for $C_{188}H_{88}N_{16}O_{16}Pd_2$ 759.8673; found 759.8696; $[C_{60}@Pd_2\mathbf{L^1}_4+BF_4]^{3+}$ calcd. for $C_{188}H_{88}N_{16}O_{16}Pd_2BF_4$ 1042.1578; found 1042.1617; $[C_{60}@Pd_2\mathbf{L^1}_4+2BF_4]^{2+}$ calcd. for $C_{188}H_{88}N_{16}O_{16}Pd_2B_2F_8$ 1606.2385; found 1606.2454.

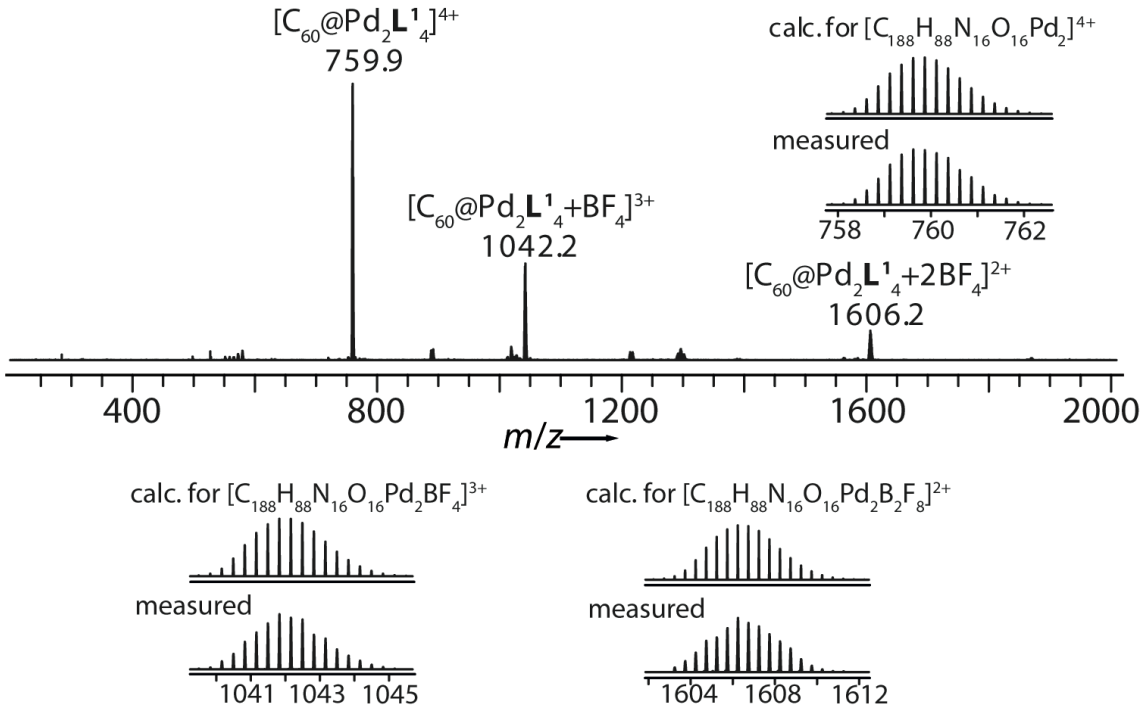


**Figure S12** ESI mass spectrum of $[C_{60}@Pd_2\mathbf{L^1}_4]^{4+}$.

## 3.3 Formation and characterization of bowl $[Pd_2\mathbf{L^2}_3(MeCN)_2]^{4+}$

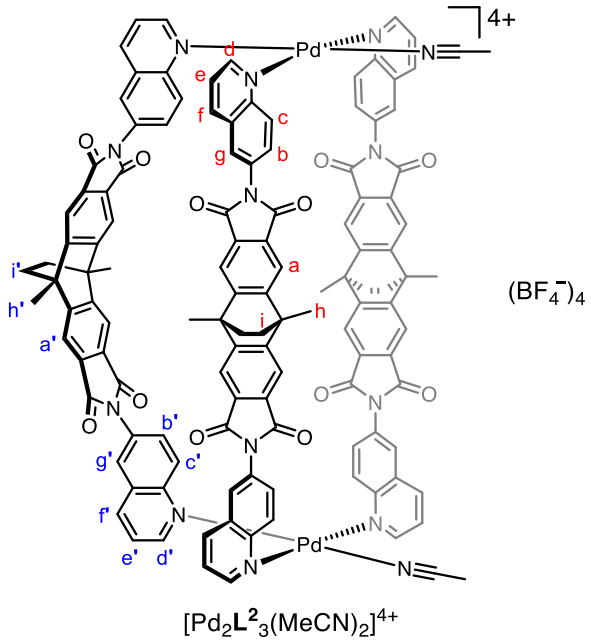

A solution of $[Pd(MeCN)_4](BF_4)_2$ (732.4 µL, 15 mM/$CD_3CN$, 10.99 µmol, 1 eq.) was combined with ligand **L²** (10.3 mg, 16.47 µmol, 1.5 eq.) in $CD_3CN$ (7848 µL) and stirred at room temperature for 2 d to give a 0.64 mM solution of bowl $[Pd_2\mathbf{L^2}_3(MeCN)_2]^{4+}$.

**$^1$H NMR** (600 MHz, 298 K, $CD_3CN$): $\delta$ (ppm) = 9.99 (d, J = 9.1 Hz, 4H), 9.85 (dd, J = 5.7, 1.3 Hz, 2H), 9.58 (dd, J = 5.5, 1.3 Hz, 4H), 9.31 (d, J = 9.0 Hz, 2H), 8.69 (d, J = 8.3 Hz, 4H), 8.51 (d, J = 8.3 Hz, 2H), 8.26 (dd, J = 9.1, 2.2 Hz, 4H), 8.16 (d, J = 2.2 Hz, 4H), 7.98 (s, 4H), 7.93 (s, 4H), 7.87 – 7.84 (m, 4H), 7.79 (dd, J = 8.3, 5.5 Hz, 4H), 7.73 (s, 4H), 7.42 (dd, J = 9.1, 2.3 Hz, 2H), 2.26 (s, 6H), 2.22 (s, 6H), 2.08 (s, 6H), 1.88 (s, 8H), 1.77 (s, 4H).

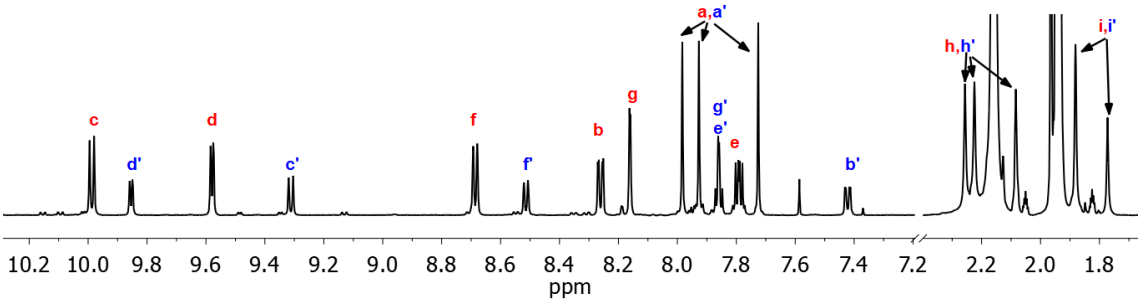


**Figure S13** $^1$H NMR spectrum (600 MHz, 298 K, $CD_3CN$) of $[Pd_2\mathbf{L^2}_3(MeCN)_2]^{4+}$.

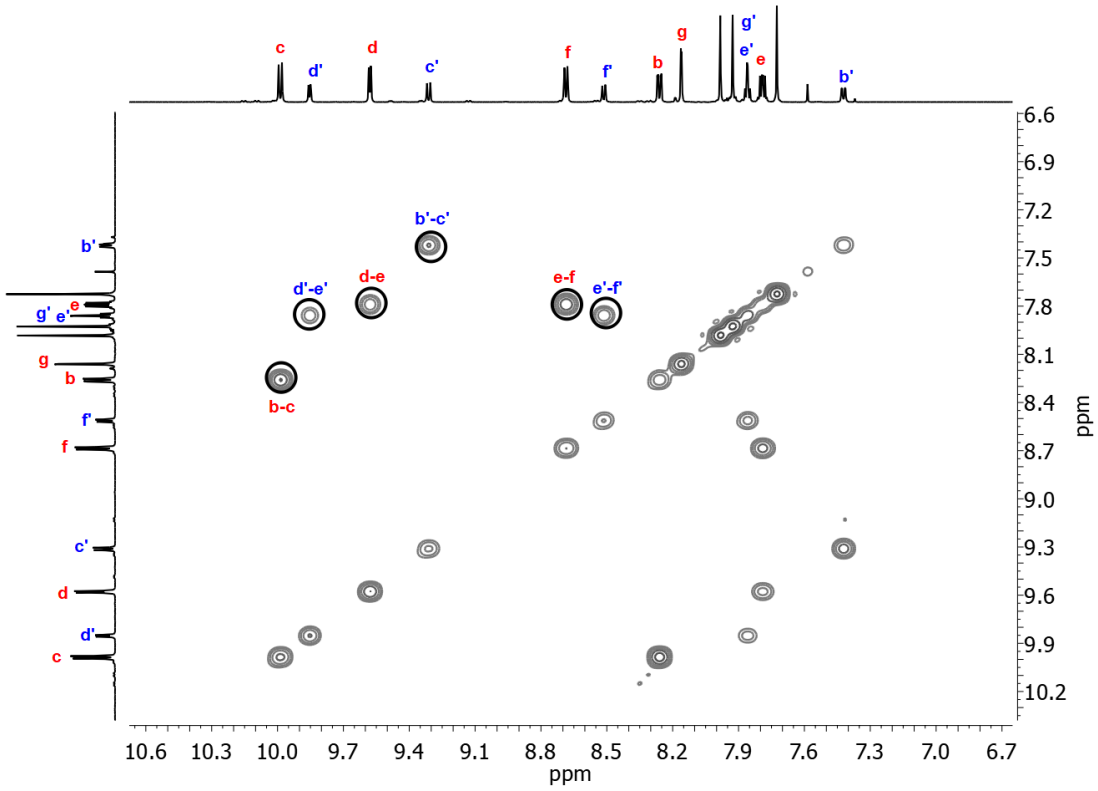


**Figure S14** Partial $^1$H – $^1$H COSY spectrum (600 MHz, 298 K, $CD_3CN$) of $[Pd_2\mathbf{L^2}_3(MeCN)_2]^{4+}$.

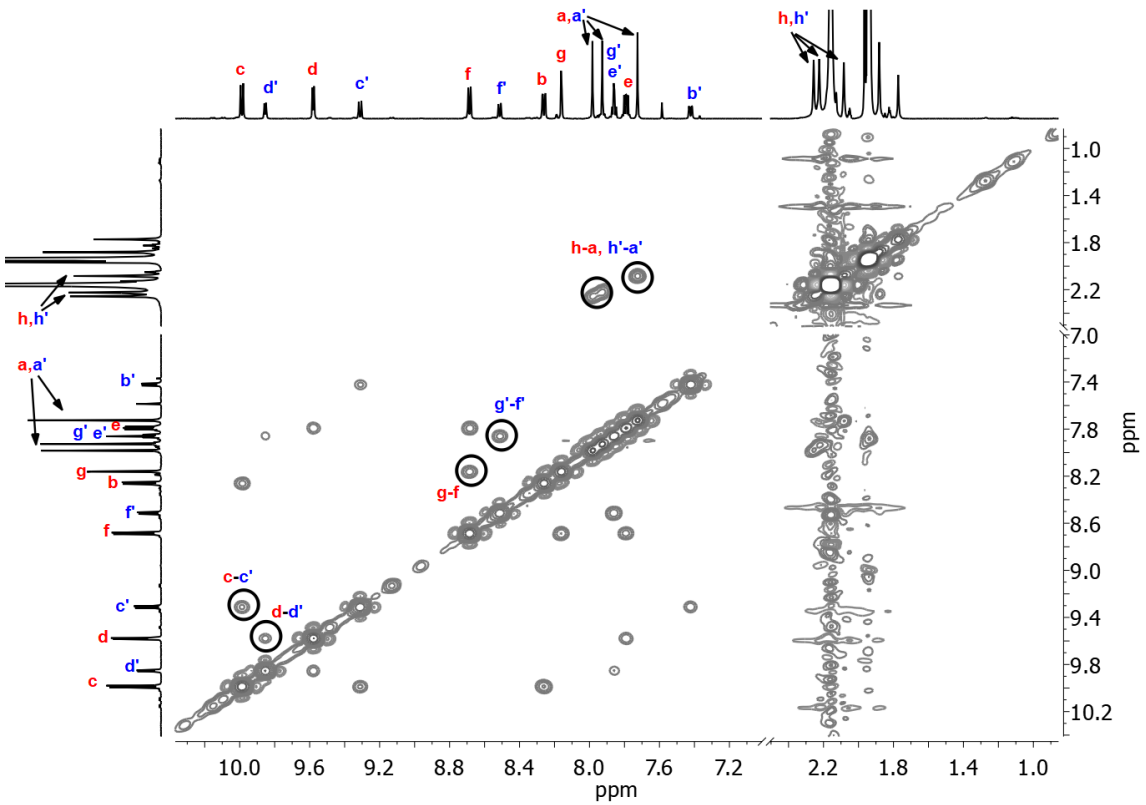


**Figure S15** Partial $^{1}H - {}^{1}H$ NOESY spectrum (600 MHz, 298 K, $CD_3CN$) of $[Pd_2\mathbf{L^2}_3(MeCN)_2]^{4+}$.

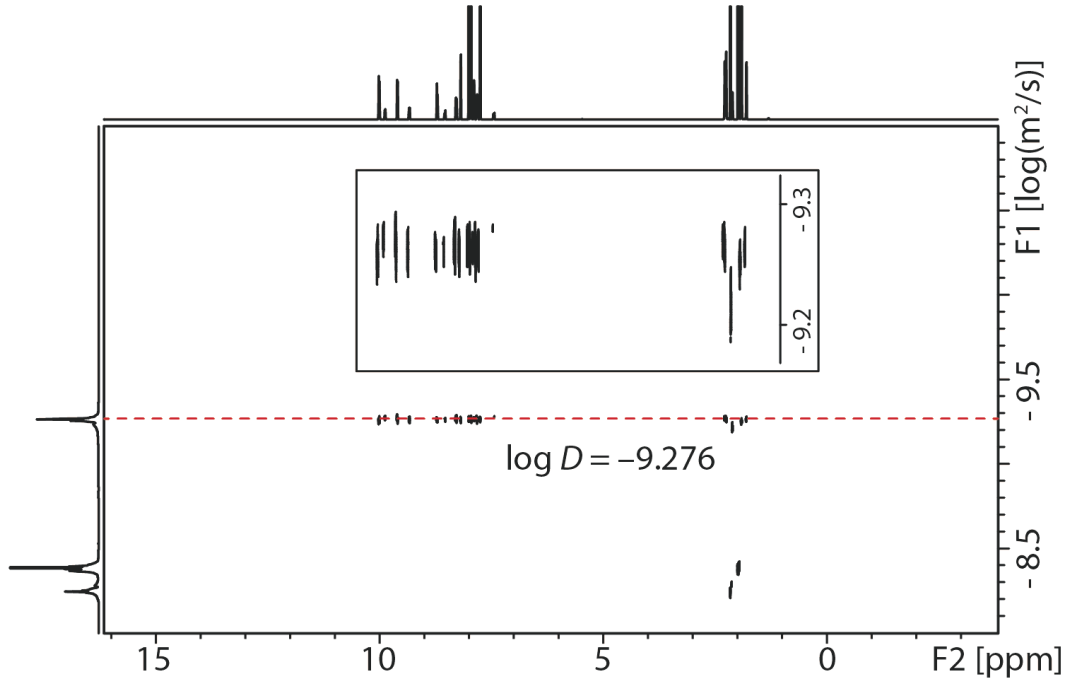


**Figure S16** DOSY spectrum (500 MHz, 298 K, $CD_3CN$) of $[Pd_2\mathbf{L^2}_3(MeCN)_2]^{4+}$: diffusion coefficient = 5.3 x $10^{-10}$ $m^2s^{-1}$, log *D* = –9.28, r = 12.0 Å.

**ESI HRMS** ($C_{124}H_{84}N_{14}O_{12}Pd_2B_4F_{16}$): $[Pd_2\mathbf{L^2}_3(MeCN)_2]^{4+}$ calcd. for $C_{124}H_{84}N_{14}O_{12}Pd_2$ 543.6123; found 543.6134; $[Pd_2\mathbf{L^2}_3(MeCN)+F]^{3+}$ calcd. for $C_{122}H_{81}N_{13}O_{12}Pd_2F$ 717.4739; found 717.4762; $[Pd_2\mathbf{L^2}_3(MeCN)+Cl]^{3+}$ calcd. for

$C_{122}H_{81}N_{13}O_{12}Pd_2Cl$ 723.1307; found 723.1325; $[Pd_2\mathbf{L^2}_3+BF_4]^{3+}$ calcd. for $C_{120}H_{78}N_{12}O_{12}Pd_2BF_4$ 726.1335; found 726.1418; $[Pd_2\mathbf{L^2}_3+2F]^{2+}$ calcd. for $C_{120}H_{78}N_{12}O_{12}Pd_2F_2$ 1065.1970; found 1065.2010.

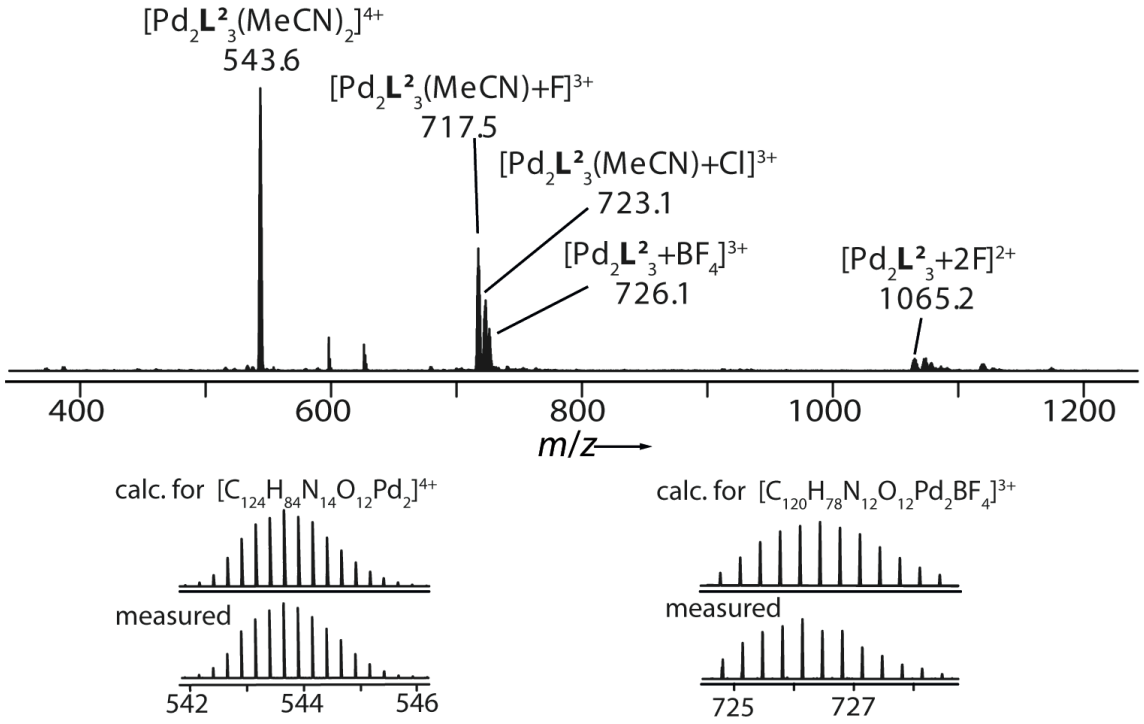


**Figure S17** ESI mass spectrum of $[Pd_2\mathbf{L^2}_3(MeCN)_2]^{4+}$. The presence of the $[Pd_2\mathbf{L^2}_3(MeCN)+F]^{3+}$, $[Pd_2\mathbf{L^2}_3(MeCN)+Cl]^{3+}$ and $[Pd_2\mathbf{L^2}_3+2F]^{2+}$ species is due to substitution of coordinated $CH_3CN$ by traces of various anions under the measurement conditions.

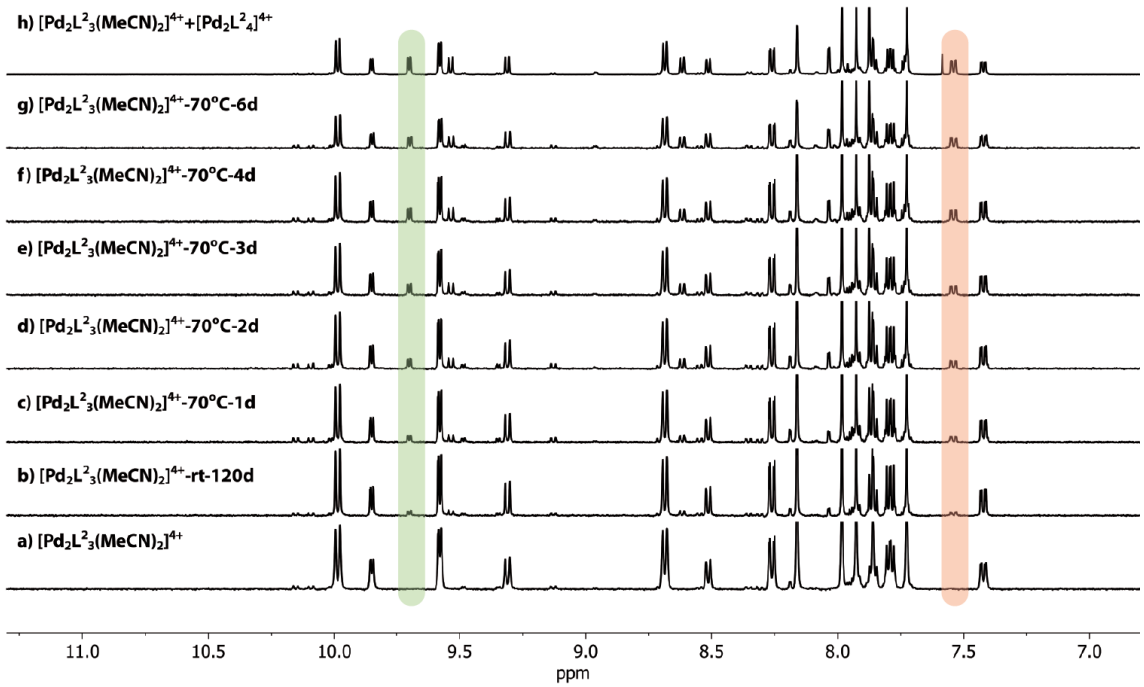


**Figure S18** $^1$H NMR spectra (500 MHz, 298 K, $CD_3CN$) following the integrity of $[Pd_2\mathbf{L^2}_3(MeCN)_2]^{4+}$ at rt or 70 °C, indicating partial conversion into cage $[Pd_2\mathbf{L^2}_4]^{4+}$ after heating for several days. The quinoline proton D and proton B of $[Pd_2\mathbf{L^2}_4]^{4+}$ are highlighted in green and red, respectively.

## 3.4 Formation and characterization of the mixture of bowl $[Pd_2L^2_3(MeCN)_2]^{4+}$ and cage $[Pd_2L^2_4]^{4+}$

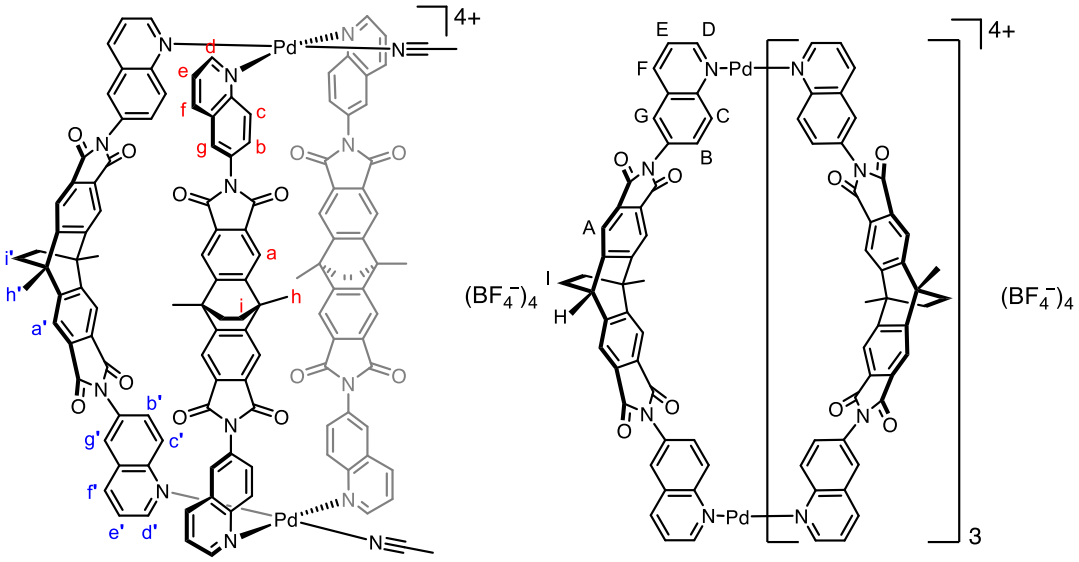


A solution of $[Pd(CH_3CN)_4](BF_4)_2$ (281.9 µL, 15 mM/$CD_3CN$, 4.23 µmol, 1 eq.) was combined with ligand **L²** (5.3 mg, 8.46 µmol, 2 eq.) in $CD_3CN$ (3020 µL) and heated at 70 °C for 3 d. Remaining ligand was removed by filtration to give a mixture of bowl $[Pd_2L^2_3(MeCN)_2]^{4+}$ and cage $[Pd_2L^2_4]^{4+}$ (ratio: ca. 4:1).

**$^1$H NMR** (600 MHz, 298 K, $CD_3CN$): $\delta$ (ppm) = δ 9.99 (d, J = 9.1 Hz, 2H), 9.85 (dd, J = 5.7, 1.3 Hz, 1H), 9.70 (dd, J = 5.5, 1.3 Hz, 1H), 9.58 (dd, J = 5.5, 1.3 Hz, 2H), 9.54 (d, J = 9.2 Hz, 1H), 9.31 (d, J = 9.0 Hz, 1H), 8.69 (d, J = 8.3 Hz, 2H), 8.62 (d, J = 8.3 Hz, 1H), 8.51 (d, J = 8.3 Hz, 1H), 8.26 (dd, J = 9.1, 2.3 Hz, 2H), 8.16 (d, J = 2.3 Hz, 2H), 8.03 (d, J = 2.2 Hz, 1H), 7.98 (s, 2H), 7.93 (s, 2H), 7.87 (s, 2H), 7.86 (d, J = 2.4 Hz, 2H), 7.79 (dd, J = 8.2, 5.5 Hz, 2H), 7.75 – 7.72 (m, 3H), 7.54 (dd, J = 9.2, 2.3 Hz, 1H), 7.42 (dd, J = 9.0, 2.3 Hz, 1H), 2.26 (s, 3H), 2.22 (s, 3H), 2.20 (s, 3H), 1.89 (d, J = 5.6 Hz, 6H), 1.77 (s, 2H).

All the signals in the aromatic region could be assigned via 2D NMR spectroscopy.

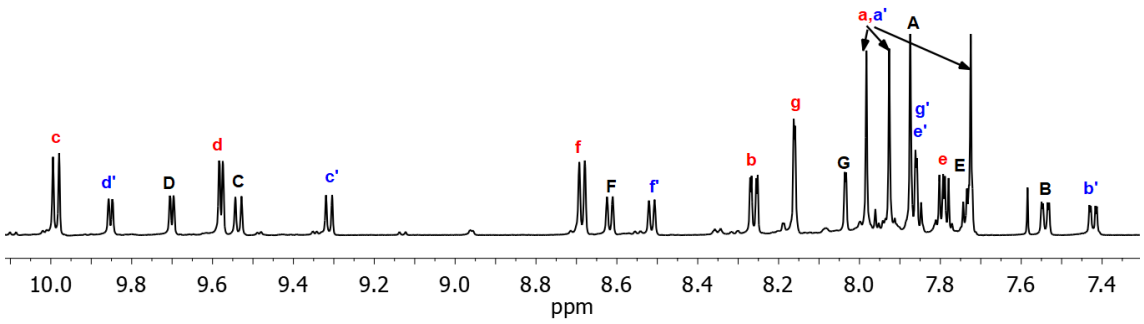


**Figure S19** $^1$H NMR spectrum (600 MHz, 298 K, $CD_3CN$) of the mixture of bowl $[Pd_2L^2_3(MeCN)_2]^{4+}$ and cage $[Pd_2L^2_4]^{4+}$.

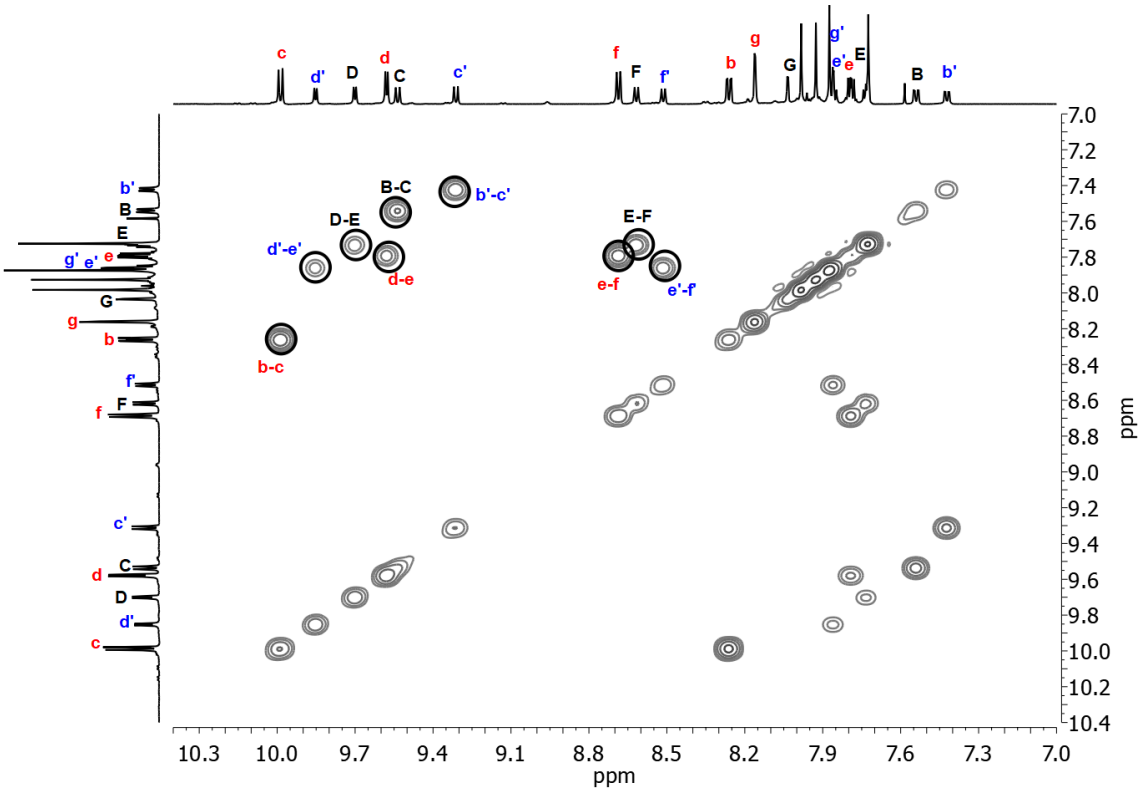


**Figure S20** Partial $^{1}H - {}^{1}H$ COSY spectrum (600 MHz, 298 K, $CD_3CN$) of the mixture of bowl $[Pd_2\mathbf{L^2}_3(MeCN)_2]^{4+}$ and cage $[Pd_2\mathbf{L^2}_4]^{4+}$.

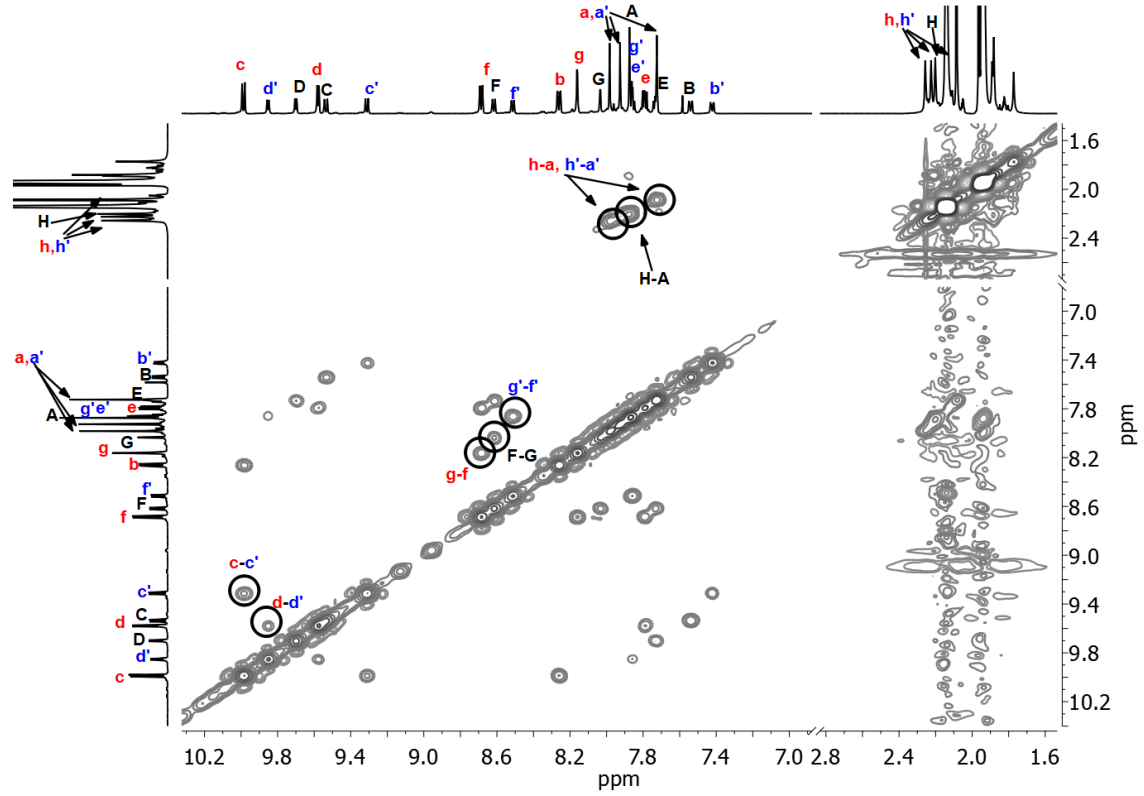


**Figure S21** Partial $^{1}H - {}^{1}H$ NOESY spectrum (600 MHz, 298 K, $CD_3CN$) of the mixture of bowl $[Pd_2\mathbf{L^2}_3(MeCN)_2]^{4+}$ and cage $[Pd_2\mathbf{L^2}_4]^{4+}$.

**ESI HRMS** ($C_{124}H_{84}N_{14}O_{12}Pd_2B_4F_{16}$ and $C_{160}H_{104}N_{16}O_{16}Pd_2B_4F_{16}$): $[Pd_2\mathbf{L^2}_4]^{4+}$ calcd. for $C_{160}H_{104}N_{16}O_{16}Pd_2$ 679.8984; found 679.8983; $[Pd_2\mathbf{L^2}_4+BF_4]^{3+}$ calcd. for $C_{160}H_{104}N_{16}O_{16}Pd_2BF_4$ 935.1988; found 935.2001; $[Pd_2\mathbf{L^2}_4+2BF_4]^{2+}$ calcd. for $C_{160}H_{104}N_{16}O_{16}Pd_2B_2F_8$ 1446.3000; found 1446.3028. Other peaks come from the bowl $[Pd_2\mathbf{L^2}_3(MeCN)_2]^{4+}$ species as shown before.

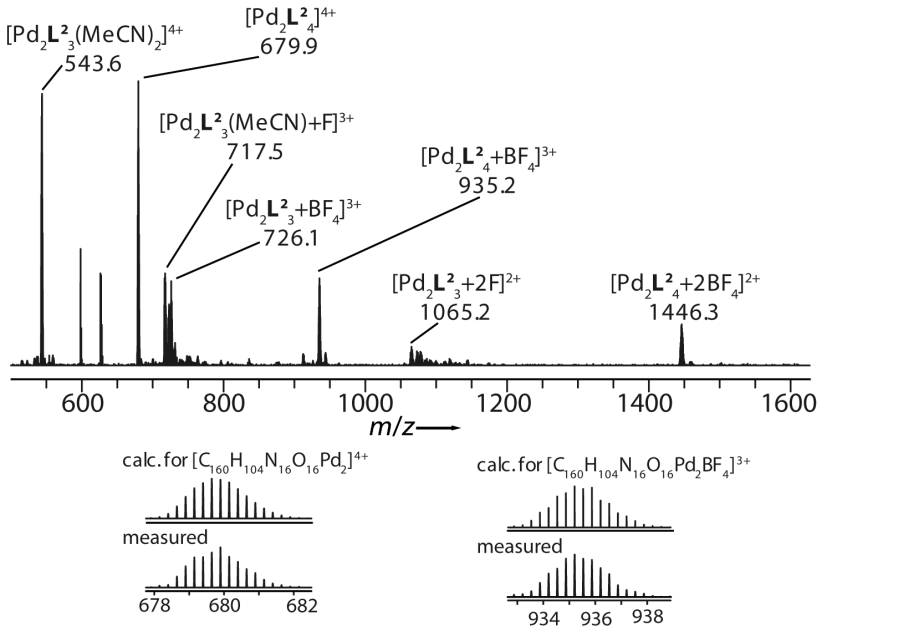


**Figure S22** ESI mass spectrum of the mixture of bowl $[Pd_2\mathbf{L^2}_3(MeCN)_2]^{4+}$ and cage $[Pd_2\mathbf{L^2}_4]^{4+}$. The presence of the $[Pd_2\mathbf{L^2}_3(MeCN)+F]^{3+}$ and $[Pd_2\mathbf{L^2}_3+2F]^{2+}$ species is due to substitution of coordinated $CH_3CN$ by traces of various anions under the measurement conditions.

## 3.5 Formation and characterization of bowl $[C_{60}@Pd_2\mathbf{L^2}_3(MeCN)_2]^{4+}$

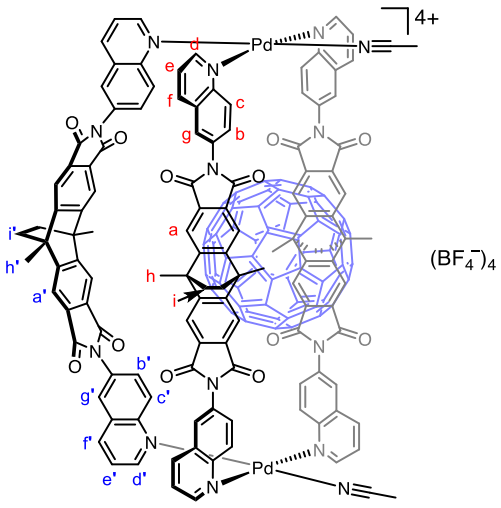


$[C_{60}@Pd_2\mathbf{L^2}_3(MeCN)_2]^{4+}$

A solution of $[Pd(MeCN)_4](BF_4)_2$ (797.0 µL, 15 mM/$CD_3CN$, 11.96 µmol, 1 eq.) was combined with ligand $\mathbf{L^2}$ (11.2 mg, 17.92 µmol, 1.5 eq.) and $C_{60}$ (5.0 mg, 6.97 µmol, 0.6 eq.) in $CD_3CN$ (8540 µL) and stirred at room temperature for 2 d (or at 70°C for 1 d). Excess $C_{60}$ solid was removed by filtration to give a 0.64 mM pale purple solution of bowl $[C_{60}@Pd_2\mathbf{L^2}_3(MeCN)_2]^{4+}$.

**$^1$H NMR** (600 MHz, 298 K, $CD_3CN$): $\delta$ (ppm) = 10.32 (d, J = 9.1 Hz, 4H), 9.84 (dd, J = 5.7, 1.3 Hz, 2H), 9.46 (dd, J = 5.5, 1.3 Hz, 4H), 9.07 (d, J = 9.0 Hz, 2H), 8.68 (d, J = 8.2 Hz, 4H), 8.44 (d, J = 8.2 Hz, 2H), 8.33 (dd, J = 9.1, 2.3 Hz, 4H), 8.18 (d, J = 2.3 Hz, 4H), 8.04 (s, 4H), 7.96 (s, 4H), 7.84 – 7.80 (m, 4H), 7.77 (dd, J = 8.3, 5.5 Hz, 4H), 7.73 (s, 4H), 7.00 (dd, J = 9.1, 2.2 Hz, 2H), 2.26 (s, 6H), 2.24 (s, 6H), 2.09 (s, 6H), 1.79 (s, 8H), 1.67 (s, 4H).

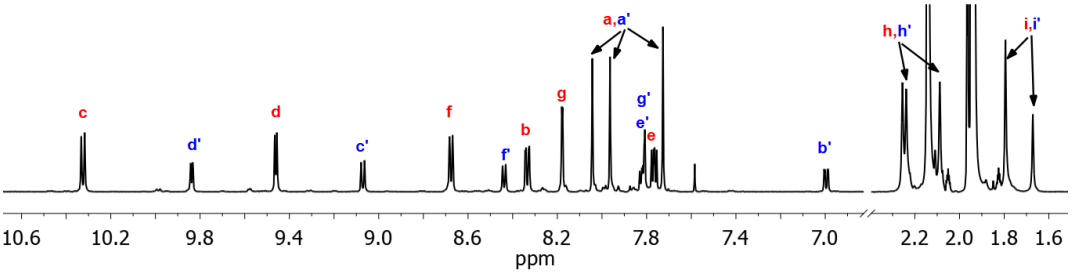


**Figure S23** $^1$H NMR spectrum (600 MHz, 298 K, $CD_3CN$) of $[C_{60}@Pd_2\mathbf{L^2}_3(MeCN)_2]^{4+}$.

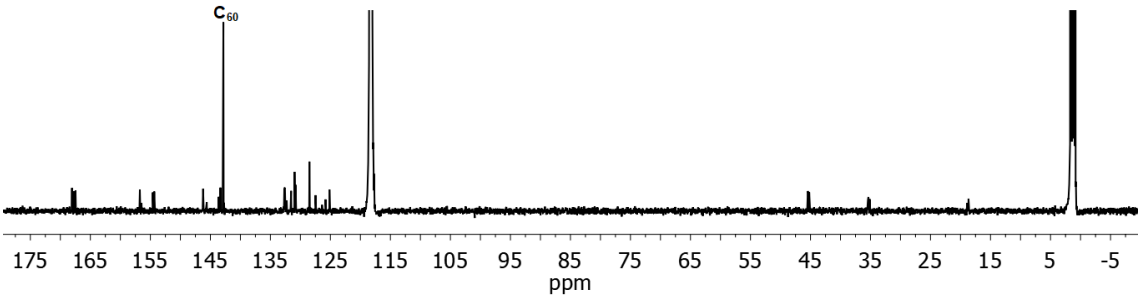


**Figure S24** $^{13}$C NMR spectrum (151 MHz, 298 K, $CD_3CN$) of $[C_{60}@Pd_2\mathbf{L^2}_3(MeCN)_2]^{4+}$. A single signal at 142.83 ppm corresponds to the encapsulated $C_{60}$.

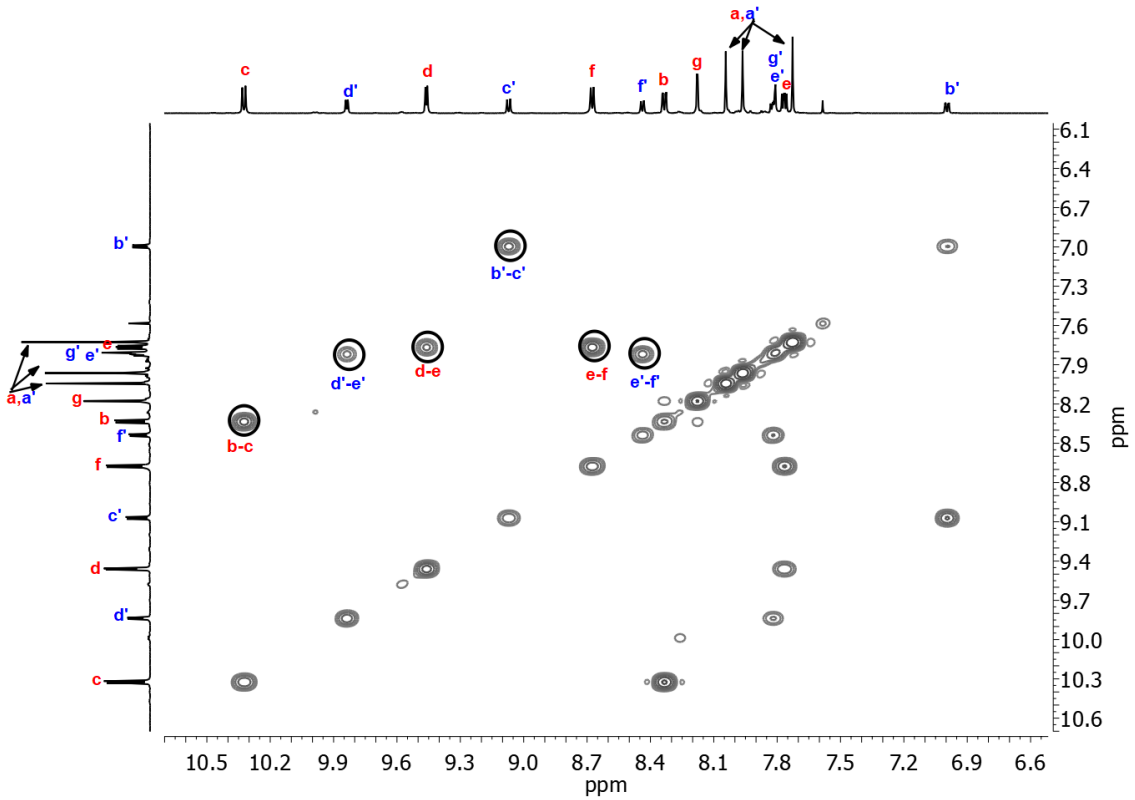


**Figure S25** Partial $^1$H – $^1$H COSY spectrum (600 MHz, 298 K, $CD_3CN$) of $[C_{60}@Pd_2\mathbf{L^2}_3(MeCN)_2]^{4+}$.

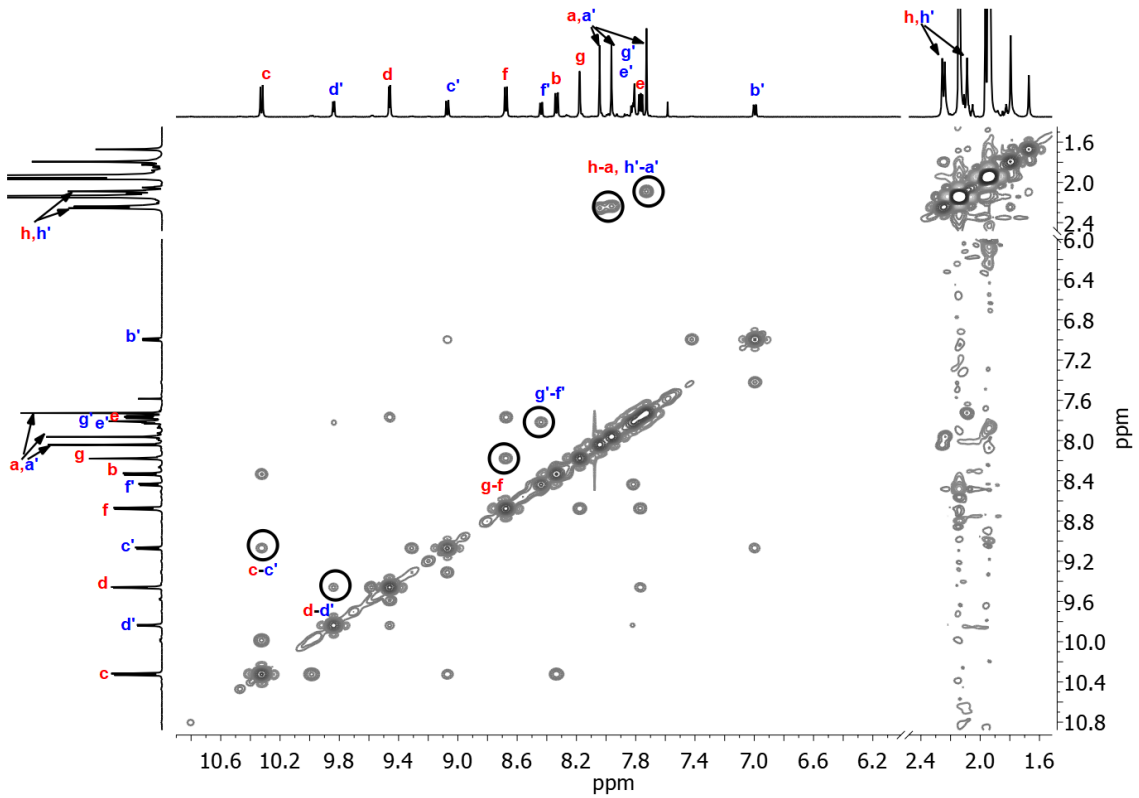


**Figure S26** Partial $^{1}H - {}^{1}H$ NOESY spectrum (600 MHz, 298 K, $CD_3CN$) of $[C_{60}@Pd_2\mathbf{L^2}_3(MeCN)_2]^{4+}$.

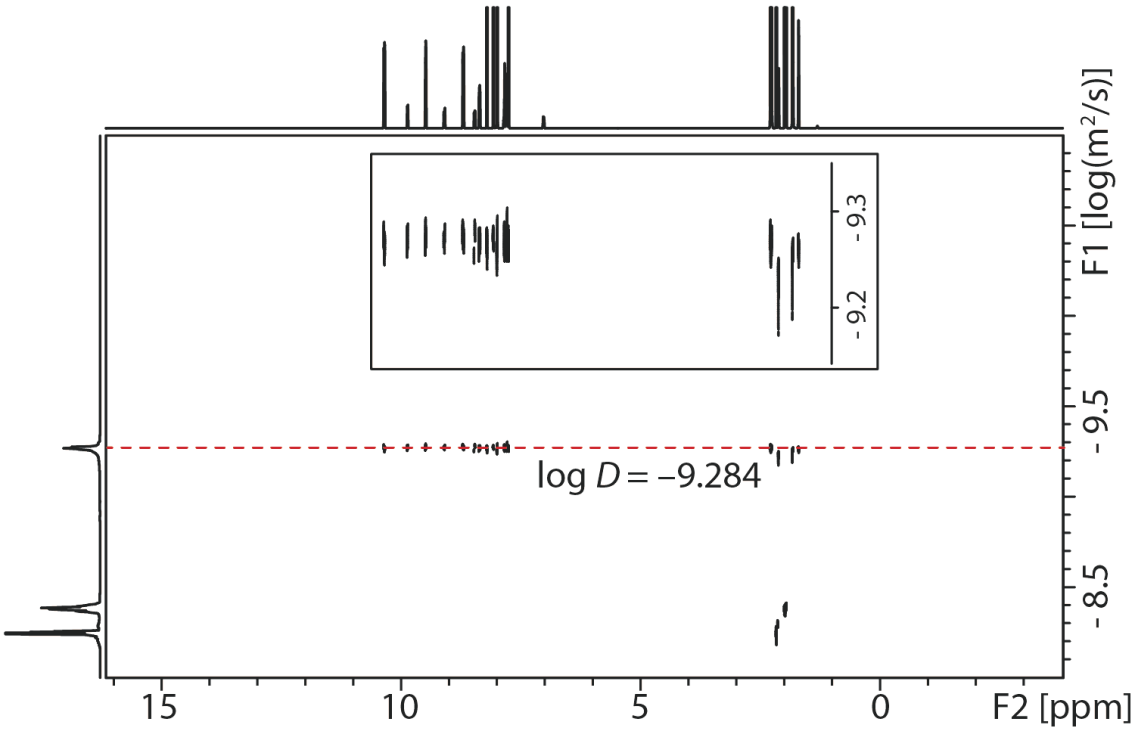


**Figure S27** DOSY spectrum (500 MHz, 298 K, $CD_3CN$) of $[C_{60}@Pd_2\mathbf{L^2}_3(MeCN)_2]^{4+}$: diffusion coefficient = 5.2 x $10^{-10}$ $m^2s^{-1}$, log $D$ = –9.28, r = 12.2 Å.

**ESI HRMS** ($C_{184}H_{84}N_{14}O_{12}Pd_2B_4F_{16}$): $[C_{60}@Pd_2\mathbf{L^2}_3(MeCN)_2]^{4+}$ calcd. for $C_{184}H_{84}N_{14}O_{12}Pd_2$ 723.6129; found 723.6137; $[C_{60}@Pd_2\mathbf{L^2}_3(MeCN)+F]^{3+}$ calcd. for $C_{182}H_{81}N_{13}O_{12}Pd_2F$ 957.4745; found 957.4773; $[C_{60}@Pd_2\mathbf{L^2}_3+BF_4]^{3+}$ calcd. for $C_{180}H_{78}N_{12}O_{12}Pd_2BF_4$ 966.1340; found 966.1425; $[C_{60}@Pd_2\mathbf{L^2}_3+F+HCOO]^{2+}$ calcd. for $C_{181}H_{79}N_{12}O_{14}Pd_2F$ 1438.1976; found 1438.2014.

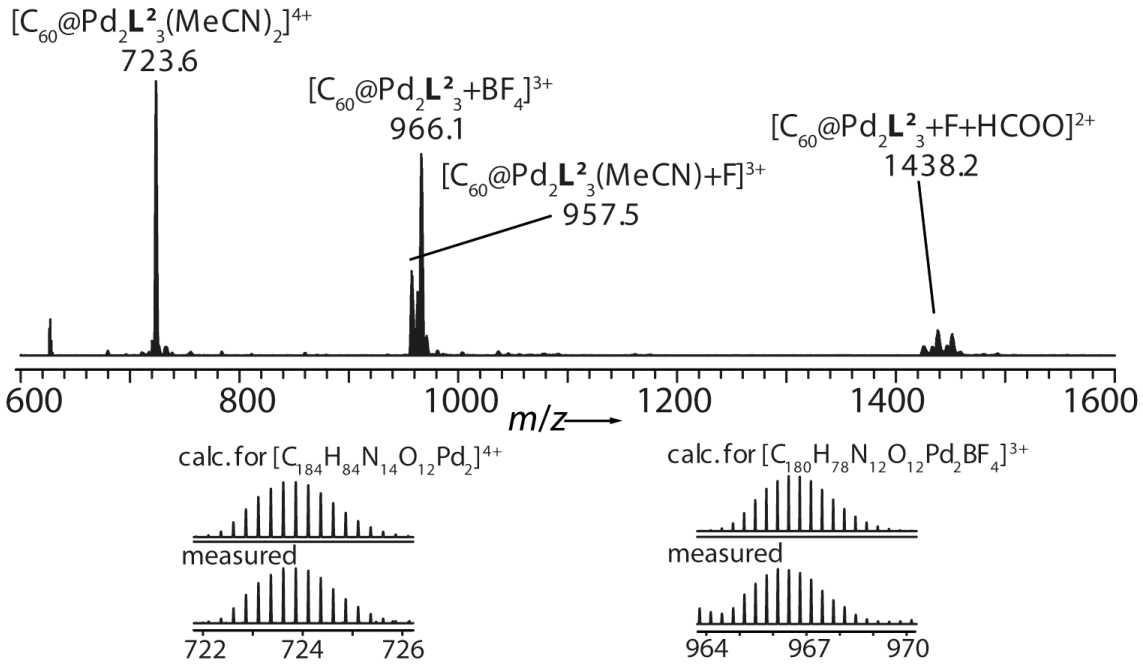


**Figure S28** ESI mass spectrum of $[C_{60}@Pd_2\mathbf{L^2}_3(MeCN)_2]^{4+}$. The presence of the $[C_{60}@Pd_2\mathbf{L^2}_3(MeCN)+F]^{3+}$, $[C_{60}@Pd_2\mathbf{L^2}_3+F+HCOO]^{3+}$ and species is due to substitution of coordinated $CH_3CN$ by traces of various anions under the measurement conditions.

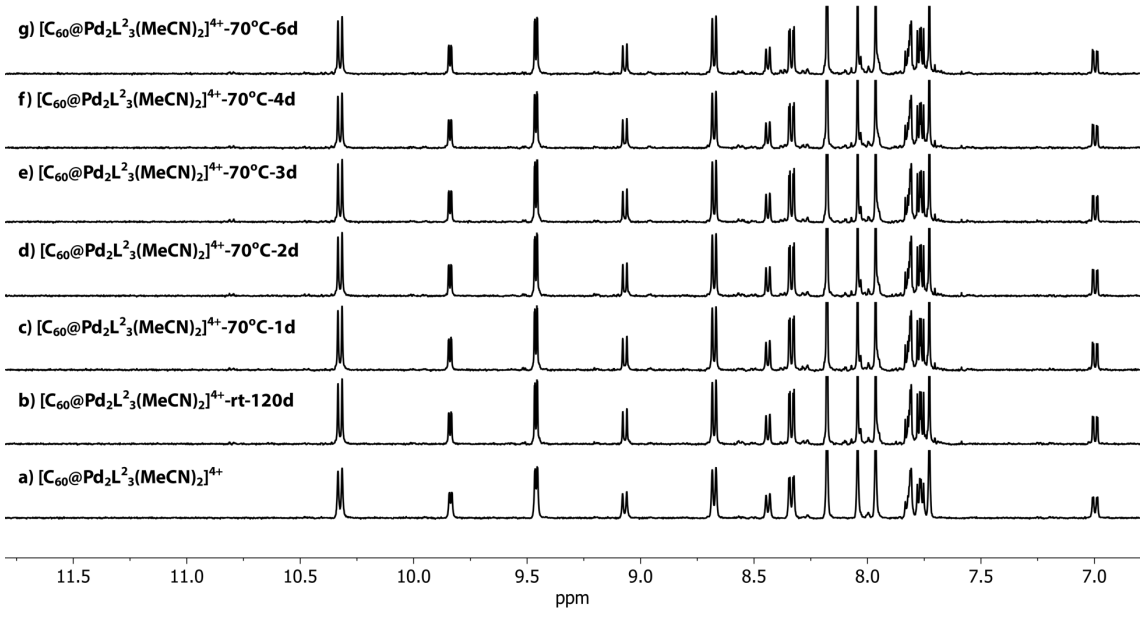


**Figure S29** $^1H$ NMR spectra (500 MHz, 298 K, $CD_3CN$) following the integrity of $[C_{60}@Pd_2\mathbf{L^2}_3(MeCN)_2]^{4+}$ at rt or 70 °C, indicating its high thermal stability at 70 °C.

## 3.6 Formation and characterization of bowl $[C_{70}@Pd_2L^2_3(MeCN)_2]^{4+}$

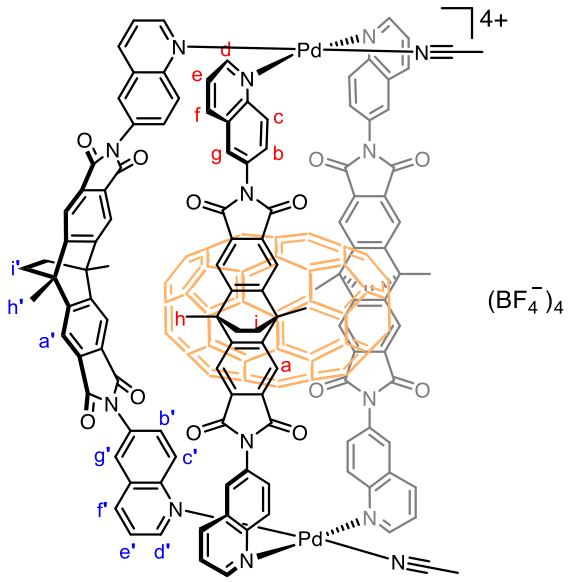


A solution of $[Pd(MeCN)_4](BF_4)_2$ (772.2 µL, 15 mM/$CD_3CN$, 11.58 µmol, 1 eq.) was combined with ligand **L²** (10.9 mg, 17.36 µmol, 1.5 eq.) and $C_{70}$ (5.6 mg, 6.67 µmol, 0.6 eq.) in $CD_3CN$ (8273 µL) and stirred at room temperature for 2 d. Excess $C_{70}$ solid was removed by filtration to give a 0.64 mM brown solution of the bowl $[C_{70}@Pd_2L^2_3(MeCN)_2]^{4+}$.

**$^1$H NMR** (600 MHz, 298 K, $CD_3CN$): $\delta$ (ppm) = 9.93 (d, J = 9.1 Hz, 4H), 9.82 (dd, J = 5.7, 1.3 Hz, 2H), 9.43 (dd, J = 5.5, 1.3 Hz, 4H), 8.74 (d, J = 9.1 Hz, 2H), 8.67 (d, J = 8.3 Hz, 4H), 8.46 (d, J = 8.3 Hz, 2H), 8.18 (d, J = 2.3 Hz, 4H), 8.10 (s, 4H), 8.08 (s, 4H), 8.06 (dd, J = 9.1, 2.3 Hz, 4H), 7.84 – 7.80 (m, 4H), 7.76 – 7.73 (m, 8H), 6.59 (dd, J = 9.1, 2.2 Hz, 2H), 2.34 (s, 6H), 2.31 (s, 6H), 2.11 (s, 6H), 1.86 (s, 8H), 1.67 (s, 4H).

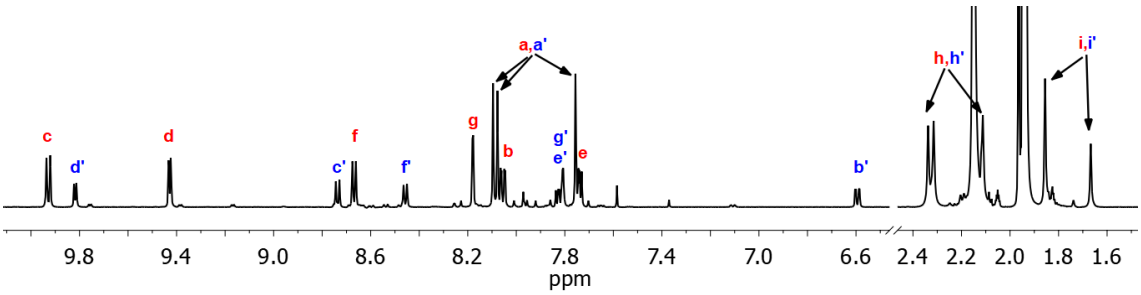


**Figure S30** $^1$H NMR spectrum (600 MHz, 298 K, $CD_3CN$) of $[C_{70}@Pd_2L^2_3(MeCN)_2]^{4+}$.

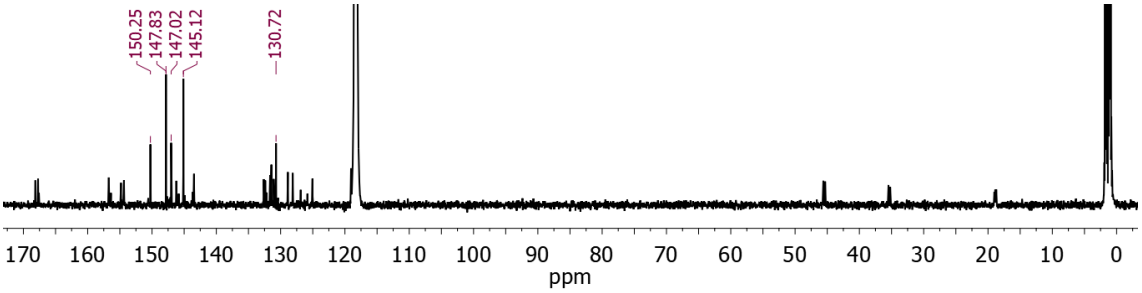


**Figure S31** $^{13}C$ NMR spectrum (151 MHz, 298 K, $CD_3CN$) of $[C_{70}@Pd_2\mathbf{L^2}_3(MeCN)_2]^{4+}$. Five single signals at 150.25, 147.83, 147.02, 145.12, 130.72 ppm correspond to the encapsulated $C_{70}$.

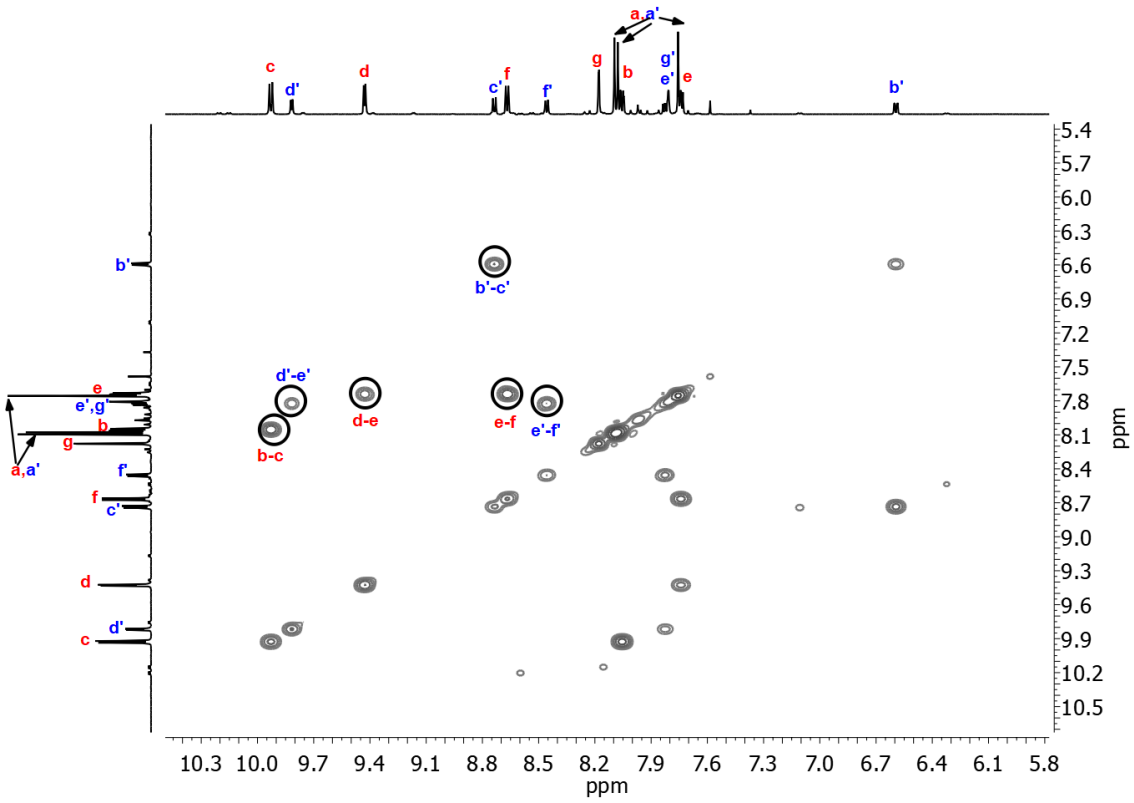


**Figure S32** Partial $^1H - ^1H$ COSY spectrum (600 MHz, 298 K, $CD_3CN$) of $[C_{70}@Pd_2\mathbf{L^2}_3(MeCN)_2]^{4+}$.

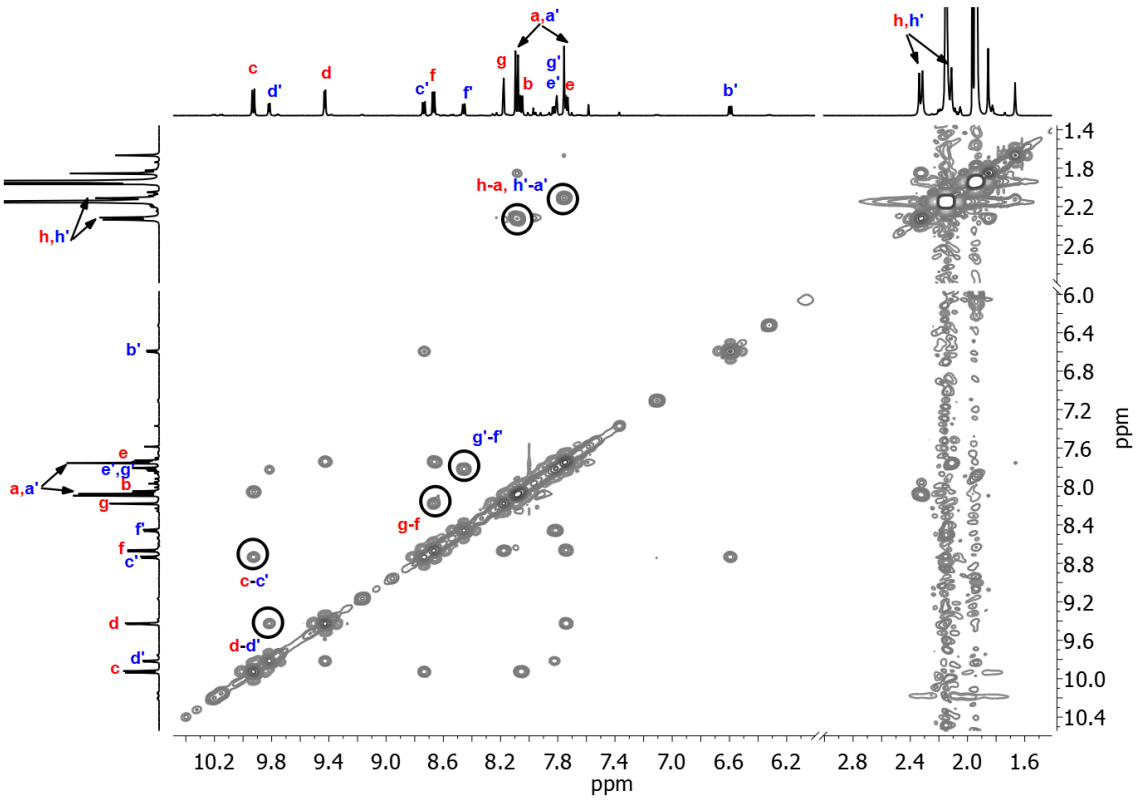


**Figure S33** Partial $^{1}H - {}^{1}H$ NOESY spectrum (600 MHz, 298 K, $CD_3CN$) of $[C_{70}@Pd_2\mathbf{L^2}_3(MeCN)_2]^{4+}$.

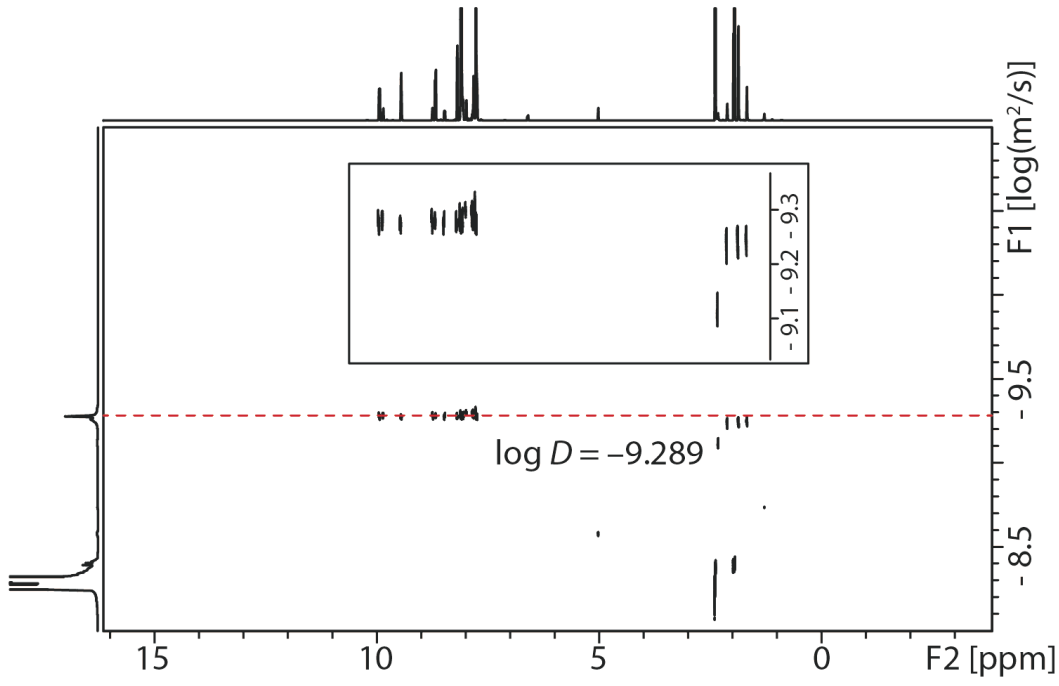


**Figure S34** DOSY spectrum (500 MHz, 298 K, $CD_3CN$) of $[C_{70}@Pd_2\mathbf{L^2}_3(MeCN)_2]^{4+}$: diffusion coefficient = 5.1 x $10^{-10}$ $m^2s^{-1}$, log *D* = –9.29, r = 12.4 Å.

**ESI HRMS** ($C_{194}H_{84}N_{14}O_{12}Pd_2B_4F_{16}$): $[C_{70}@Pd_2\mathbf{L^2}_3(MeCN)_2]^{4+}$ calcd. for $C_{194}H_{84}N_{14}O_{12}Pd_2$ 753.6130; found 753.6165; $[C_{70}@Pd_2\mathbf{L^2}_3+BF_4]^{3+}$ calcd. for $C_{190}H_{78}N_{12}O_{12}Pd_2BF_4$ 1006.4675; found 1006.4797; $[C_{70}@Pd_2\mathbf{L^2}_3+2HCOO]^{2+}$ calcd. for $C_{192}H_{80}N_{12}O_{16}Pd_2$ 1511.6978; found 1511.7045.

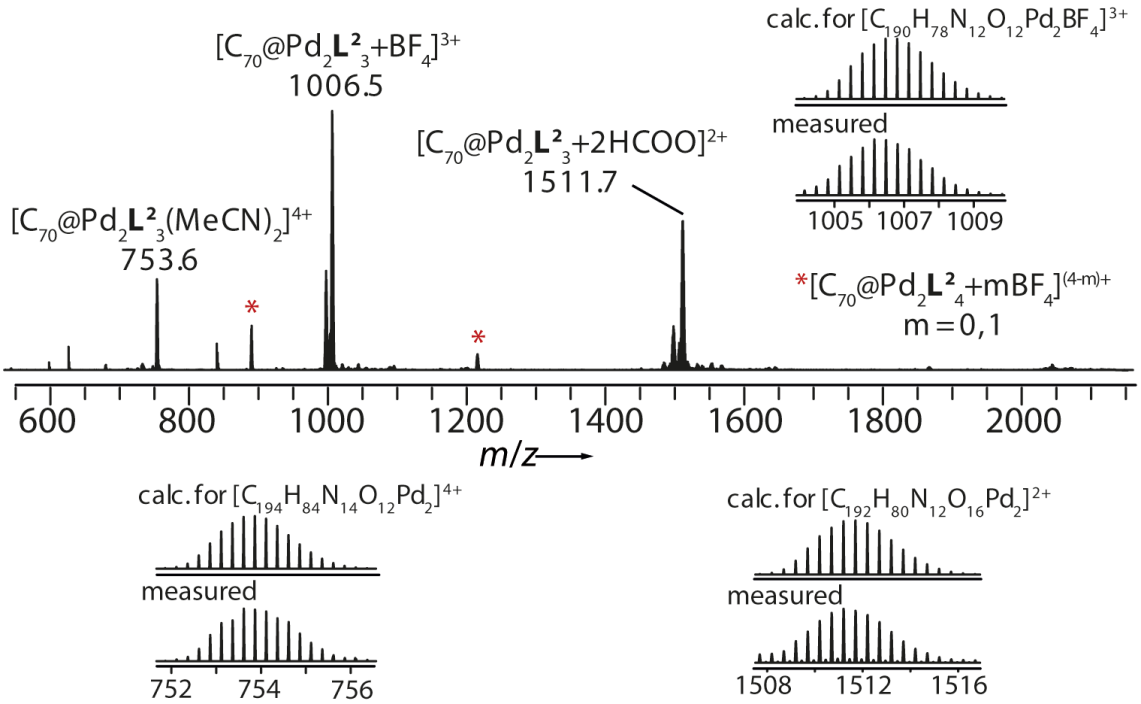


**Figure S35** ESI mass spectrum of $[C_{70}@Pd_2\mathbf{L^2}_3(MeCN)_2]^{4+}$. The presence of the $[C_{70}@Pd_2\mathbf{L^2}_3+2HCOO]^{2+}$ species is due to substitution of coordinated $CH_3CN$ by traces of formate under the measurement conditions. The $[C_{70}@Pd_2\mathbf{L^2}_4]^{4+}$ species is caused by the partial structural reorganization of the thermodynamic unstable species $[C_{70}@Pd_2\mathbf{L^2}_3(MeCN)_2]^{4+}$.

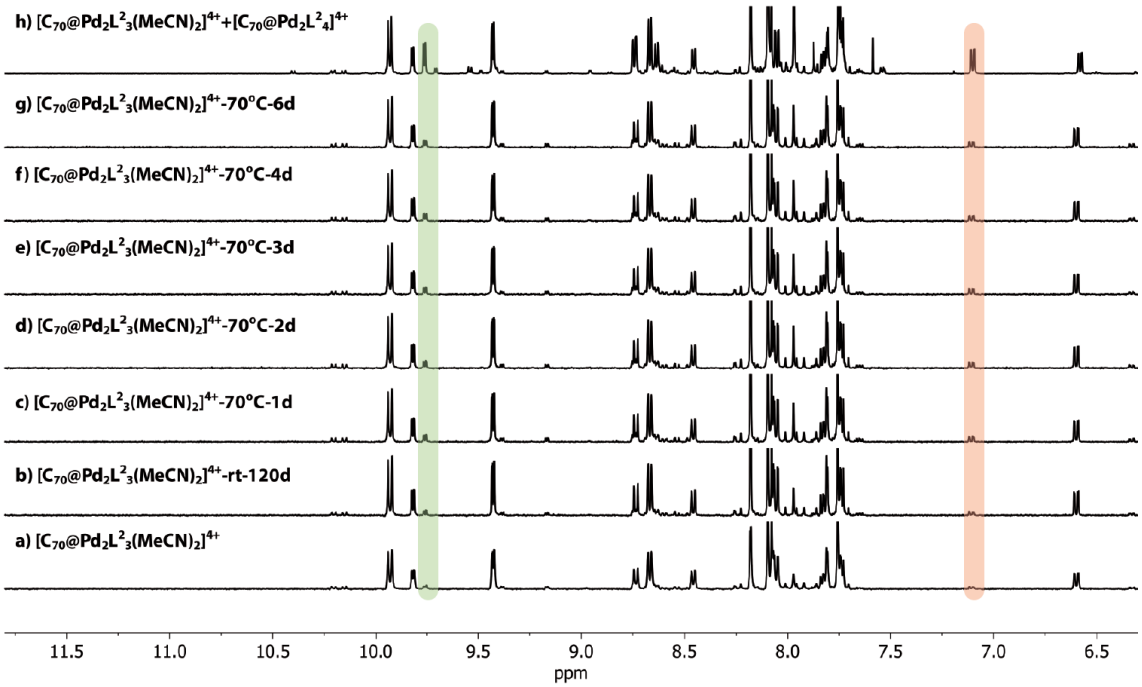


**Figure S36** $^1H$ NMR spectra (500 MHz, 298 K, $CD_3CN$) following the integrity of $[C_{70}@Pd_2\mathbf{L^2}_3(MeCN)_2]^{4+}$ at rt or 70 °C, indicating partial conversion into cage $[C_{70}@Pd_2\mathbf{L^2}_4]^{4+}$ after heating for several days. The quinoline proton D and proton B of $[C_{70}@Pd_2\mathbf{L^2}_4]^{4+}$ are highlighted in green and red, respectively.

## 3.7 Formation and characterization of the mixture of bowl $[C_{70}@Pd_2L^2_3(MeCN)_2]^{4+}$ and cage $[C_{70}@Pd_2L^2_4]^{4+}$

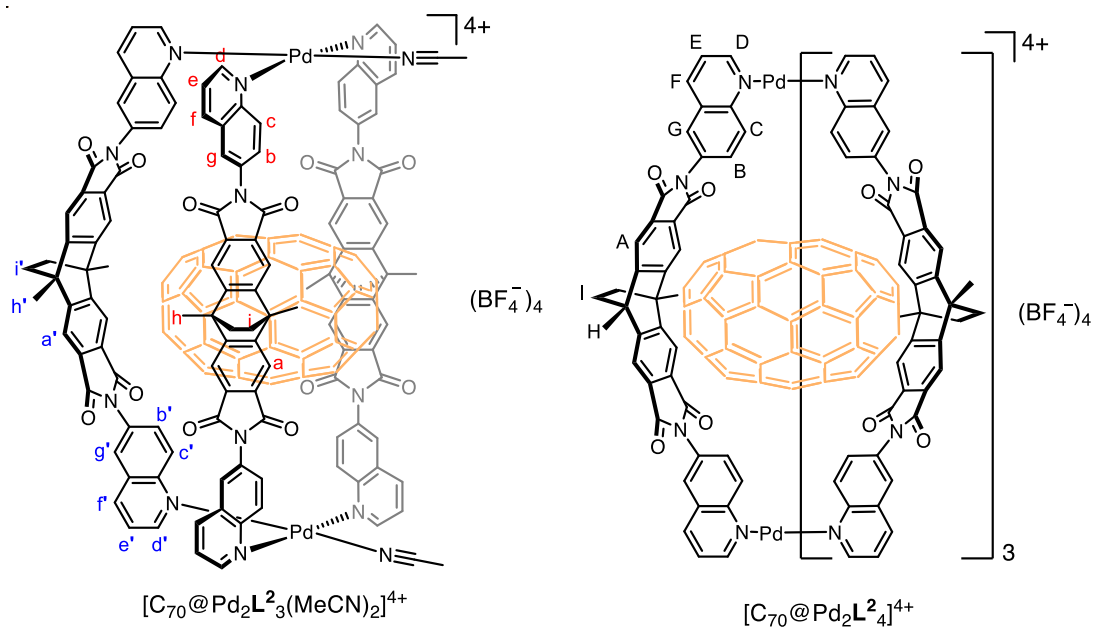


A solution of $[Pd(CH_3CN)_4](BF_4)_2$ (192.0 µL, 15 mM/$CD_3CN$, 2.88 µmol, 1 eq.) was combined with ligand **L²** (3.6 mg, 5.76 µmol, 2 eq.) and $C_{70}$ (1.3 mg, 1.55 µmol, 0.5 eq.) in $CD_3CN$ (2057 µL) and heated at 70 °C for 3 d. Remaining ligand and $C_{70}$ were removed by filtration to give bowl $[C_{70}@Pd_2L^2_3(MeCN)_2]^{4+}$ and cage $[C_{70}@Pd_2L^2_4]^{4+}$ (ratio: ca. 4:1).

**$^1$H NMR** (600 MHz, 298 K, $CD_3CN$): $\delta$ (ppm) = 9.93 (d, J = 9.2 Hz, 2H), 9.82 (dd, J = 5.6, 1.3 Hz, 1H), 9.76 (dd, J = 5.5, 1.3 Hz, 1H), 9.43 (dd, J = 5.4, 1.3 Hz, 2H), 8.74 (dd, J = 9.2, 2.5 Hz, 2H), 8.67 (d, J = 8.3 Hz, 2H), 8.64 (d, J = 8.4 Hz, 1H), 8.46 (d, J = 8.4 Hz, 1H), 8.18 (d, J = 2.4 Hz, 2H), 8.09 (d, J = 3.0 Hz, 3H), 8.08 (s, 2H), 8.05 (dd, J = 9.1, 2.3 Hz, 2H), 7.97 (s, 2H), 7.84 – 7.80 (m, 2H), 7.77 – 7.72 (m, 5H), 7.10 (dd, J = 9.2, 2.3 Hz, 1H), 6.58 (dd, J = 9.1, 2.2 Hz, 1H), 2.36 – 2.30 (m, 9H), 2.11 (s, 3H), 1.85 (d, J = 9.1 Hz, 6H), 1.66 (s, 2H).

All the signals in the aromatic region could be assigned via 2D NMR spectroscopy.

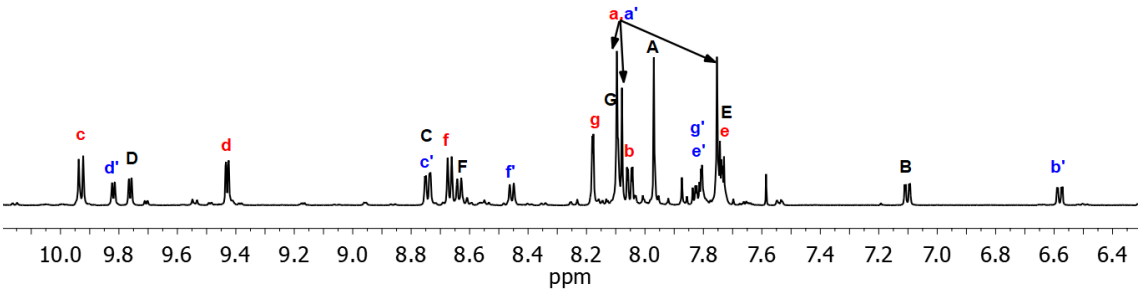


**Figure S37** $^1$H NMR spectrum (600 MHz, 298 K, $CD_3CN$) of the mixture of bowl $[C_{70}@Pd_2L^2_3(MeCN)_2]^{4+}$ and cage $[C_{70}@Pd_2L^2_4]^{4+}$.

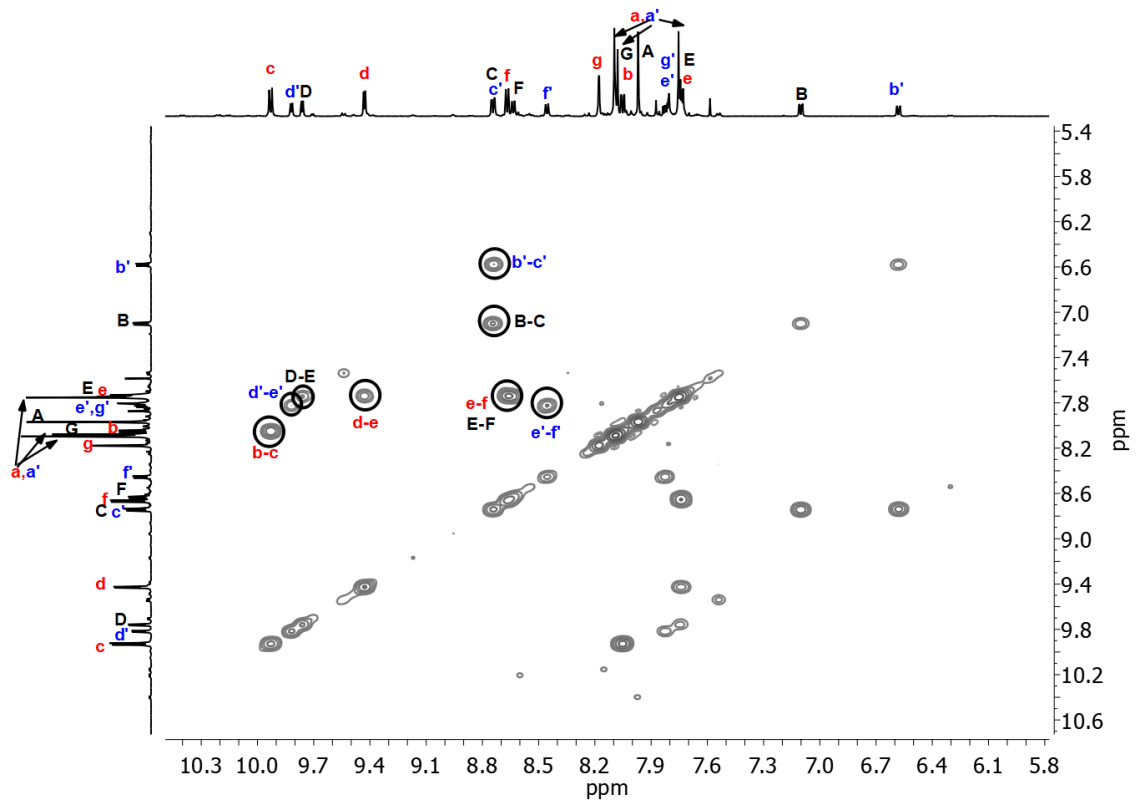


**Figure S38** Partial $^{1}H$ – $^{1}H$ COSY spectrum (600 MHz, 298 K, $CD_3CN$) of the mixture of bowl $[C_{70}@Pd_2\mathbf{L^2}_3(MeCN)_2]^{4+}$ and cage $[C_{70}@Pd_2\mathbf{L^2}_4]^{4+}$.

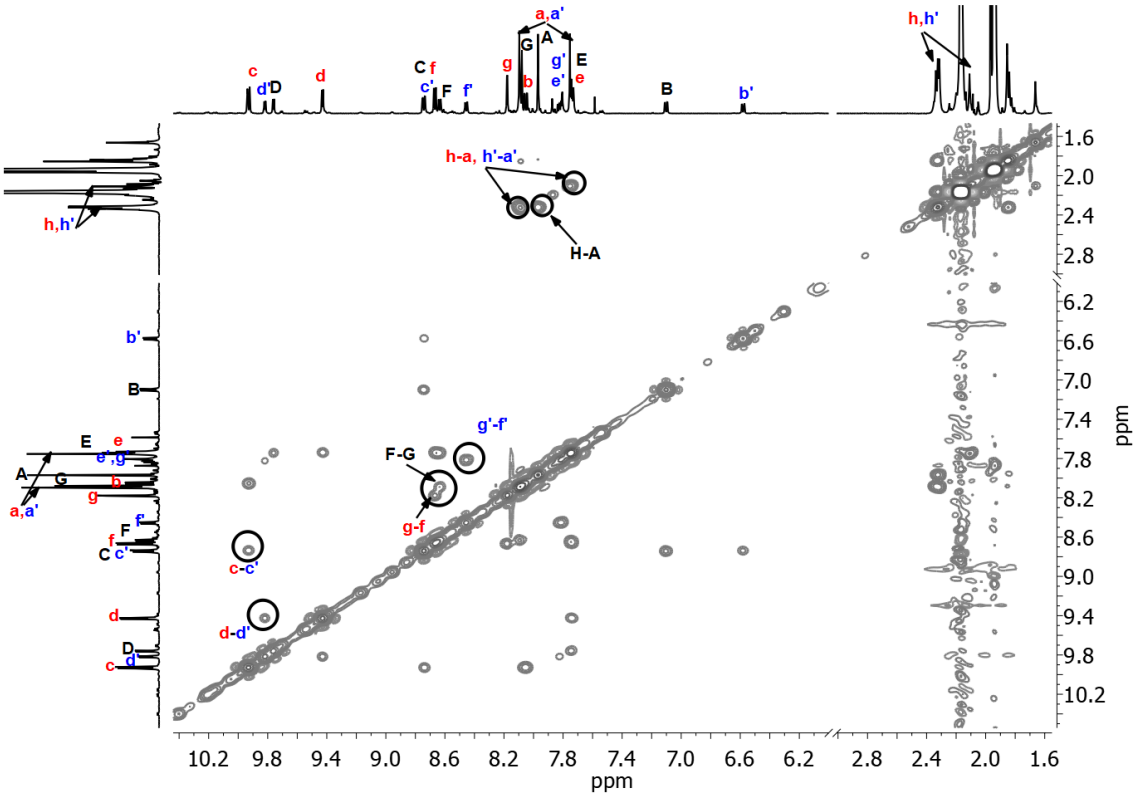


**Figure S39** Partial $^{1}H$ – $^{1}H$ NOESY spectrum (600 MHz, 298 K, $CD_3CN$) of the mixture of bowl $[C_{70}@Pd_2\mathbf{L^2}_3(MeCN)_2]^{4+}$ and cage $[C_{70}@Pd_2\mathbf{L^2}_4]^{4+}$.

**ESI HRMS** ($C_{194}H_{84}N_{14}O_{12}Pd_2B_4F_{16}$ and $C_{230}H_{104}N_{16}O_{16}Pd_2B_4F_{16}$): $[C_{70}@Pd_2\mathbf{L^2}_4]^{4+}$ calcd. for $C_{230}H_{104}N_{16}O_{16}Pd_2$ 889.8989; found 889.9022; $[C_{70}@Pd_2\mathbf{L^2}_4+BF_4]^{3+}$ calcd. for $C_{230}H_{104}N_{16}O_{16}Pd_2BF_4$ 1215.5333; found 1215.5389. Other peaks come from the bowl $[C_{70}@Pd_2\mathbf{L^2}_3(MeCN)_2]^{4+}$ species as shown before.

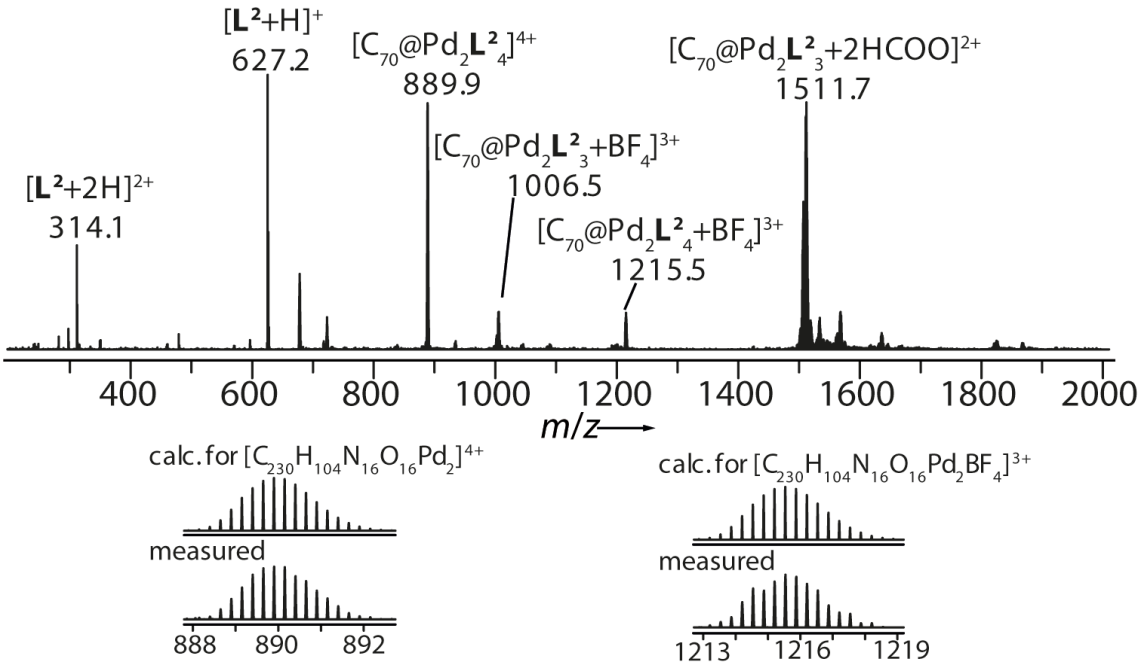


**Figure S40** ESI mass spectrum of the mixture of bowl $[C_{70}@Pd_2\mathbf{L^2}_3(MeCN)_2]^{4+}$ and cage $[C_{70}@Pd_2\mathbf{L^2}_4]^{4+}$. The presence of the $[C_{70}@Pd_2\mathbf{L^2}_3+2HCOO]^{2+}$ species is due to substitution of coordinated $CH_3CN$ by traces of forma under the measurement conditions.

## 3.8 Titration of bowl $[Pd_2\mathbf{L^2}_3(MeCN)_2]^{4+}$ with chloride anions

A 500 µL solution of the bowl $[Pd_2\mathbf{L^2}_3(MeCN)_2]^{4+}$ (0.64 mM) in $CD_3CN$ was titrated with a concentrated solution of tetrabutylammonium chloride ($NBu_4Cl$) (8.75 mM) in $CD_3CN$. Upon each addition, the solution was shaken before acquiring the spectrum, which allowed equilibrium to be reached.

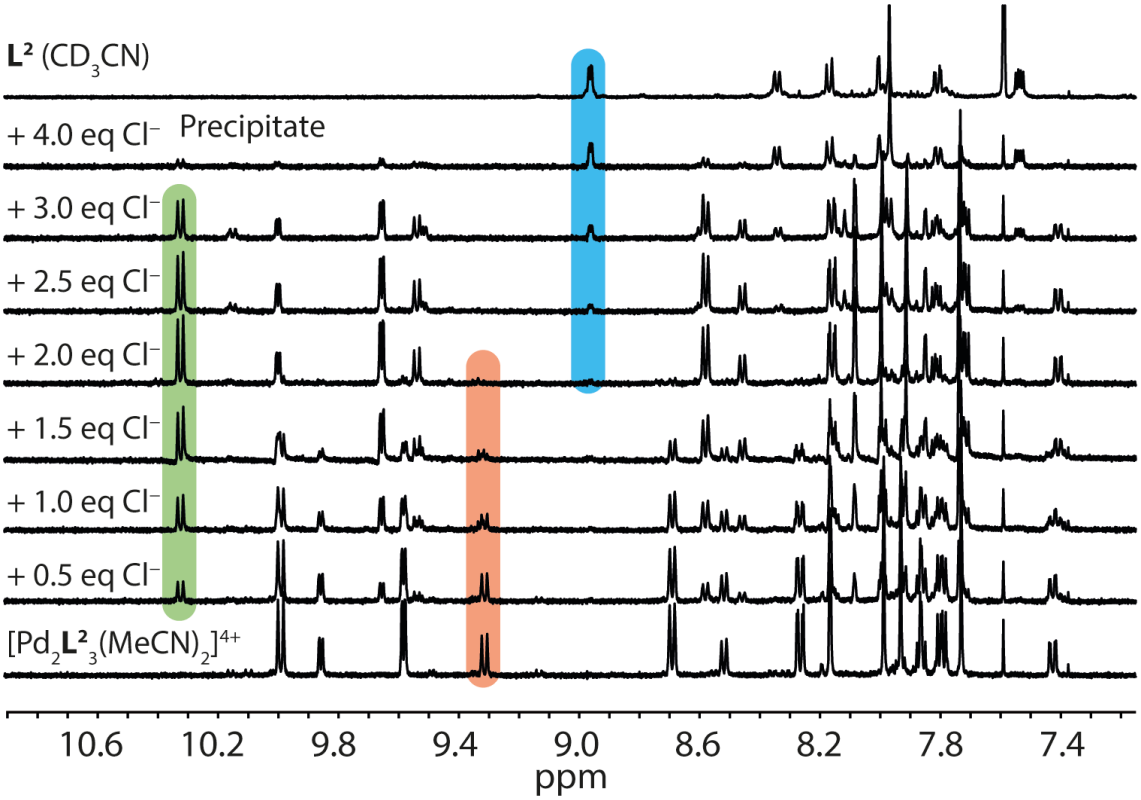


**Figure S41** $^1$H NMR titration (500 MHz, 298 K, $CD_3CN$) of $[Pd_2\mathbf{L^2}_3(MeCN)_2]^{4+}$ with $NBu_4Cl$. Upon addition of two equivalents of chloride, bowl $[Pd_2\mathbf{L^2}_3(MeCN)_2]^{4+}$ transforms into bowl $[Pd_2\mathbf{L^2}_3Cl_2]^{2+}$. Excess addition of chloride leads to disassembly of the bowl. The quinoline proton c of $[Pd_2\mathbf{L^2}_3Cl_2]^{2+}$, proton c' of $[Pd_2\mathbf{L^2}_3(MeCN)_2]^{4+}$ and proton d of $\mathbf{L^2}$ are highlighted in green, red and blue, respectively.

## 3.9 Formation and characterization of bowl $[Pd_2L^2{}_3Cl_2]^{2+}$

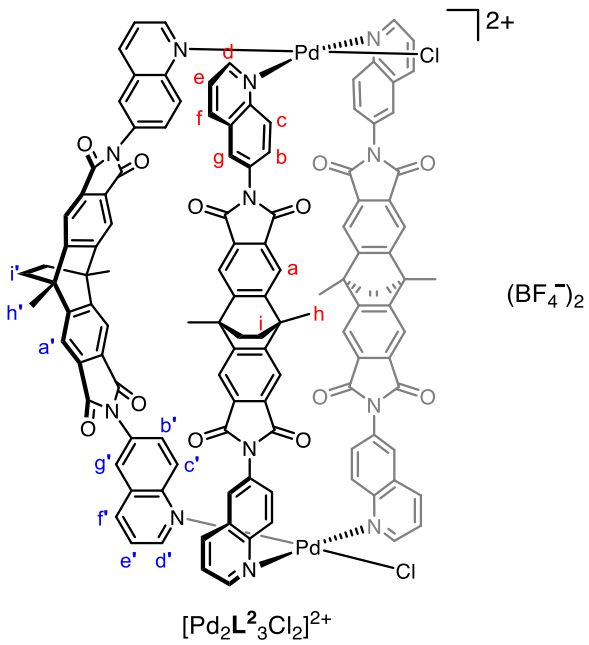


The $[Pd_2\mathbf{L^2}_3Cl_2]^{2+}$ solution (0.56 mM) was formed by stirring a mixture of the $CD_3CN$ solution of $[Pd_2\mathbf{L^2}_3(MeCN)_2]^{4+}$ (4000 µL, 0.64 mM, 2.56 µmol, 1 eq.) and $CD_3CN$ solution of $NBu_4Cl$ (585.4 µL, 8.75 mM, 5.12 µmol, 2 eq.) at room temperature for 2 min.

**$^1$H NMR** (600 MHz, 298 K, $CD_3CN$): $\delta$ (ppm) = 10.32 (d, J = 9.1 Hz, 4H), 10.00 (dd, J = 5.4, 1.4 Hz, 2H), 9.65 (dd, J = 5.4, 1.3 Hz, 4H), 9.54 (d, J = 9.0 Hz, 2H), 8.58 (d, J = 8.3 Hz, 4H), 8.45 (d, J = 8.3 Hz, 2H), 8.16 (dd, J = 9.1, 2.2 Hz, 4H), 8.08 (d, J = 2.2 Hz, 4H), 7.99 (s, 4H), 7.91 (s, 4H), 7.84 (d, J = 2.2 Hz, 2H), 7.81 (dd, J = 8.4, 5.4 Hz, 2H), 7.74 – 7.70 (m, 8H), 7.40 (dd, J = 9.0, 2.2 Hz, 2H), 2.26 (s, 6H), 2.22 (s, 6H), 2.09 (s, 6H), 1.87 (s, 8H), 1.77 (s, 4H).

All the peaks in aromatic region could be assigned via 2D NMR spectroscopy.

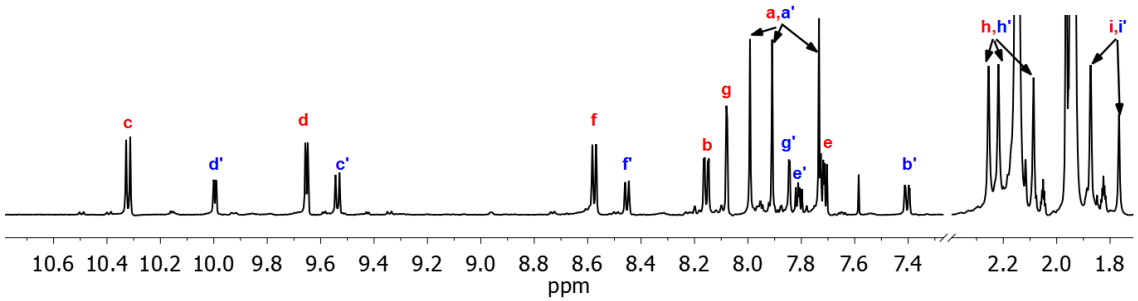


**Figure S42** $^1$H NMR spectrum (600 MHz, 298 K, $CD_3CN$) of $[Pd_2\mathbf{L^2}_3Cl_2]^{2+}$.

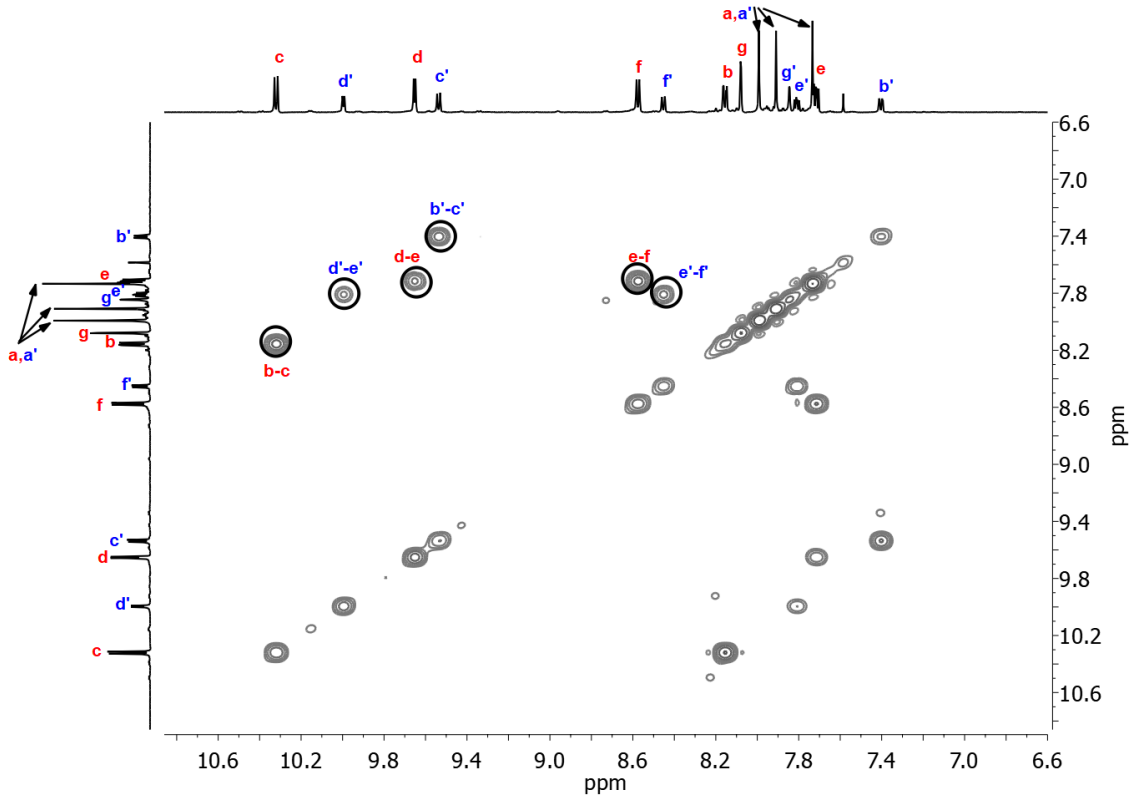


**Figure S43** Partial $^1$H – $^1$H COSY spectrum (600 MHz, 298 K, $CD_3CN$) of $[Pd_2\mathbf{L^2}_3Cl_2]^{2+}$.

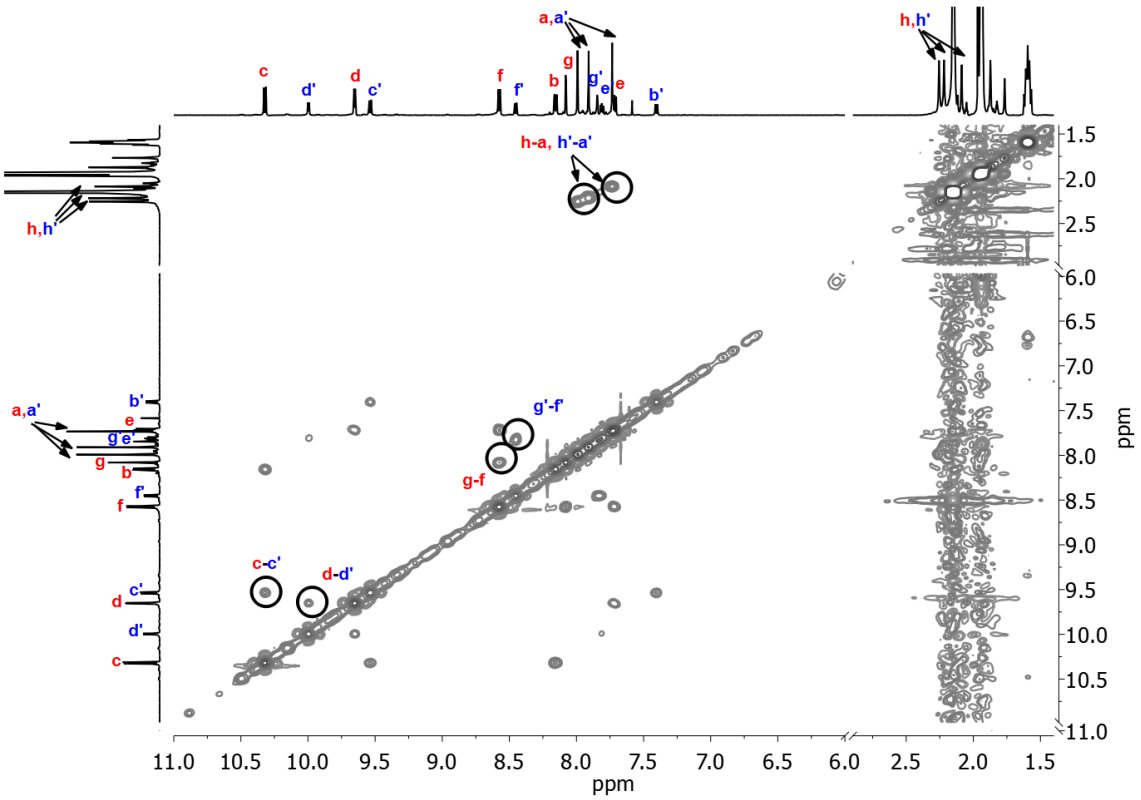


**Figure S44** Partial $^{1}H - {}^{1}H$ NOESY spectrum (600 MHz, 298 K, $CD_3CN$) of $[Pd_2\mathbf{L^2}_3Cl_2]^{2+}$.

**ESI HRMS** ($C_{120}H_{78}N_{12}O_{12}Pd_2Cl_2B_2F_8$): $[Pd_2\mathbf{L^2}_3Cl_2]^{2+}$ calcd. for $C_{120}H_{78}N_{12}O_{12}Pd_2Cl_2$ 1081.1668; found 1081.1723.

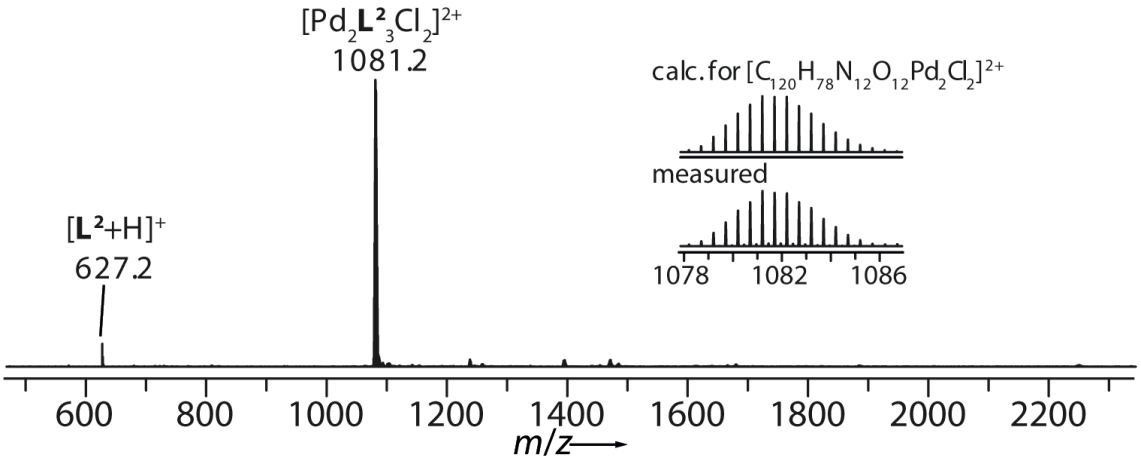


**Figure S45** ESI mass spectrum of $[Pd_2\mathbf{L^2}_3Cl_2]^{2+}$.

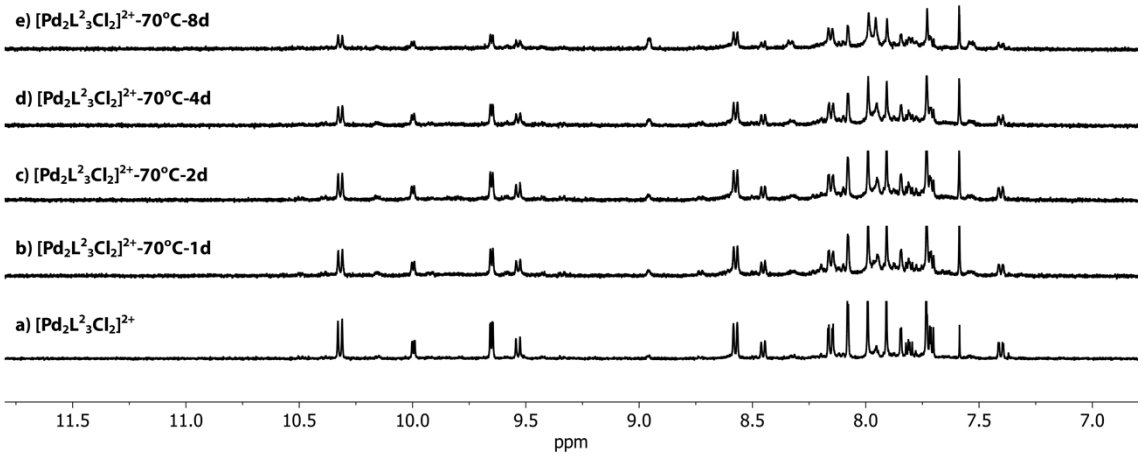


**Figure S46** $^1$H NMR spectra (500 MHz, 298 K, $CD_3CN$) following the integrity of $[Pd_2\mathbf{L^2}_3Cl_2]^{2+}$ at 70 °C, indicating partial decomposition after several days.

## 3.10 Formation and characterization of bowl $[C_{60}@Pd_2\mathbf{L^2}_3Cl_2]^{2+}$

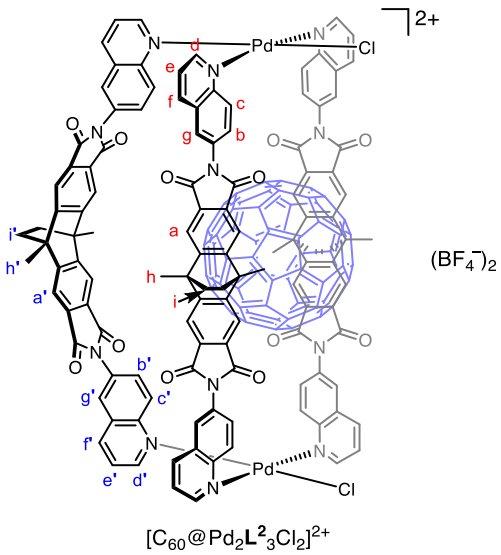


The $[C_{60}@Pd_2\mathbf{L^2}_3Cl_2]^{2+}$ solution (0.56 mM) was formed by stirring a mixture of the $CD_3CN$ solution of $[C_{60}@Pd_2\mathbf{L^2}_3(MeCN)_2]^{4+}$ (3000 µL, 0.64 mM, 1.92 µmol, 1 eq.) and the $CD_3CN$ solution of $NBu_4Cl$ (439.0 µL, 8.75 mM, 3.84 µmol, 2 eq.) at room temperature for 2 min.

**$^1$H NMR** (600 MHz, 298 K, $CD_3CN$): $\delta$ (ppm) = 10.80 (d, J = 9.1 Hz, 4H), 10.01 (d, J = 5.4 Hz, 2H), 9.51 (dd, J = 5.4, 1.3 Hz, 4H), 9.18 (d, J = 9.1 Hz, 2H), 8.56 (d, J = 8.3 Hz, 4H), 8.38 (d, J = 8.3 Hz, 2H), 8.27 (dd, J = 9.1, 2.3 Hz, 4H), 8.09 (d, J = 2.2 Hz, 4H), 8.06 (s, 4H), 7.94 (s, 4H), 7.79 (d, J = 2.2 Hz, 2H), 7.77 (dd, J = 8.3, 5.4 Hz, 2H), 7.73 (s, 4H), 7.68 (dd, J = 8.3, 5.4 Hz, 4H), 7.01 (dd, J = 9.0, 2.2 Hz, 2H), 2.24 (s, 6H), 2.22 (s, 6H), 2.09 (s, 6H), 1.77 (s, 8H), 1.67 (s, 4H).

All the peaks in aromatic region could be assigned via 2D NMR spectroscopy.

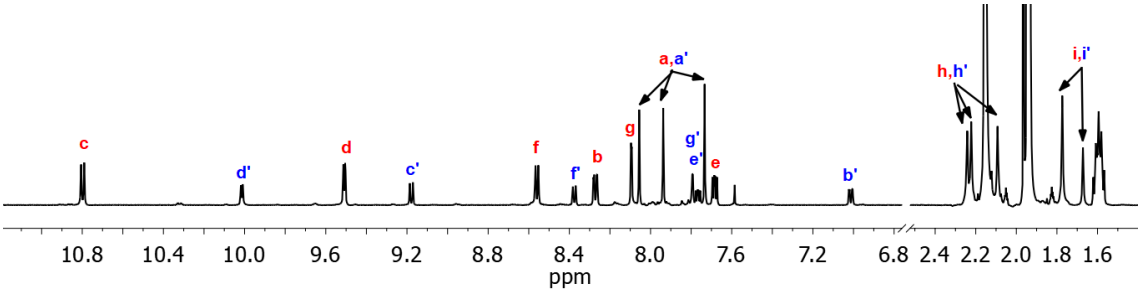


**Figure S47** $^{1}$H NMR spectrum (600 MHz, 298 K, $CD_3CN$) of $[C_{60}@Pd_2\mathbf{L^2}_3Cl_2]^{2}$.

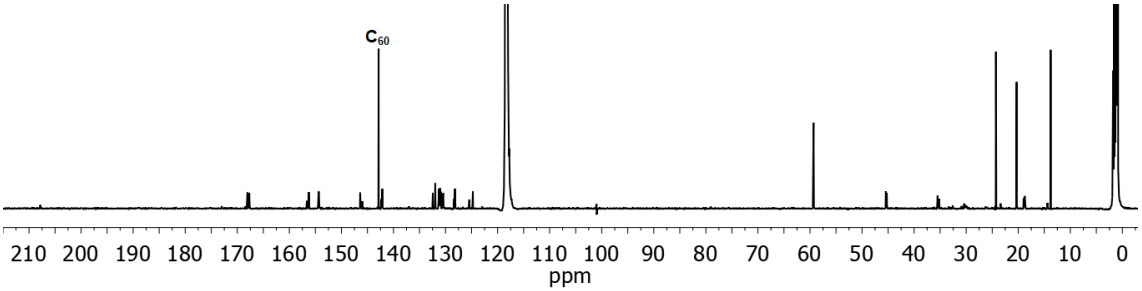


**Figure S48** $^{13}$C NMR spectrum (151 MHz, 298 K, $CD_3CN$) of $[C_{60}@Pd_2\mathbf{L^2}_3Cl_2]^{2+}$. A single signal at 142.85 ppm corresponds to encapsulated $C_{60}$.

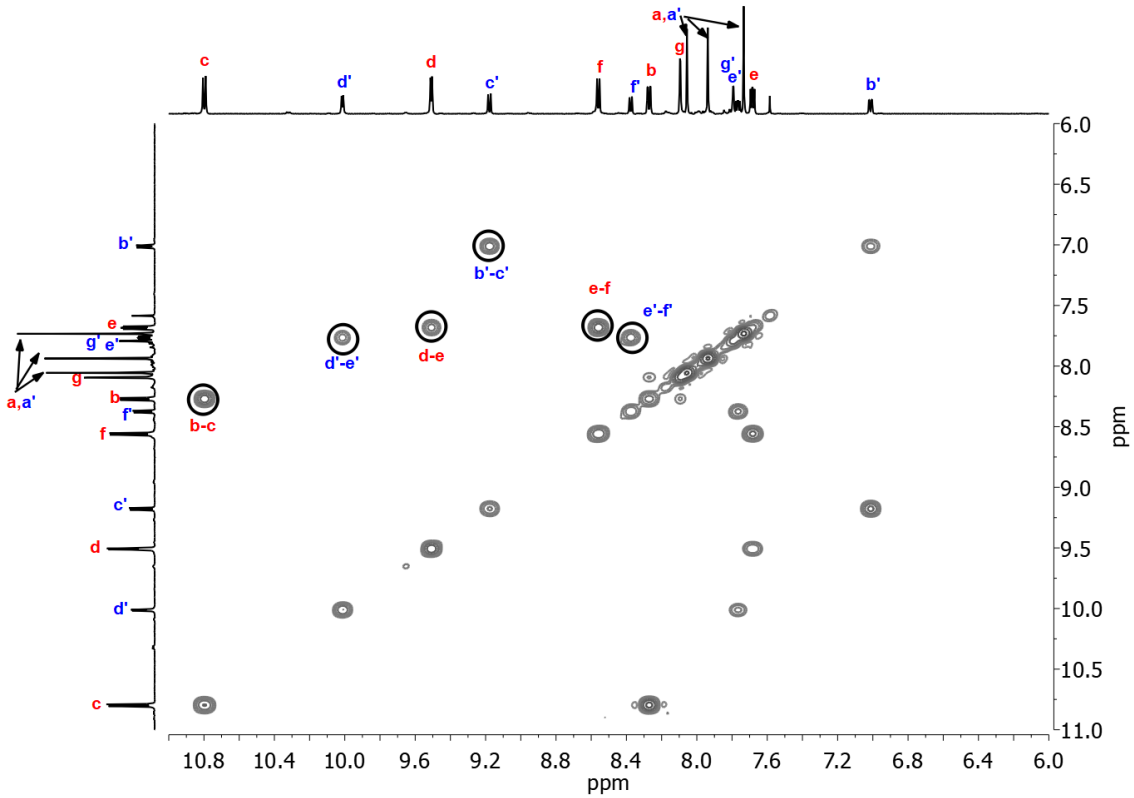


**Figure S49** Partial $^{1}$H – $^{1}$H COSY spectrum (600 MHz, 298 K, $CD_3CN$) of $[C_{60}@Pd_2\mathbf{L^2}_3Cl_2]^{2+}$.

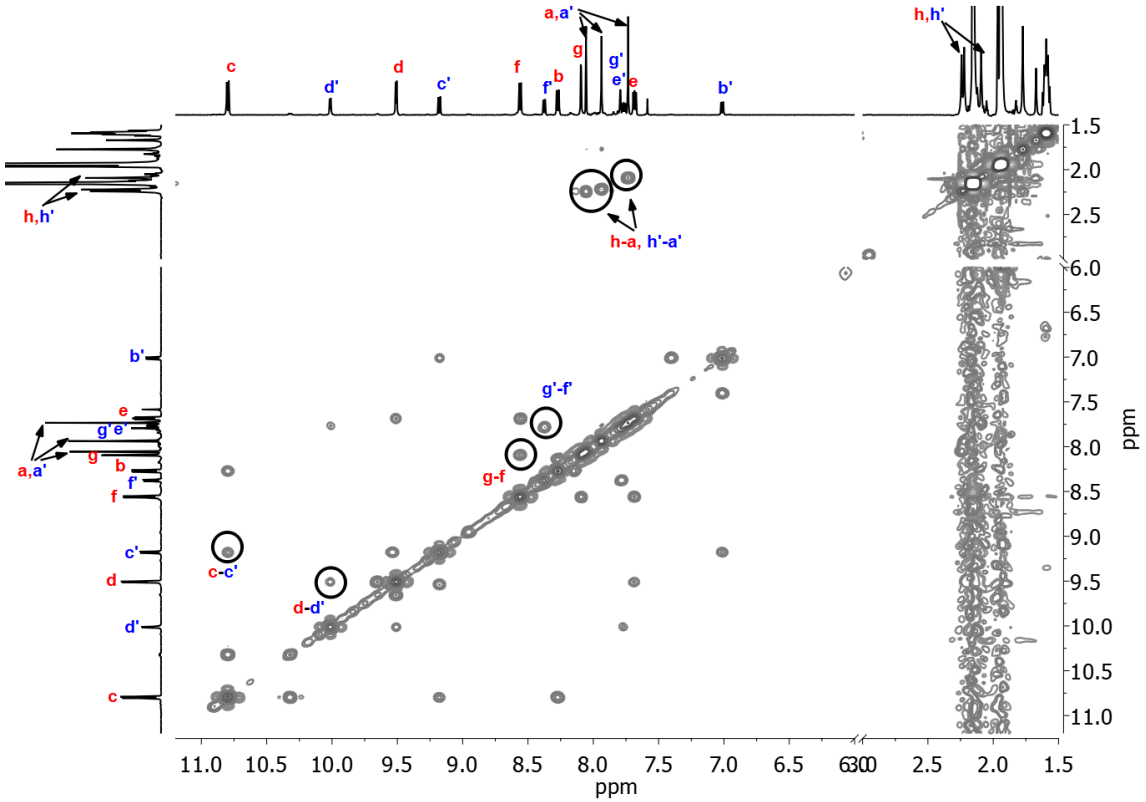


**Figure S50** Partial $^{1}H - ^{1}H$ NOESY spectrum (600 MHz, 298 K, $CD_3CN$) of $[C_{60}@Pd_2\mathbf{L^2}_3Cl_2]^{2+}$.

**ESI HRMS** ($C_{180}H_{78}Cl_2N_{12}O_{12}Pd_2B_2F_8$): $[C_{60}@Pd_2\mathbf{L^2}_3Cl_2]^{2+}$ calcd. for $C_{180}H_{78}Cl_2N_{12}O_{12}Pd_2$ 1441.6679; found 1441.6661.

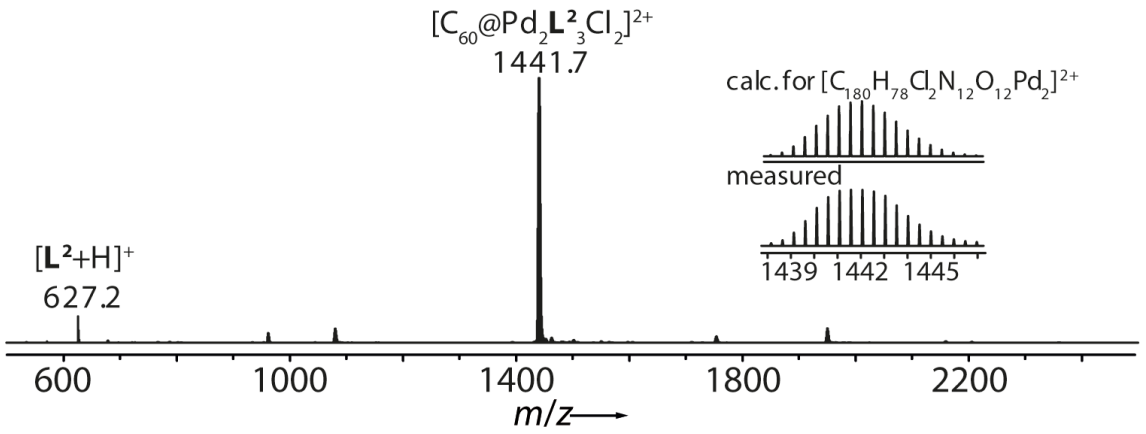


**Figure S51** ESI mass spectrum of $[C_{60}@Pd_2\mathbf{L^2}_3Cl_2]^{2+}$.

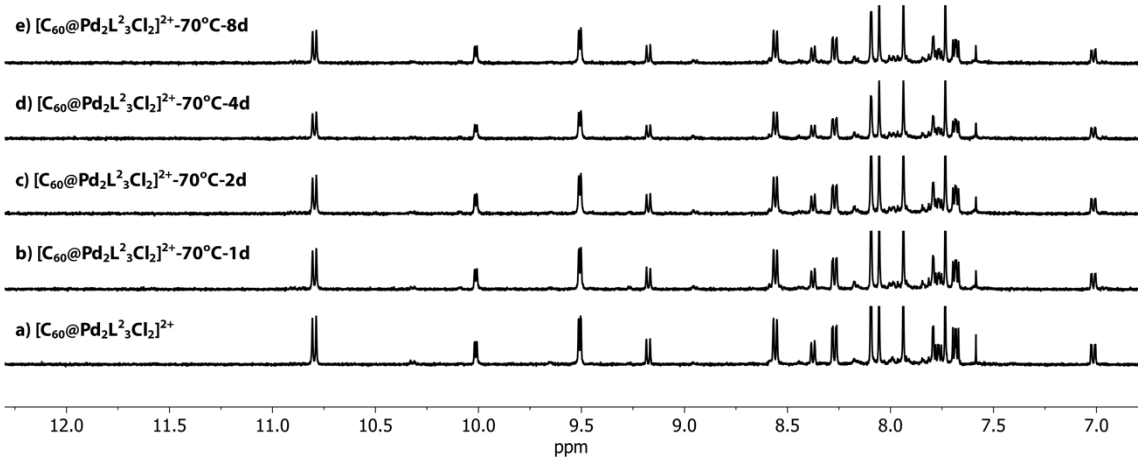


**Figure S52** $^{1}$H NMR spectra (500 MHz, 298 K, $CD_3CN$) following the integrity of $[C_{60}@Pd_2\mathbf{L^2}_3Cl_2]^{2+}$ at 70 °C, indicating stability for several days.

## 3.11 Formation and characterization of dimer $[Pd_4\mathbf{L^2}_6(BDC)_2]^{4+}$

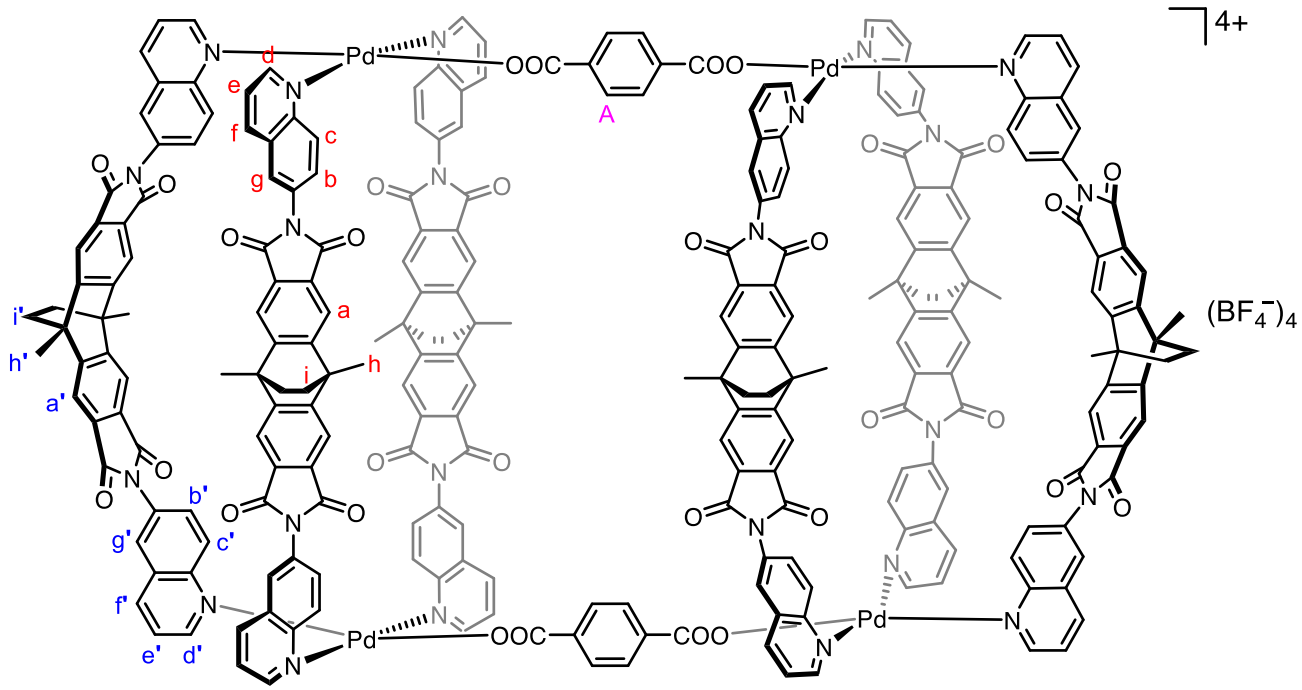


$[Pd_4\mathbf{L^2}_6(BDC)_2]^{4+}$

The $CD_3CN$ solution of $(Et_3NH)_2BDC$ (15 mM) was prepared by mixing 1,4-benzenedioic acid (BDC, 1,4-benzeneterephthalic acid) and 2 eq. trimethylamine in $CD_3CN$ at room temperature. The $CD_3CN$ solution $[Pd_4\mathbf{L^2}_6(BDC)_2]^{4+}$ (0.31 mM) was formed by stirring a mixture of the $CD_3CN$ solution of $[Pd_2\mathbf{L^2}_3(MeCN)_2]^{4+}$ (500 µL, 0.64 mM, 0.32 µmol, 1 eq.) and $CD_3CN$ solution of $(Et_3NH)_2BDC$ (21.3 µL, 15 mM, 0.32 µmol, 1 eq.) at room temperature for 2 min. NMR spectra were recorded of the freshly prepared sample.

**$^1$H NMR** (500 MHz, 298 K, $CD_3CN$): $\delta$ (ppm) = 10.16 (d, $J$ = 9.8 Hz, 8H), 9.80 (dd, $J$ = 5.5, 1.4 Hz, 4H), 9.66 (dd, $J$ = 5.5, 1.4 Hz, 8H), 9.61 (d, $J$ = 9.1 Hz, 4H), 8.53 – 8.47 (m, 12H), 8.00 – 7.96 (m, 16H), 7.96 – 7.93 (m, 12H), 7.92 (s, 8H), 7.83 (s, 8H), 7.70 (dd, $J$ = 8.3, 5.6 Hz, 4H), 7.63 (dd, $J$ = 8.3, 5.4 Hz, 8H), 7.51 (dd, $J$ = 9.1, 2.3 Hz, 4H), 7.44 (s, 8H), 2.26 – 2.19 (m, 24H), 2.16 (s, overlapping with water peak in $CD_3CN$ ), 1.94 (overlapping with solvent residual peak), 1.82 (s, 8H).

Overlapping signals in the aliphatic region could be assigned via 2D NMR spectroscopy.

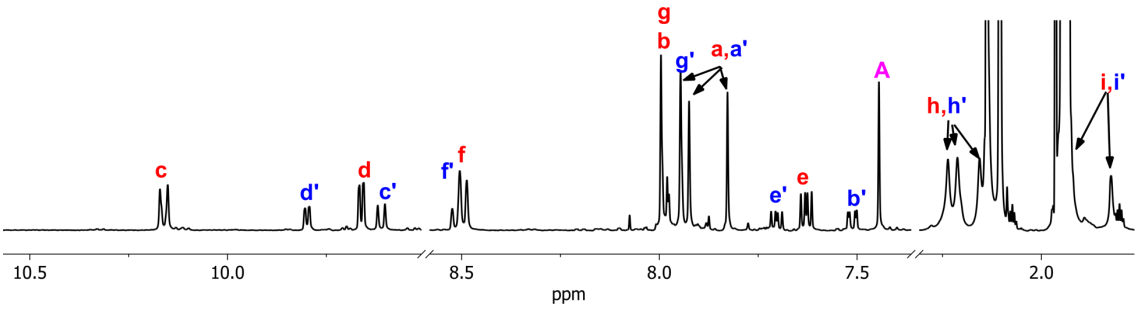


**Figure S53** $^1$H NMR spectrum (500 MHz, 298 K, $CD_3CN$) of $[Pd_4\mathbf{L^2}_6(BDC)_2]^{4+}$.

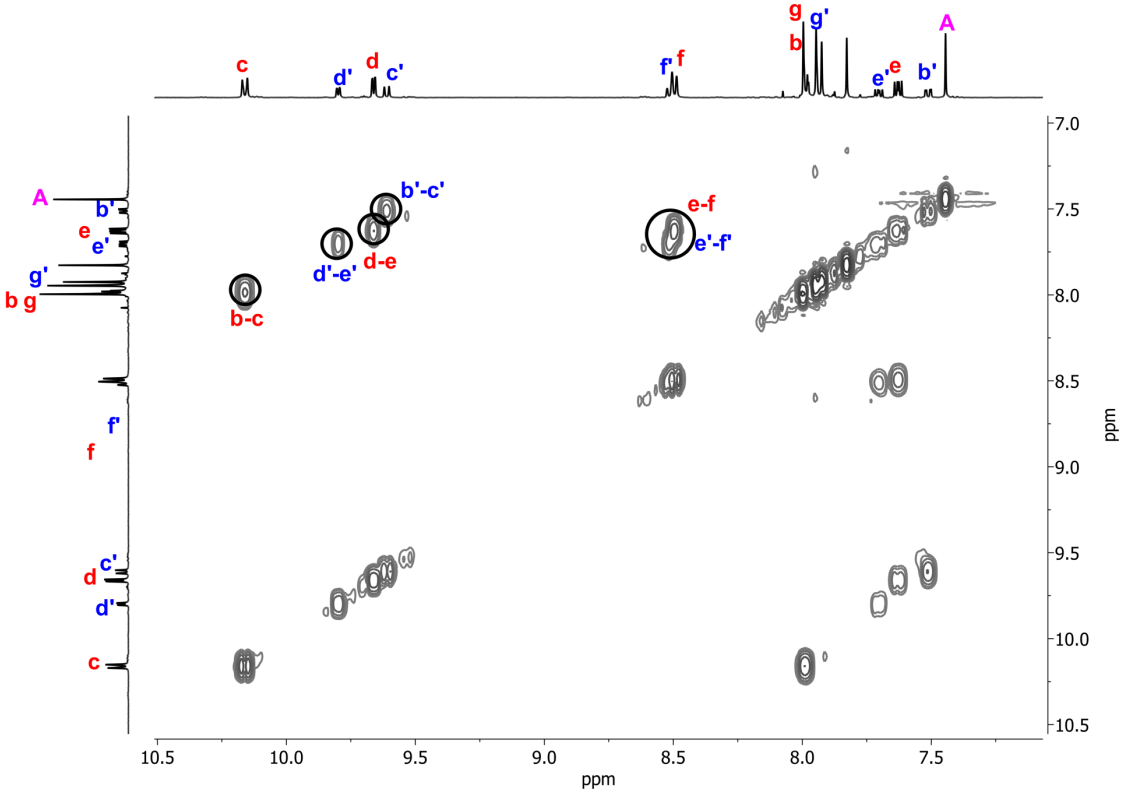


**Figure S54** Partial $^1$H – $^1$H COSY spectrum (500 MHz, 298 K, $CD_3CN$) of $[Pd_4\mathbf{L^2}_6(BDC)_2]^{4+}$.

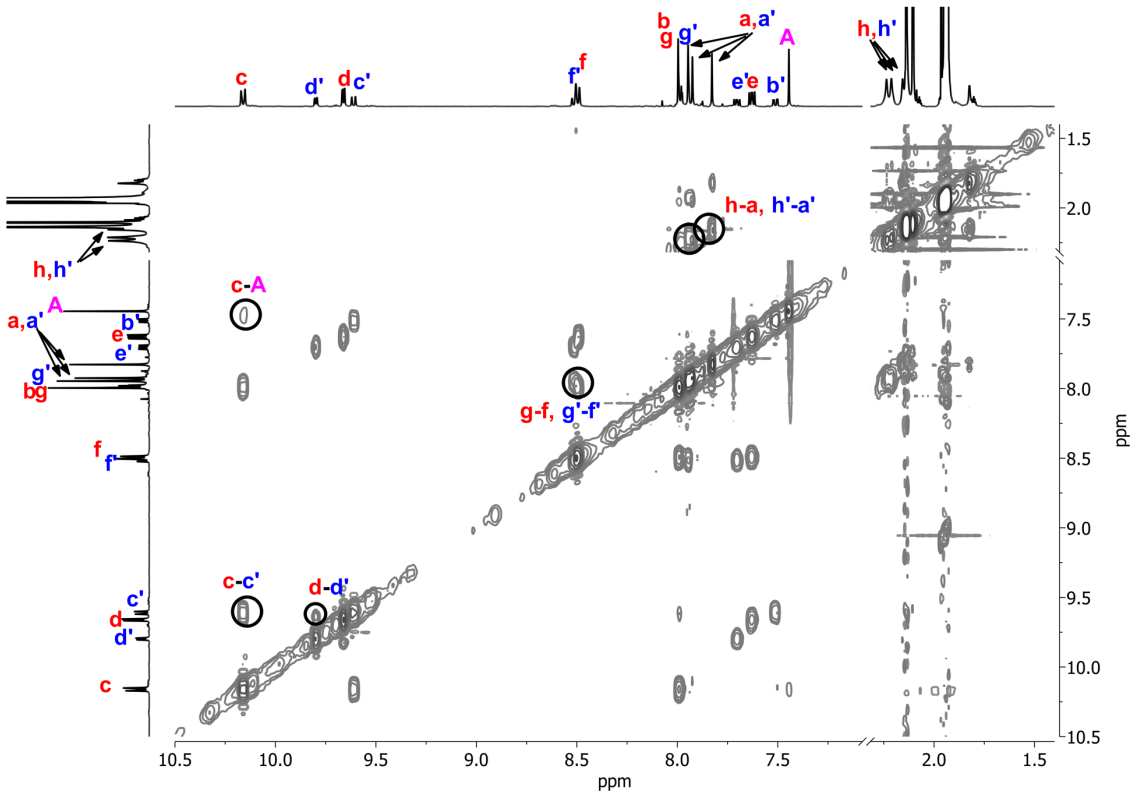


**Figure S55** Partial $^{1}H - {}^{1}H$ NOESY spectrum (500 MHz, 298 K, $CD_3CN$) of $[Pd_4\mathbf{L^2}_6(BDC)_2]^{4+}$.

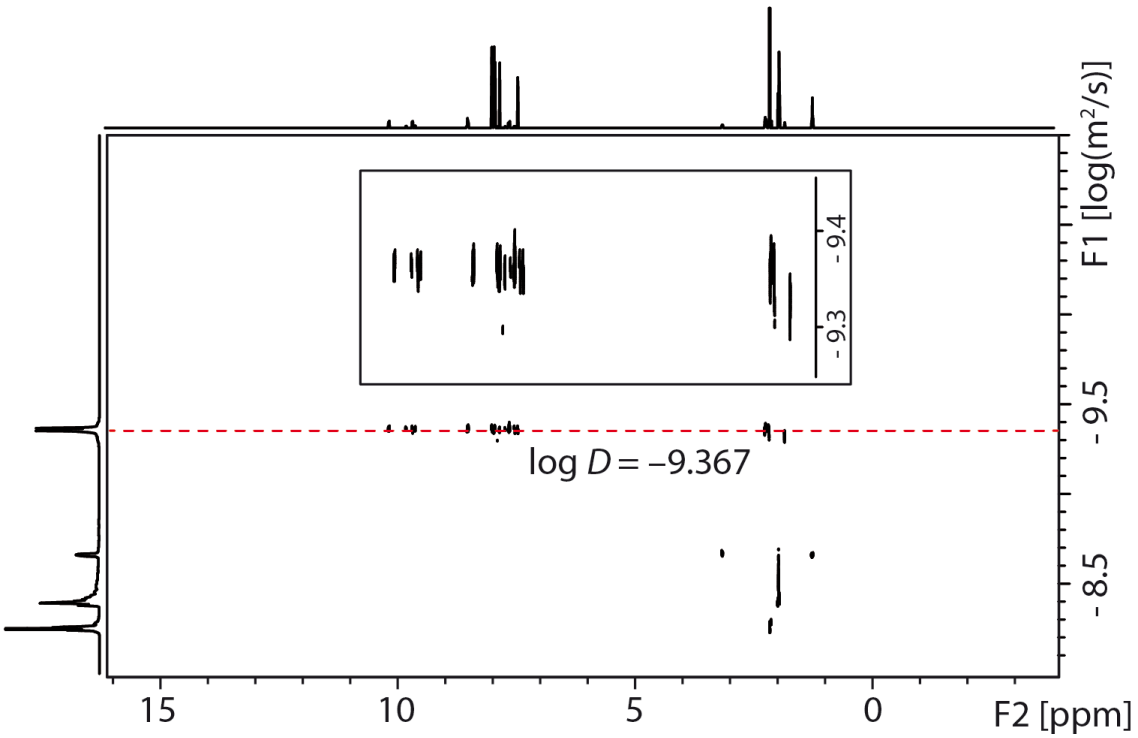


**Figure S56** DOSY spectrum (500 MHz, 298 K, $CD_3CN$) of $[Pd_4\mathbf{L^2}_6(BDC)_2]^{4+}$: diffusion coefficient = 4.3 x $10^{-10}$ $m^2s^{-1}$, log *D* = –9.37, r = 14.8 Å.

**ESI HRMS** ($C_{256}H_{164}N_{24}O_{32}Pd_4B_4F_{16}$): $[Pd_4\mathbf{L^2}_6(BDC)_2]^{4+}$ calcd. for $C_{256}H_{164}N_{24}O_{32}Pd_4$ 1128.2015; found 1128.2084; $[Pd_4\mathbf{L^2}_6(BDC)_2{+}BF_4]^{3+}$ calcd. for $C_{256}H_{164}N_{24}O_{32}Pd_4BF_4$ 1533.2740; found 1533.2740.

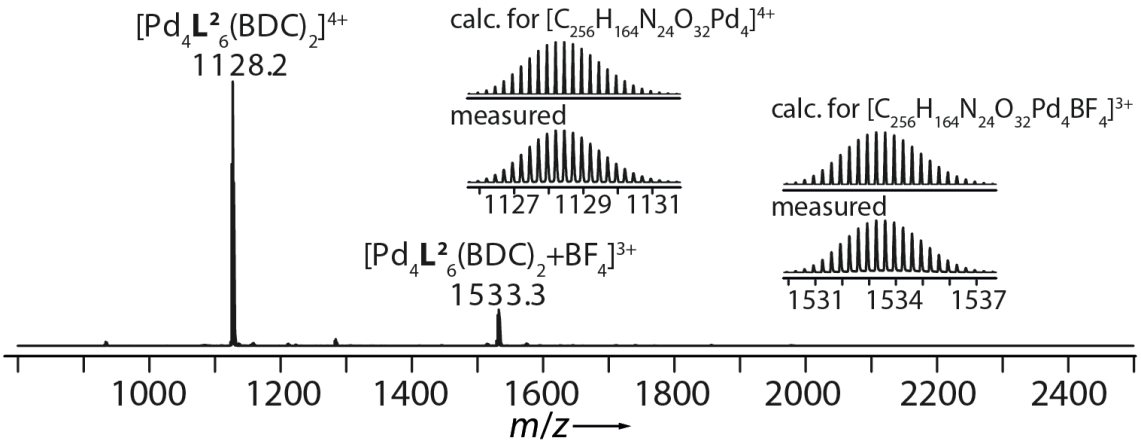


**Figure S57** ESI mass spectrum of $[Pd_4\mathbf{L}^{2}_{6}(BDC)_2]^{4+}$.

## 3.12 Formation and characterization of dimer $[2C_{60}@Pd_4L^{2}_{6}(BDC)_2]^{4+}$

The $CD_3CN$ solution $[2C_{60}@Pd_4\mathbf{L}^{2}_{6}(BDC)_2]^{4+}$ (0.31 mM) was formed by stirring a mixture of the $CD_3CN$ solution of $[C_{60}@Pd_2\mathbf{L}^{2}_{3}(MeCN)_2]^{4+}$ (500 µL, 0.64 mM, 0.32 µmol, 1 eq.) and $CD_3CN$ solution of $(Et_3NH)_2BDC$ (21.3 µL, 15 mM, 0.32 µmol, 1.0 eq.) at room temperature for 2 min.

**$^1$H NMR** (600 MHz, 298 K, $CD_3CN$): $\delta$ (ppm) = 10.60 (d, *J* = 9.0 Hz, 8H), 9.95 (dd, *J* = 5.5, 1.4 Hz, 4H), 9.62 (dd, *J* = 5.5, 1.4 Hz, 8H), 9.43 (d, *J* = 8.9 Hz, 4H), 8.49 (d, *J* = 8.1 Hz, 8H), 8.41 (d, *J* = 8.5 Hz, 4H), 8.17 (dd, *J* = 8.9, 2.3 Hz, 8H), 8.06 (s, 8H), 8.04 (d, *J* = 2.3 Hz, 8H), 7.99 (s, 8H), 7.85 (d, *J* = 2.2 Hz, 4H), 7.82 (s, 8H), 7.81 (s, 8H), 7.71 (dd, *J* = 8.1, 5.6 Hz, 4H), 7.63 (dd, *J* = 8.1, 5.5 Hz, 8H), 7.10 (dd, *J* = 8.9, 2.3 Hz, 4H), 2.34 (s, 12H), 2.28 (s, 12H), 2.17 (s, overlapped with water peak in $CD_3CN$), 1.72 (s, 8H).

Overlapping signals in the aliphatic region could be assigned via 2D NMR spectroscopy.

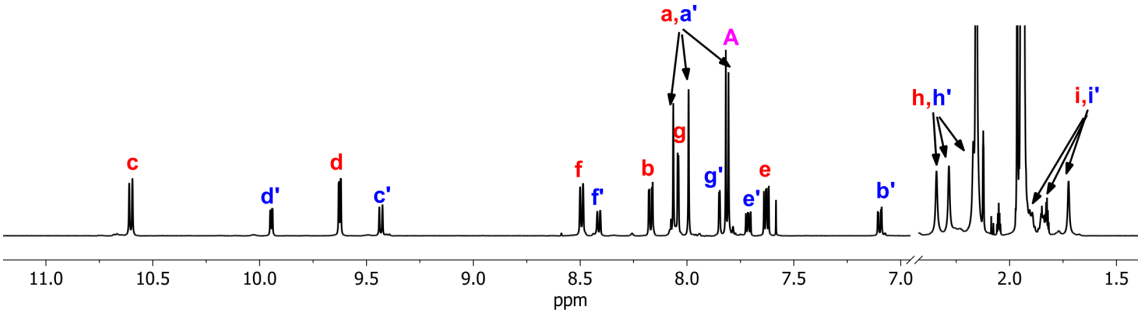


**Figure S58** $^1$H NMR spectrum (600 MHz, 298 K, $CD_3CN$) of $[2C_{60}@Pd_4\mathbf{L}^{2}_{6}(BDC)_2]^{4+}$.

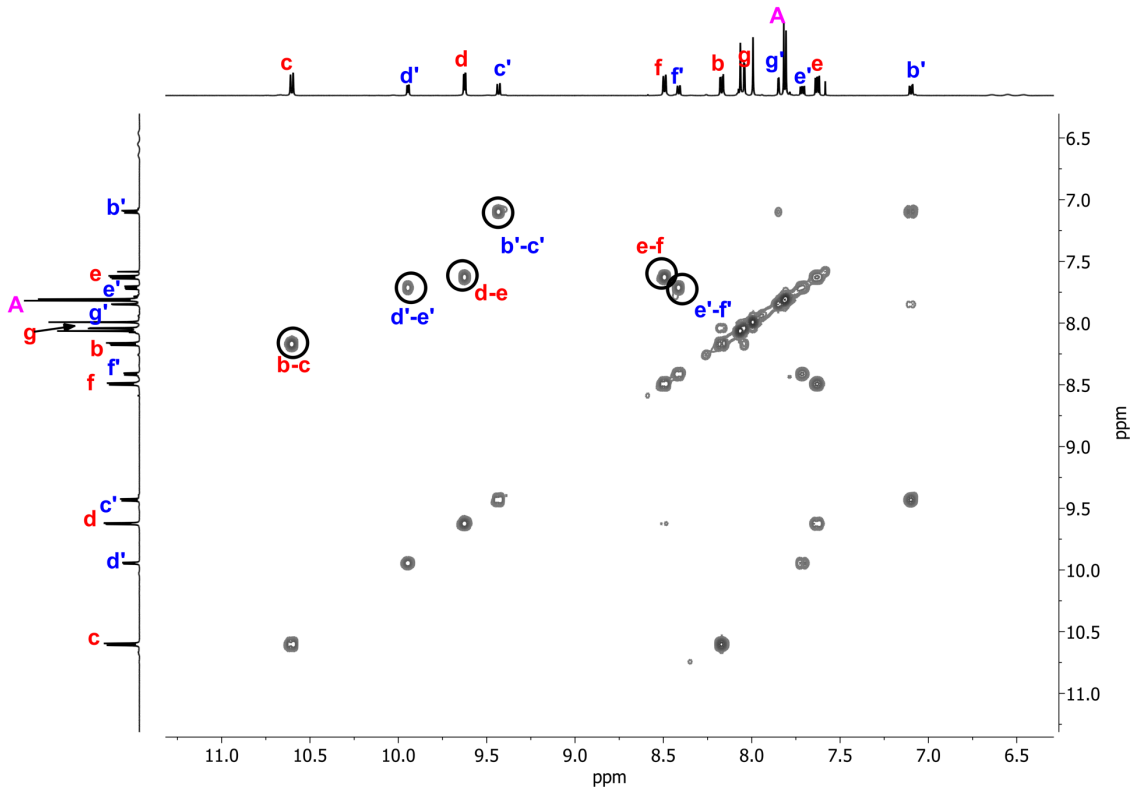


**Figure S59** Partial $^{1}H - {}^{1}H$ COSY spectrum (600 MHz, 298 K, $CD_3CN$) of $[2C_{60}@Pd_4\mathbf{L^2}_6(BDC)_2]^{4+}$.

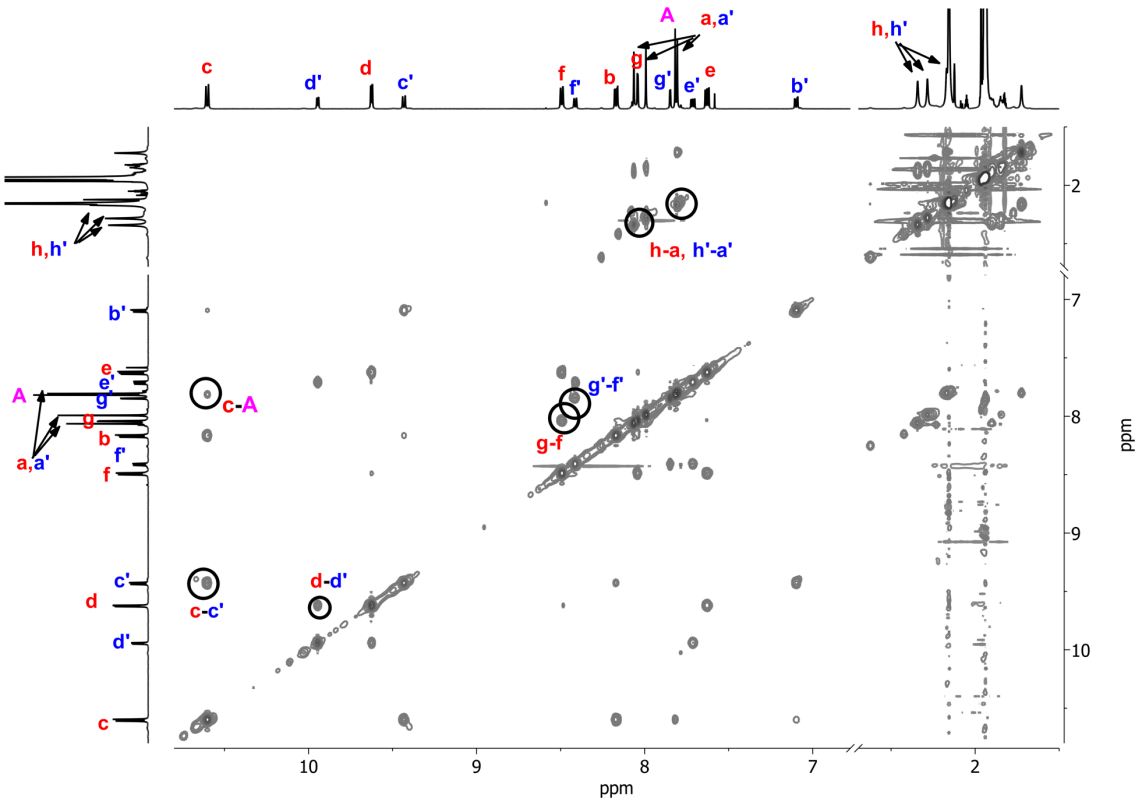


**Figure S60** Partial $^{1}H - {}^{1}H$ NOESY spectrum (600 MHz, 298 K, $CD_3CN$) of $[2C_{60}@Pd_4\mathbf{L^2}_6(BDC)_2]^{4+}$.

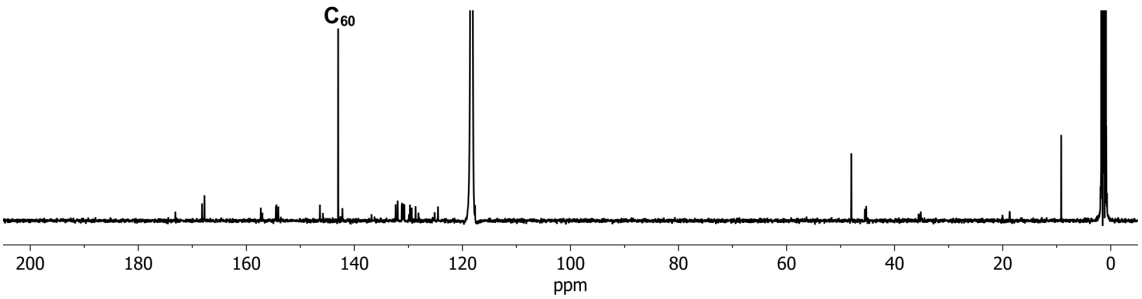


**Figure S61** $^{13}C$ NMR spectrum (151 MHz, 298 K, $CD_3CN$) of $[2C_{60}@Pd_4\mathbf{L^2}_6(BDC)_2]^{4+}$. A single signal at 143.00 ppm corresponds to the encapsulated $C_{60}$.

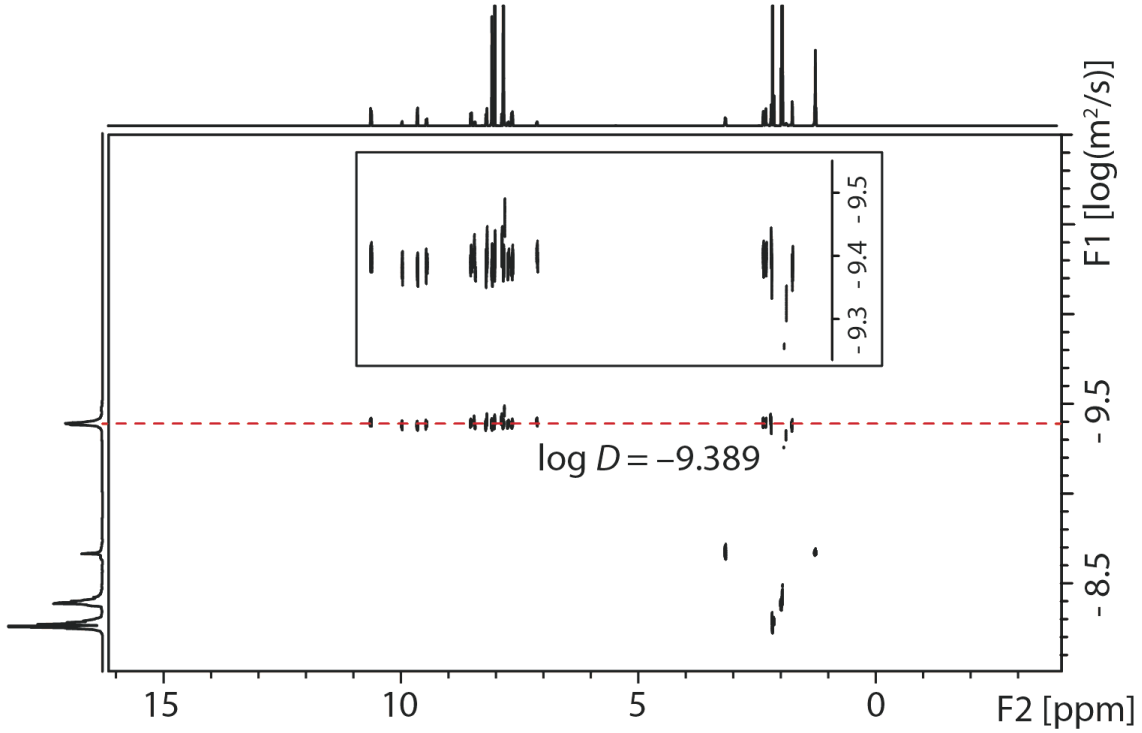


**Figure S62** DOSY spectrum (500 MHz, 298 K, $CD_3CN$) of $[2C_{60}@Pd_4\mathbf{L^2}_6(BDC)_2]^{4+}$: diffusion coefficient = 4.1 x $10^{-10}$ $m^2s^{-1}$, log *D* = −9.39, r = 15.5 Å.

**ESI HRMS** ($C_{376}H_{164}N_{24}O_{32}Pd_4B_4F_{16}$): $[2C_{60}@Pd_4\mathbf{L^2}_6(BDC)_2]^{4+}$ calcd. for $C_{376}H_{164}N_{24}O_{32}Pd_4$ 1488.7056; found 1488.7194; $[2C_{60}@Pd_4\mathbf{L^2}_6(BDC)_2{+}BF_4]^{3+}$ calcd. for $C_{376}H_{164}N_{24}O_{32}Pd_4BF_4$ 2013.9422; found 2013.9602.

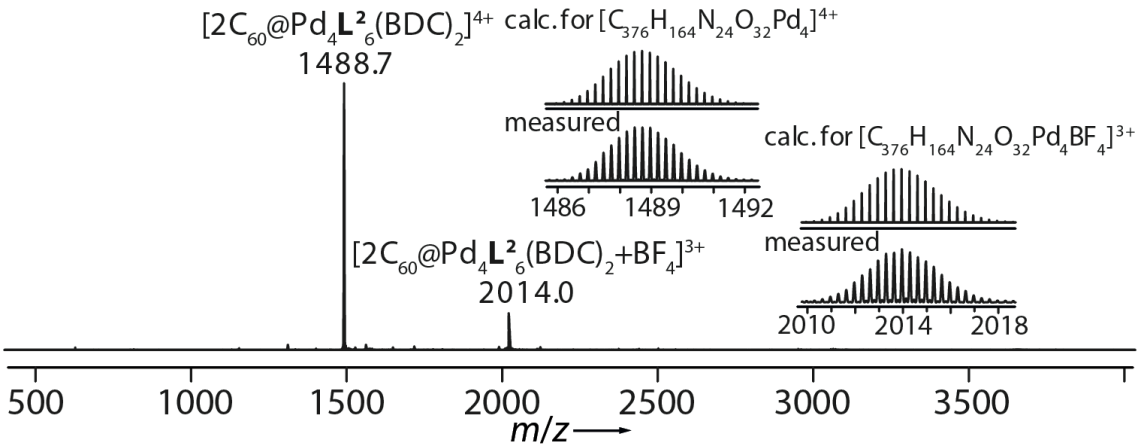


**Figure S63** ESI mass spectrum of $[2C_{60}@Pd_4\mathbf{L^2}_6(BDC)_2]^{4+}$.

## 3.13 Formation and characterization of dimer $[2C_{70}@Pd_4\mathbf{L^2}_6(BDC)_2]^{4+}$

The $CD_3CN$ solution $[2C_{70}@Pd_4\mathbf{L^2}_6(BDC)_2]^{4+}$ (0.31 mM) was formed by stirring a mixture of the $CD_3CN$ solution of $[C_{70}@Pd_2\mathbf{L^2}_3(MeCN)_2]^{4+}$ (500 µL, 0.64 mM, 0.32 µmol, 1 eq.) and $CD_3CN$ solution of $(Et_3NH)_2BDC$ (21.3 µL, 15 mM, 0.32 µmol, 1 eq.) at room temperature for 2 min.

**$^1$H NMR** (600 MHz, 298 K, $CD_3CN$): $\delta$ (ppm) = 10.11 (d, *J* = 9.1 Hz, 8H), 9.86 (dd, *J* = 5.5, 1.4 Hz, 4H), 9.58 (dd, *J* = 5.4, 1.4 Hz, 8H), 8.98 (d, *J* = 9.1 Hz, 4H), 8.49 (dd, *J* = 8.1, 1.2 Hz, 8H), 8.46 (d, *J* = 8.3 Hz, 4H), 8.06 (s, 16H), 8.03 (d, *J* = 2.3 Hz, 8H), 7.91 – 7.89 (m, 12H), 7.84 (dd, *J* = 9.1, 2.3 Hz, 8H), 7.70 – 7.67 (m, 12H), 7.60 (dd, *J* = 8.3, 5.5 Hz, 8H), 6.90 (dd, *J* = 9.1, 2.3 Hz, 4H), 2.40 (s, 12H), 2.34 (s, 12H), 2.22 (s, 12H), 1.75 (s, 8H).

Overlapping signals in the aliphatic region could be assigned via 2D NMR spectroscopy.

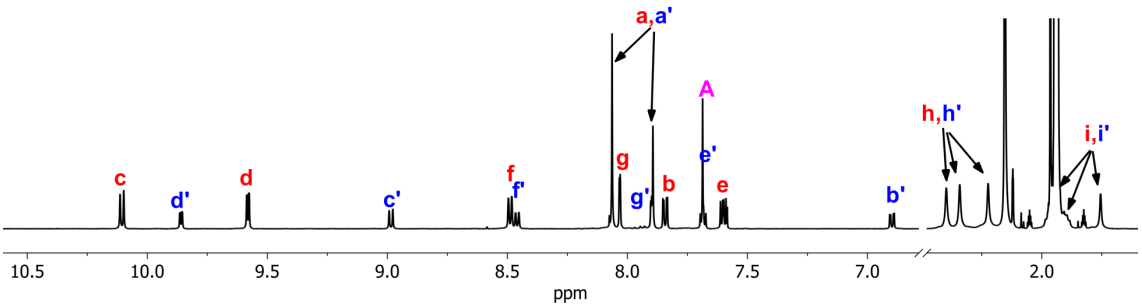


**Figure S64** $^1$H NMR spectrum (600 MHz, 298 K, $CD_3CN$) of $[2C_{70}@Pd_4\mathbf{L^2}_6(BDC)_2]^{4+}$.

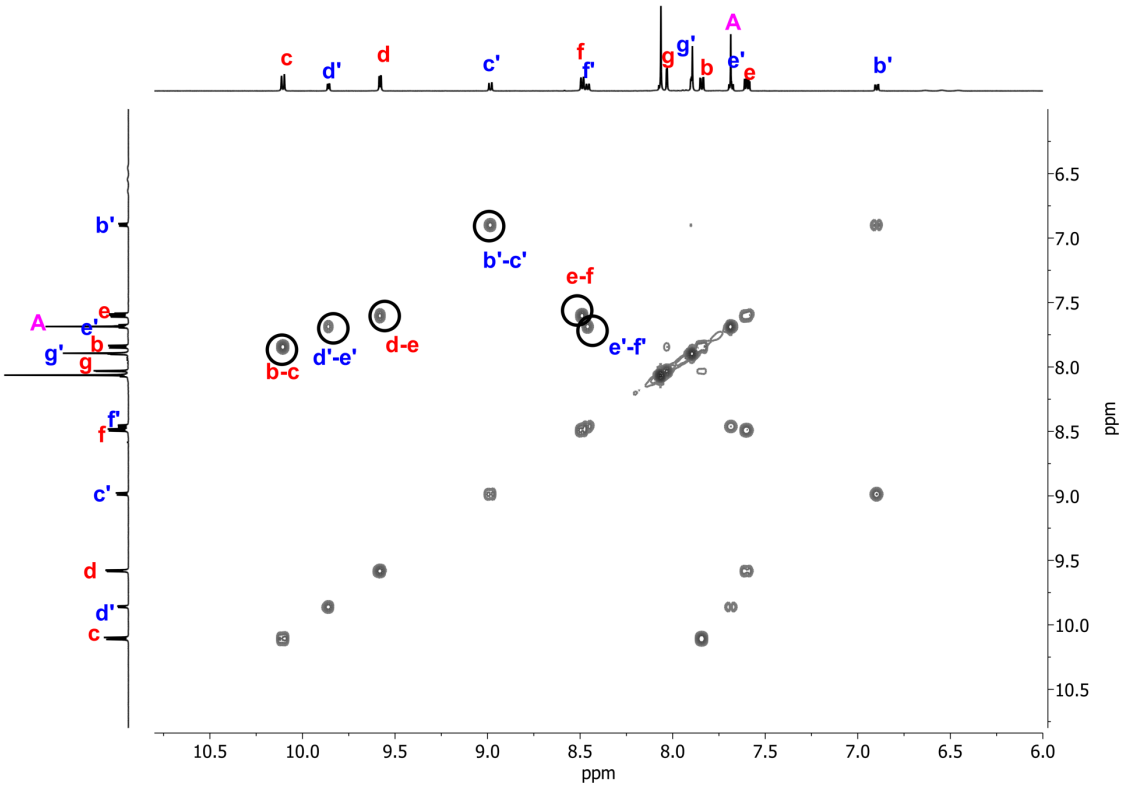


**Figure S65** Partial $^{1}H - {}^{1}H$ COSY spectrum (600 MHz, 298 K, $CD_3CN$) of $[2C_{70}@Pd_4\mathbf{L^2}_6(BDC)_2]^{4+}$.

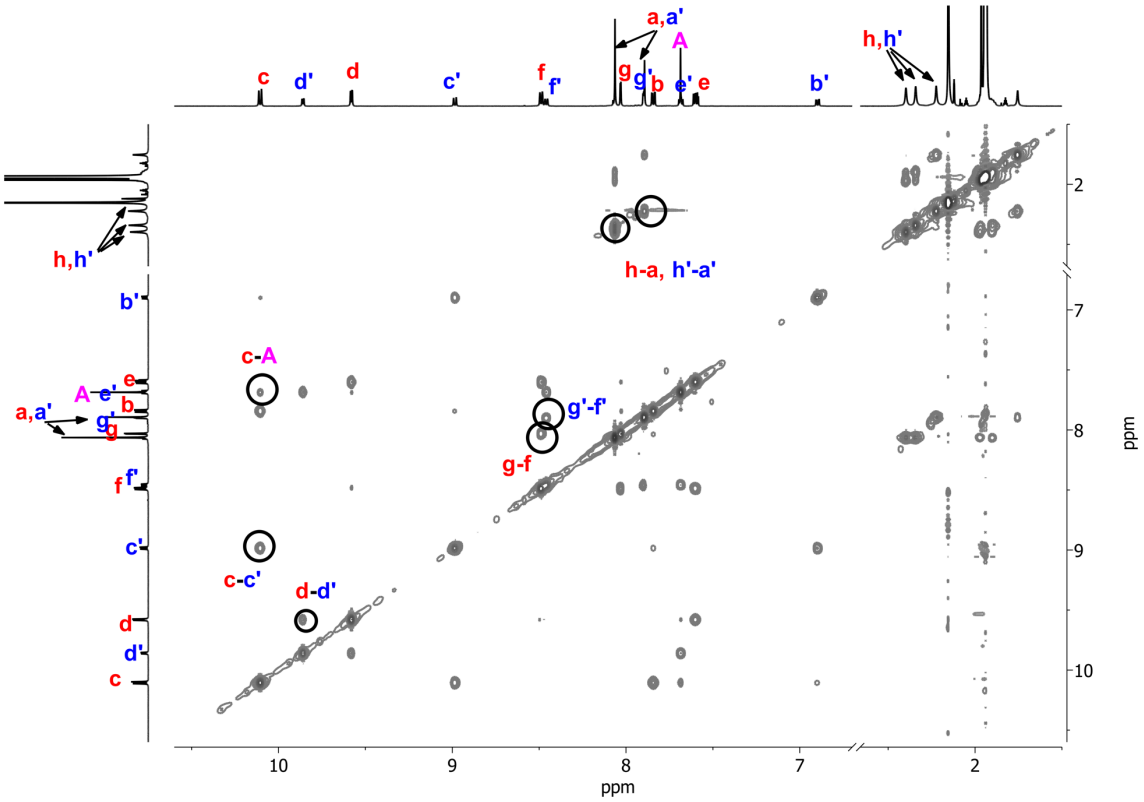


**Figure S66** Partial $^{1}H - {}^{1}H$ NOESY spectrum (600 MHz, 298 K, $CD_3CN$) of $[2C_{70}@Pd_4\mathbf{L^2}_6(BDC)_2]^{4+}$.

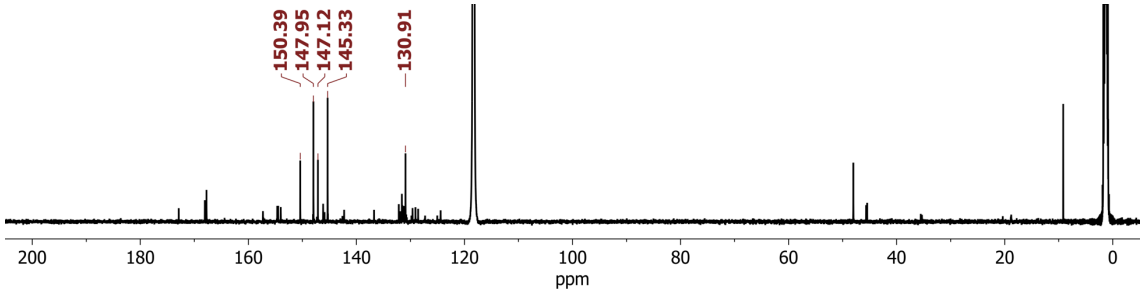


**Figure S67** $^{13}C$ NMR spectrum (151 MHz, 298 K, $CD_3CN$) of $[2C_{70}@Pd_4\mathbf{L^2}_6(BDC)_2]^{4+}$. Five single signals at 150.39, 147.95, 147.12, 145.33, 130.91 ppm correspond to the encapsulated $C_{70}$.

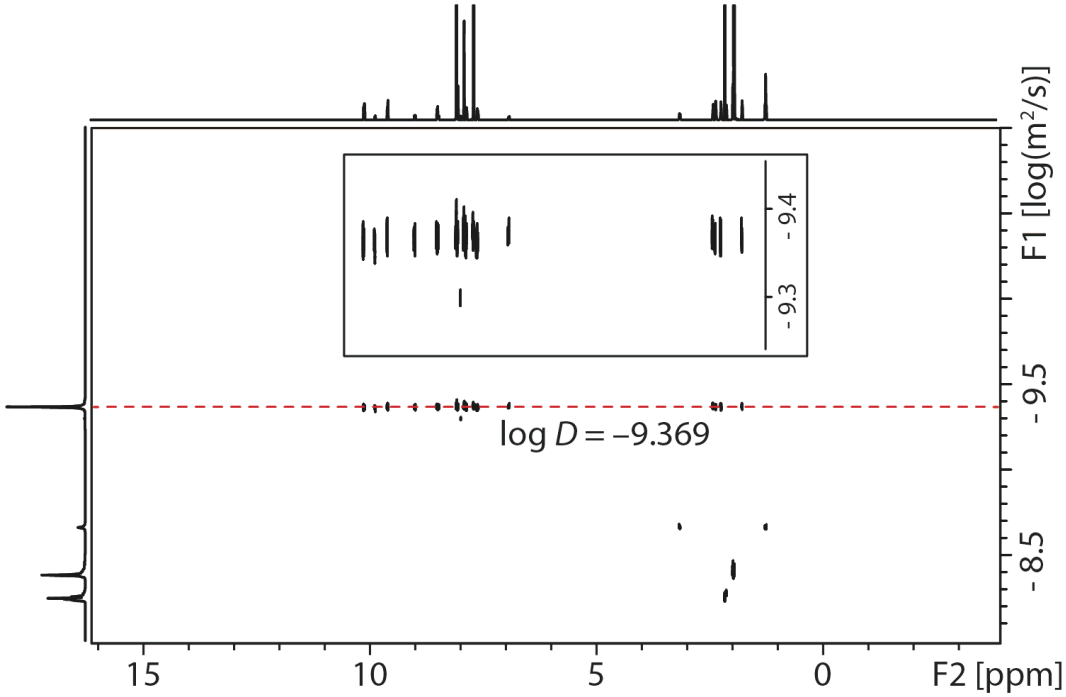


**Figure S68** DOSY spectrum (500 MHz, 298 K, $CD_3CN$) of $[2C_{70}@Pd_4\mathbf{L^2}_6(BDC)_2]^{4+}$: diffusion coefficient = 4.3 x $10^{-10}$ $m^2s^{-1}$, log *D* = –9.37, r = 14.8 Å.

**ESI HRMS** ($C_{396}H_{164}N_{24}O_{32}Pd_4B_4F_{16}$): $[2C_{70}@Pd_4\mathbf{L^2}_6(BDC)_2]^{4+}$ calcd. for $C_{396}H_{164}N_{24}O_{32}Pd_4$ 1548.4563; found 1548.4679; $[2C_{70}@Pd_4\mathbf{L^2}_6(BDC)_2{+}BF_4]^{3+}$ calcd. for $C_{396}H_{164}N_{24}O_{32}Pd_4BF_4$ 2093.9424; found 2093.9582.

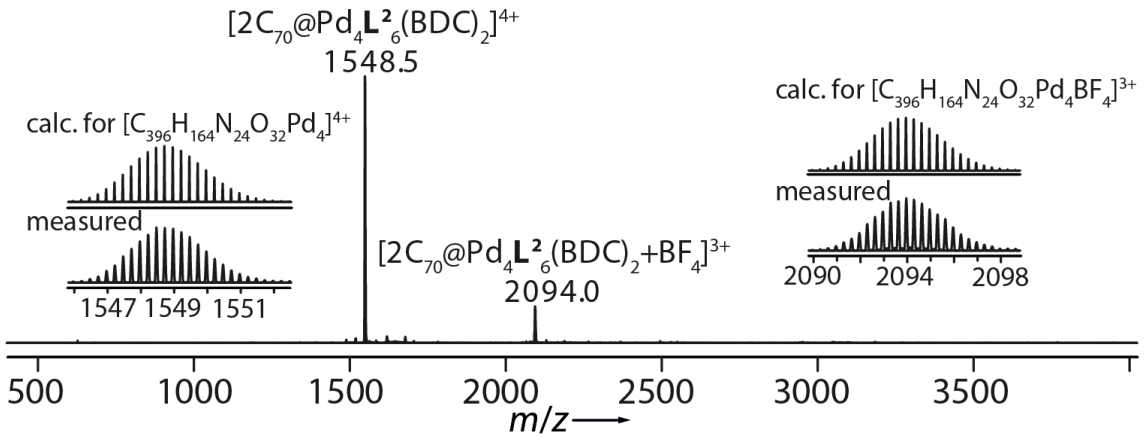


**Figure S69** ESI mass spectrum of $[2C_{70}@Pd_4\mathbf{L^2}_6(BDC)_2]^{4+}$.

# 4 Fullerene binding studies

**General procedure:** To a $CD_3CN$ solution of the host compounds (0.64 mM for $[Pd_2\mathbf{L^1}_4]^{4+}$ and $[Pd_2\mathbf{L^2}_3(MeCN)_2]^{4+}$, 0.56 mM for $[Pd_2\mathbf{L^2}_3Cl_2]^{2+}$) in a sealed vessel, excess fullerene ($C_{60}$ or $C_{70}$) was added as finely grounded powder. The mixtures were sonicated for 3 minutes, then stirred at room temperature or left standing at 70 °C for several days. Upon cooling, the supernatant was collected and transferred to NMR tubes.

## 4.1 Fullerene binding experiment with cage $[Pd_2L^1_4]^{4+}$

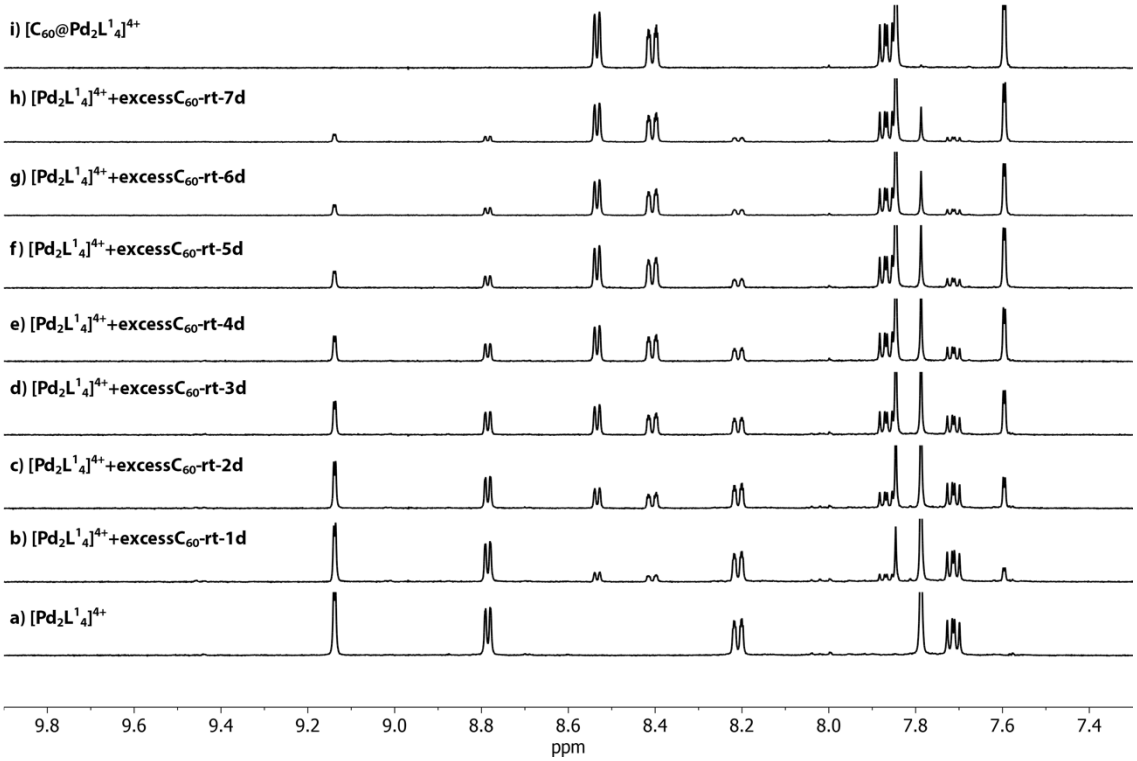


**Figure S70** $^1H$ NMR spectra (500 MHz, 298 K, $CD_3CN$) following the encapsulation of $C_{60}$ in $[Pd_2\mathbf{L^1}_4]^{4+}$ at room temperature.

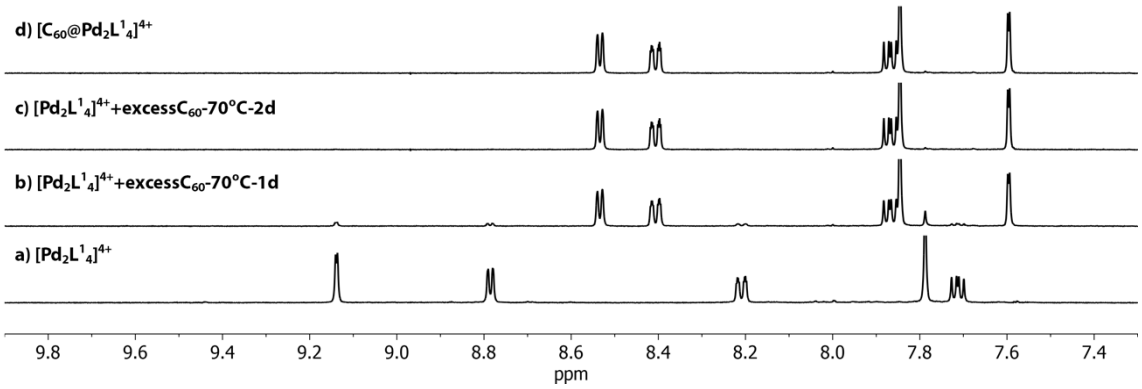


**Figure S71** $^1H$ NMR spectra (500 MHz, 298 K, $CD_3CN$) following the encapsulation of $C_{60}$ in $[Pd_2\mathbf{L^1}_4]^{4+}$ at 70 °C, indicating a faster process compared with the encapsulation performed at room temperature.

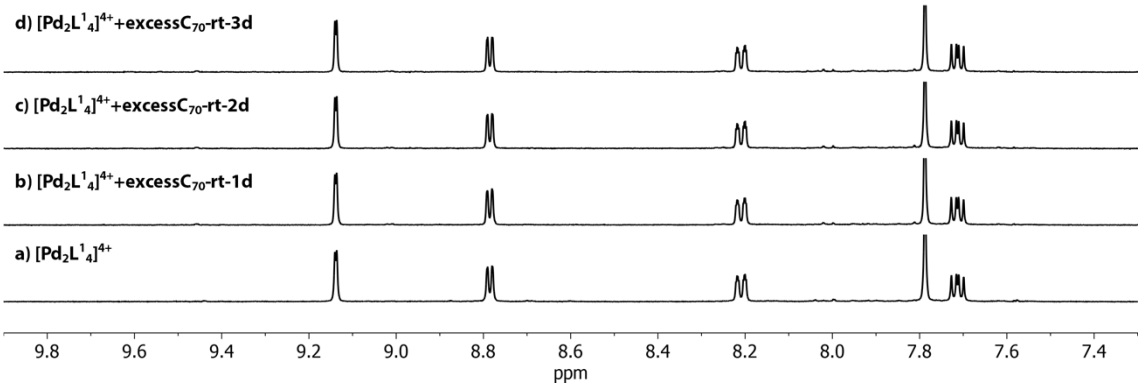


**Figure S72** $^1$H NMR spectra (500 MHz, 298 K, $CD_3CN$) monitoring the test of binding $C_{70}$ in $[Pd_2\mathbf{L^1}_4]^{4+}$ at room temperature, indicating that $C_{70}$ cannot be encapsulated in $[Pd_2\mathbf{L^1}_4]^{4+}$ at room temperature.

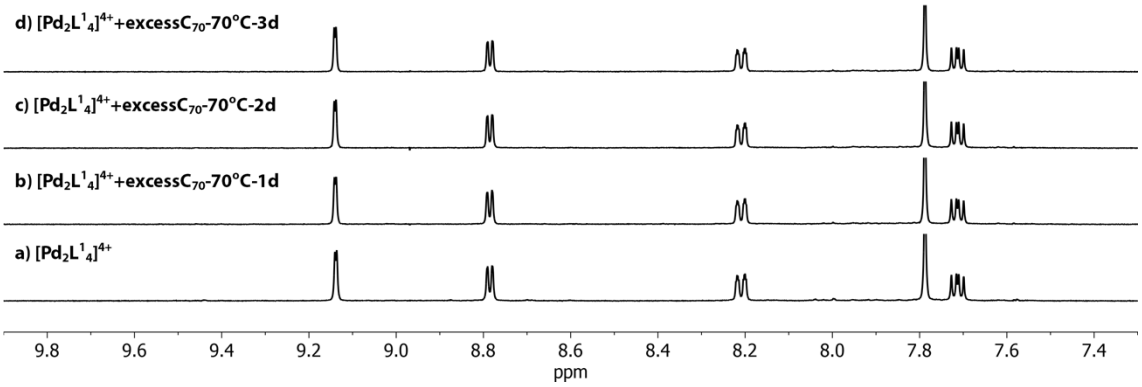


**Figure S73** $^1$H NMR spectra (500 MHz, 298 K, $CD_3CN$) monitoring the test of binding $C_{70}$ in $[Pd_2\mathbf{L^1}_4]^{4+}$ at 70 °C, indicating that $C_{70}$ cannot be encapsulated in $[Pd_2\mathbf{L^1}_4]^{4+}$.

## 4.2 Fullerene binding experiment with bowl $[Pd_2L^2_3(MeCN)_2]^{4+}$

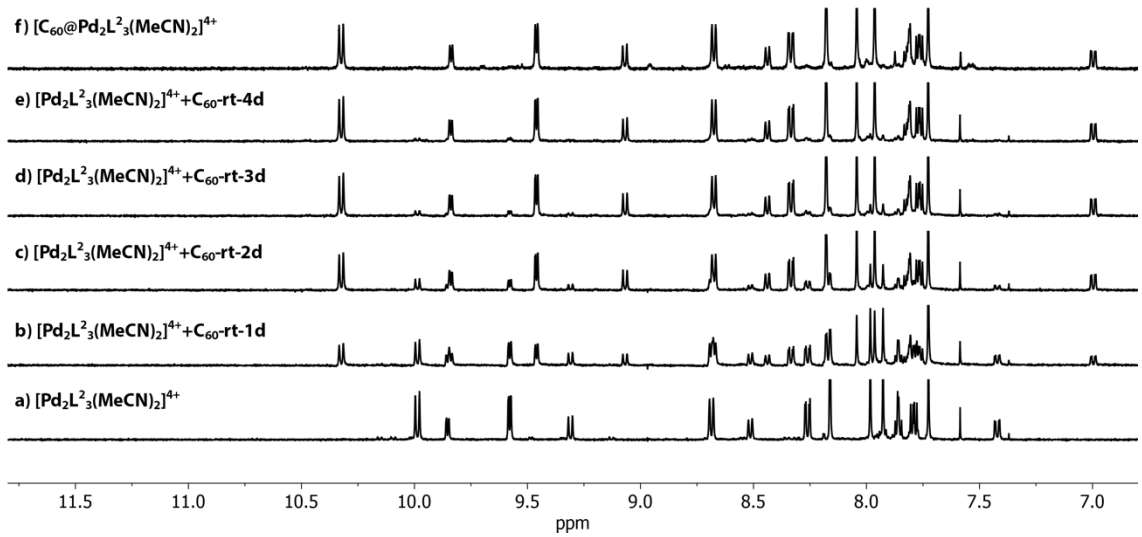


**Figure S74** $^1$H NMR spectra (500 MHz, 298 K, $CD_3CN$) following the encapsulation of $C_{60}$ in $[Pd_2\mathbf{L^2}_3(MeCN)_2]^{4+}$ at room temperature.

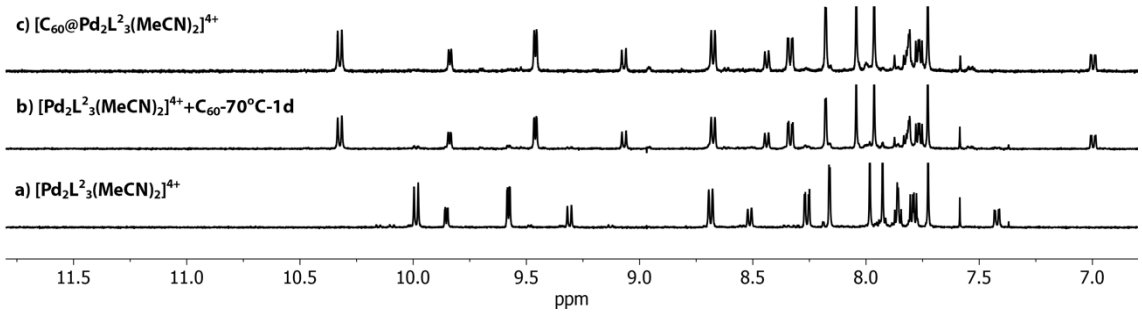


**Figure S75** $^1$H NMR spectra (500 MHz, 298 K, $CD_3CN$) following the encapsulation of $C_{60}$ in $[Pd_2\mathbf{L^2}_3(MeCN)_2]^{4+}$ at 70 °C, indicating a faster process compared with the encapsulation performed at room temperature.

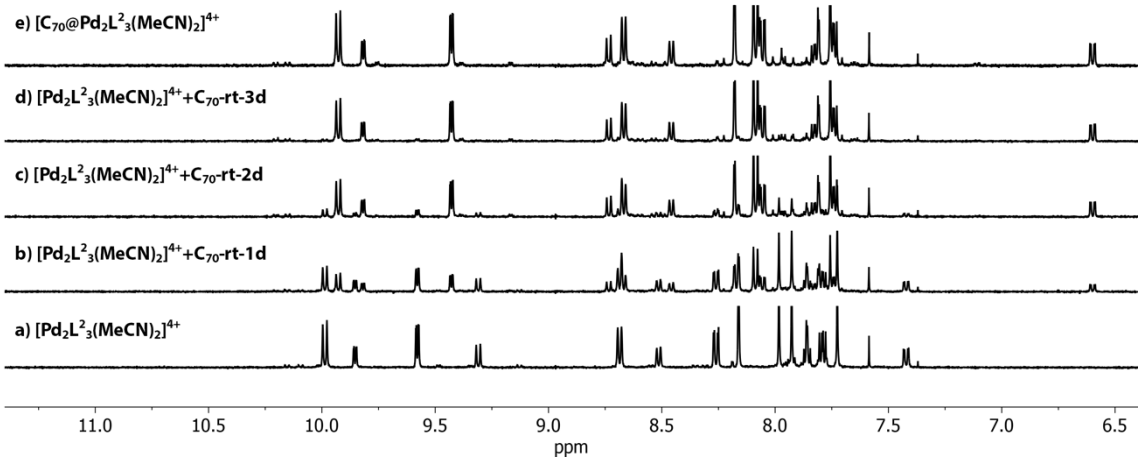


**Figure S76** $^1$H NMR spectra (500 MHz, 298 K, $CD_3CN$) following the encapsulation of $C_{70}$ in $[Pd_2\mathbf{L^2}_3(MeCN)_2]^{4+}$ at room temperature.

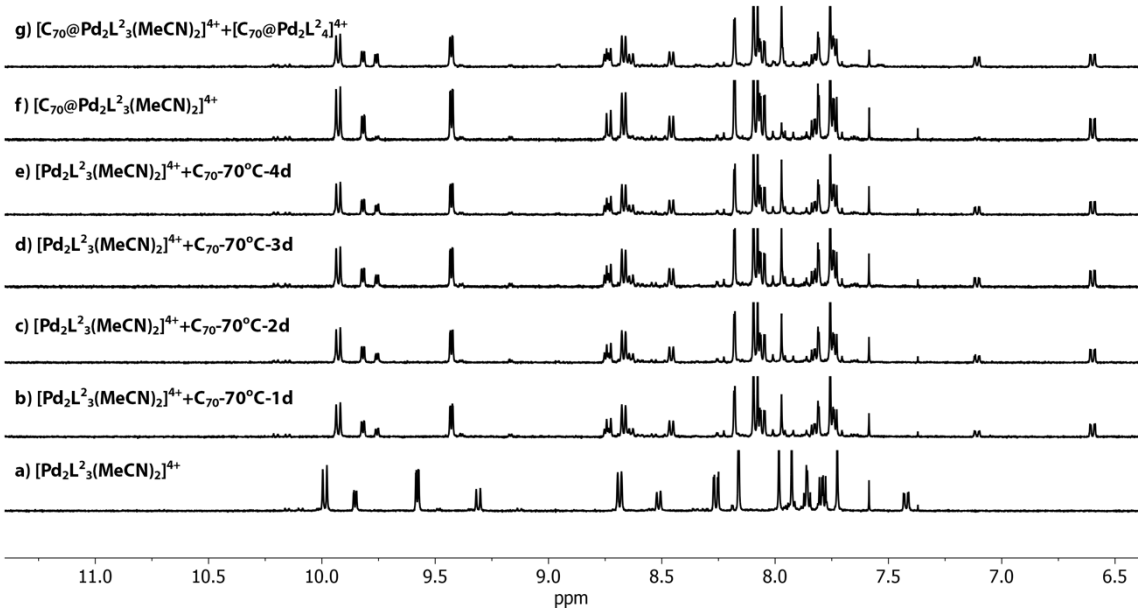


**Figure S77** $^1$H NMR spectra (500 MHz, 298 K, $CD_3CN$) following the reaction between $C_{70}$ and $[Pd_2\mathbf{L^2}_3(MeCN)_2]^{4+}$ at 70 °C, indicating the formation of the mixture of $[C_{70}@Pd_2\mathbf{L^2}_3(MeCN)_2]^{4+}$ and $[C_{70}@Pd_2\mathbf{L^2}_4]^{4+}$.

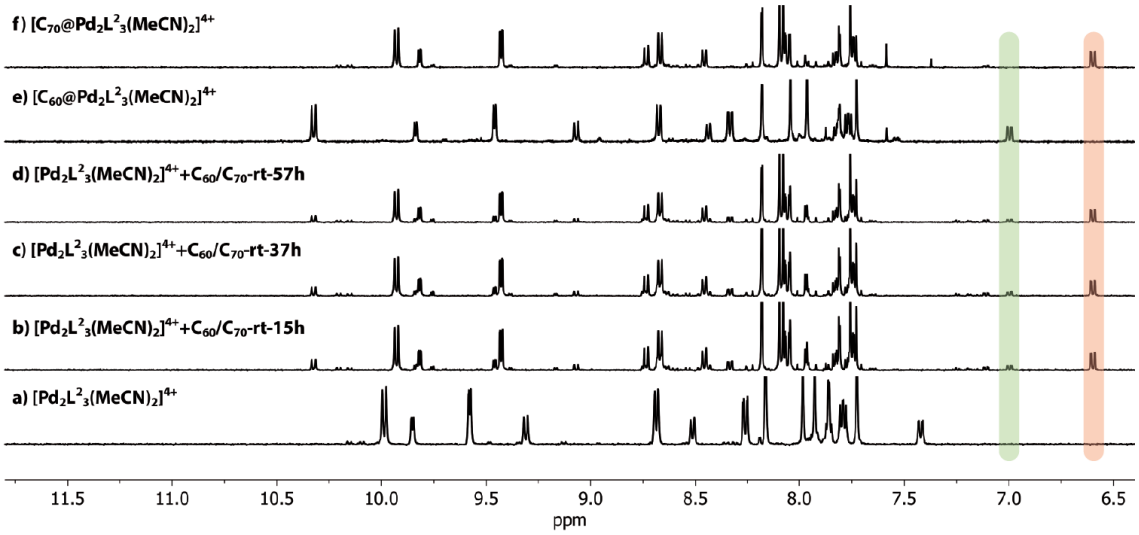


**Figure S78** $^1$H NMR spectra (500 MHz, 298 K, $CD_3CN$) following the competitive reaction between $[Pd_2\mathbf{L^2}_3(MeCN)_2]^{4+}$ (1eq.) and a powdered mixture of $C_{60}$ (5eq.) and $C_{70}$ (5eq.) at room temperature. The bowl exhibits preferred binding towards $C_{70}$ at room temperature (final ratio of $[C_{60}@Pd_2\mathbf{L^2}_3(MeCN)_2]^{4+}$ to $[C_{70}@Pd_2\mathbf{L^2}_3(MeCN)_2]^{4+} \approx 1 : 4$. The quinoline proton b' of $[C_{60}@Pd_2\mathbf{L^2}_3(MeCN)_2]^{4+}$ and proton b' of $[C_{70}@Pd_2\mathbf{L^2}_3(MeCN)_2]^{4+}$ are highlighted in green and red, respectively.

## 4.3 Fullerene binding experiment with bowl $[Pd_2L^2_3Cl_2]^{2+}$

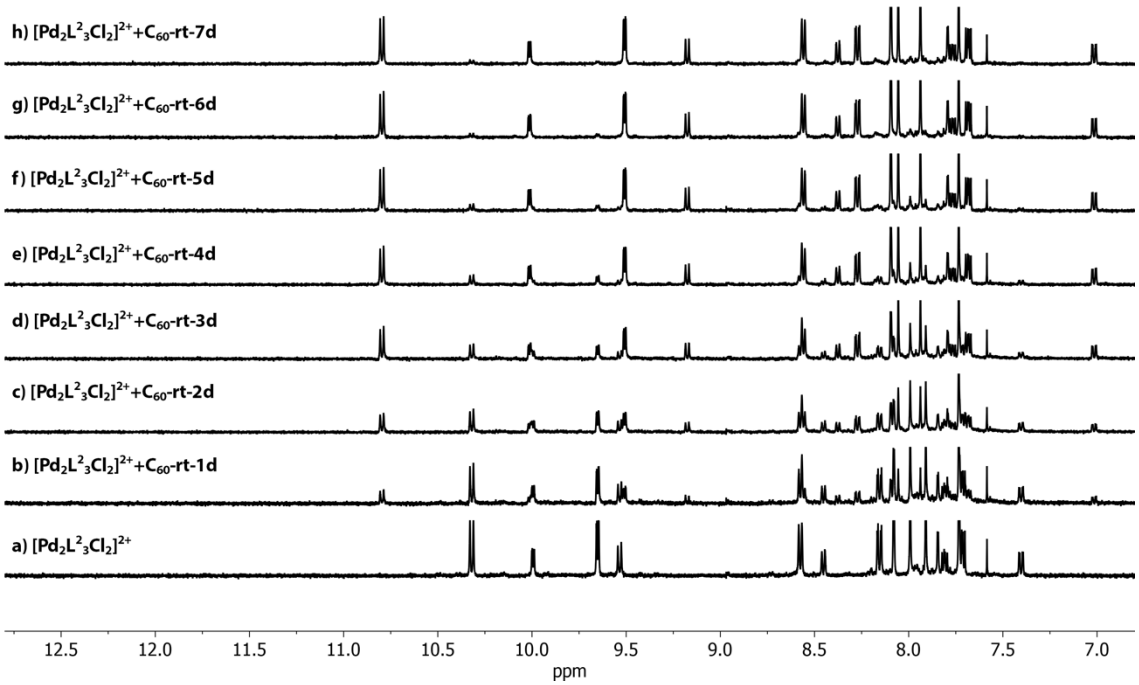


**Figure S79** $^1$H NMR spectra (500 MHz, 298 K, $CD_3CN$) following the encapsulation of $C_{60}$ in $[Pd_2\mathbf{L^2}_3Cl_2]^{2+}$ at room temperature.

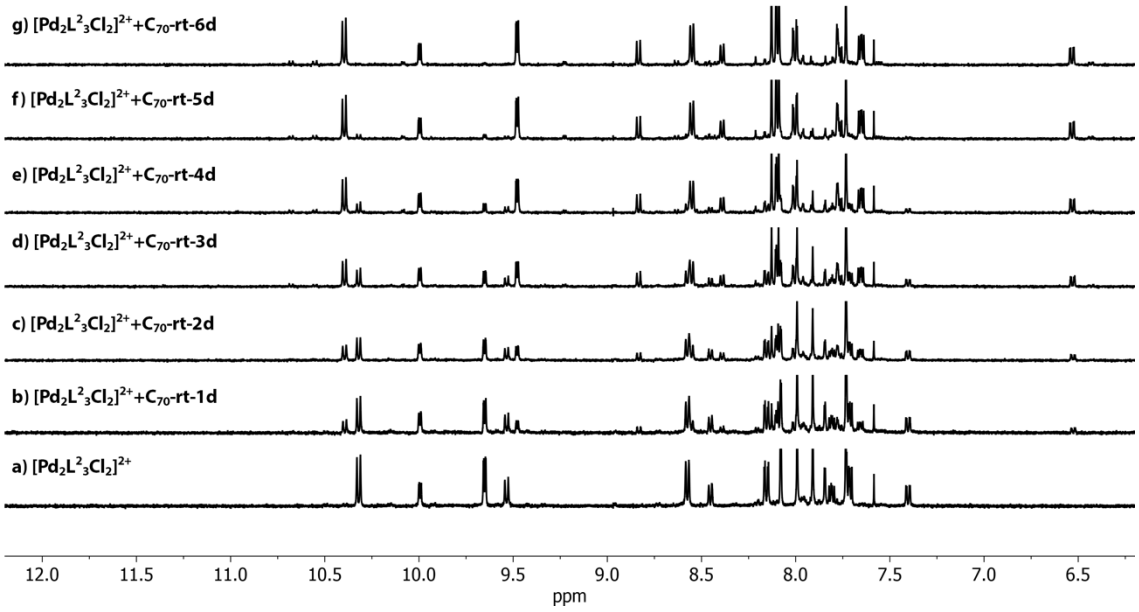


**Figure S80** $^1$H NMR spectra (500 MHz, 298 K, $CD_3CN$) following the encapsulation of $C_{70}$ in $[Pd_2\mathbf{L^2}_3Cl_2]^{2+}$ at room temperature.

# 5 Solvent studies with $[Pd_2\mathbf{L^1}_4]^{4+}$ and $[C_{60}@Pd_2\mathbf{L^1}_4]^{4+}$

In order to investigate solubility and stability of $[Pd_2\mathbf{L^1}_4]^{4+}$ and $[C_{60}@Pd_2\mathbf{L^1}_4]^{4+}$ in a wider range of organic solvents, the $CD_3CN$ solution of cage compounds $[Pd_2\mathbf{L^1}_4]^{4+}$ and $[C_{60}@Pd_2\mathbf{L^1}_4]^{4+}$ (0.64 mM, 300 µL) was evaporated, followed by adding different deuterated solvents (600 µL). NMR spectra were recorded after 1 h and 24 h.

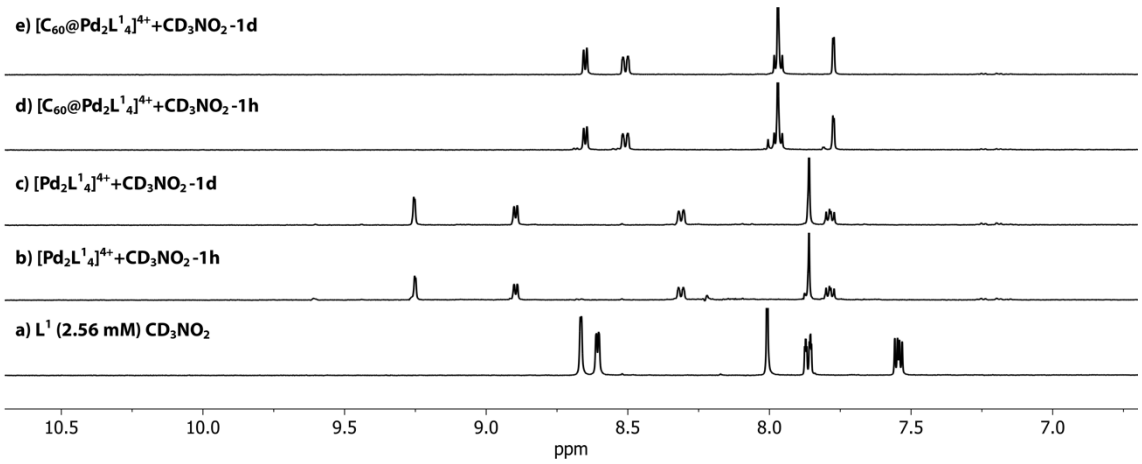


**Figure S81** $^1$H NMR spectra (500 MHz, 298 K, $CD_3NO_2$) of $\mathbf{L^1}$, re-dissolved $[Pd_2\mathbf{L^1}_4]^{4+}$ and re-dissolved $[C_{60}@Pd_2\mathbf{L^1}_4]^{4+}$ in $CD_3NO_2$ for 1 h or 1 d at room temperature, indicating good solubility and stability of $[Pd_2\mathbf{L^1}_4]^{4+}$ and $[C_{60}@Pd_2\mathbf{L^1}_4]^{4+}$ in $CD_3NO_2$.

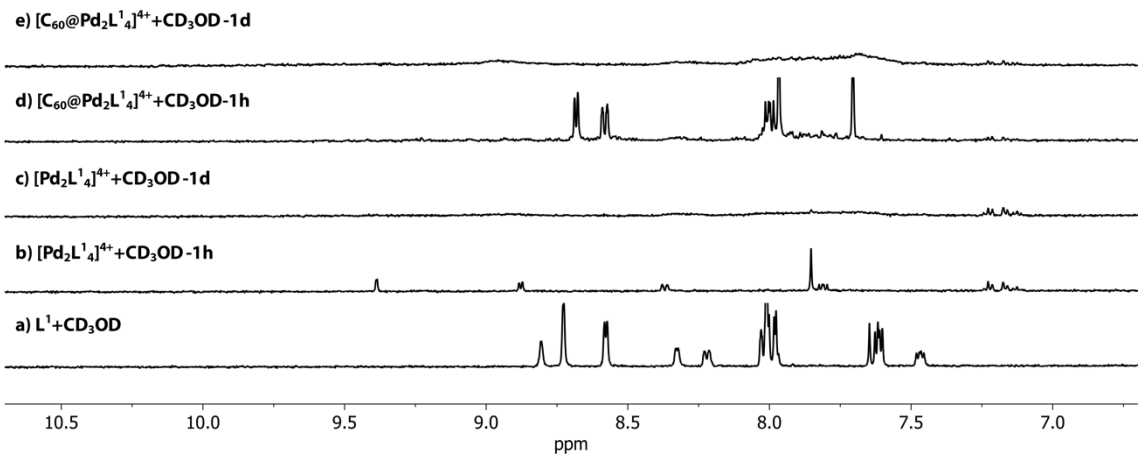


**Figure S82** $^1$H NMR spectra (500 MHz, 298 K, $CD_3OD$) of **L$^1$**, re-dissolved $[Pd_2\mathbf{L^1}_4]^{4+}$ and re-dissolved $[C_{60}@Pd_2\mathbf{L^1}_4]^{4+}$ in $CD_3OD$ for 1 h or 1 d at room temperature, indicating decomposition and limited solubility of **L$^1$**, $[Pd_2\mathbf{L^1}_4]^{4+}$ and $[C_{60}@Pd_2\mathbf{L^1}_4]^{4+}$ in $CD_3OD$.

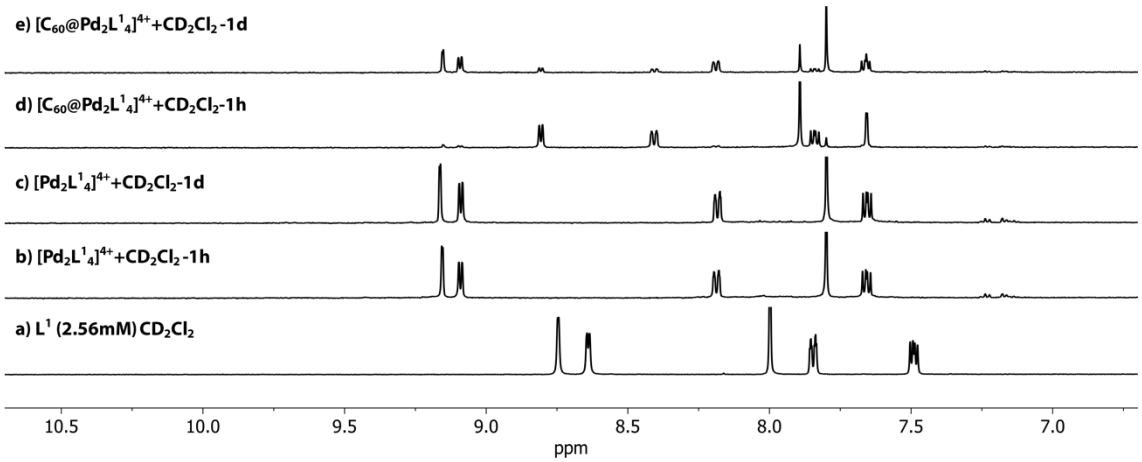


**Figure S83** $^1$H NMR spectra (500 MHz, 298 K, $CD_2Cl_2$) of **L$^1$**, re-dissolved $[Pd_2\mathbf{L^1}_4]^{4+}$ and re-dissolved $[C_{60}@Pd_2\mathbf{L^1}_4]^{4+}$ in $CD_2Cl_2$ for 1 h or 1 d at room temperature, indicating good solubility and stability of $[Pd_2\mathbf{L^1}_4]^{4+}$ in $CD_2Cl_2$, but conversion of $[C_{60}@Pd_2\mathbf{L^1}_4]^{4+}$ into $[Pd_2\mathbf{L^1}_4]^{4+}$ under ejection of $C_{60}$ in $CD_2Cl_2$.

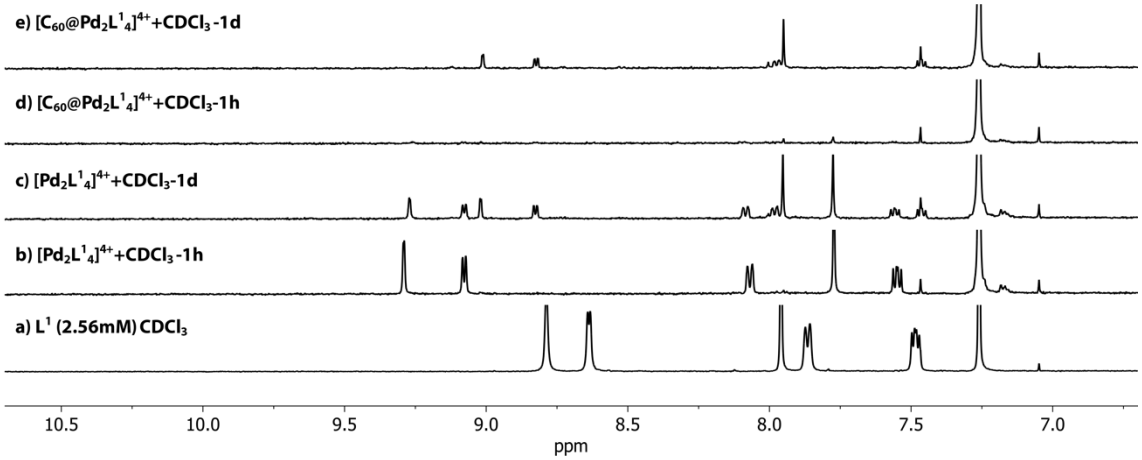


**Figure S84** $^1$H NMR spectra (500 MHz, 298 K, $CDCl_3$) of **L$^1$**, re-dissolved $[Pd_2\mathbf{L^1}_4]^{4+}$ and re-dissolved $[C_{60}@Pd_2\mathbf{L^1}_4]^{4+}$ in $CDCl_3$ for 1 h or 1 d at room temperature, indicating decomposition of $[Pd_2\mathbf{L^1}_4]^{4+}$ and $[C_{60}@Pd_2\mathbf{L^1}_4]^{4+}$ in $CDCl_3$.

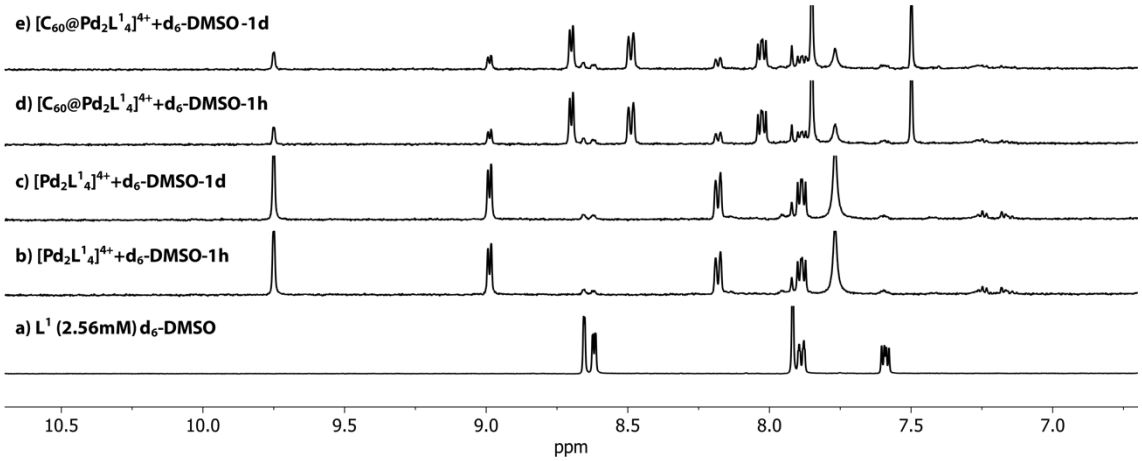


**Figure S85** $^1$H NMR spectra (500 MHz, 298 K, $d_6$-DMSO) of **L¹**, re-dissolved $[Pd_2\mathbf{L^1}_4]^{4+}$ and re-dissolved $[C_{60}@Pd_2\mathbf{L^1}_4]^{4+}$ in $d_6$-DMSO for 1 h or 1 d at room temperature, indicating good solubility and stability of $[Pd_2\mathbf{L^1}_4]^{4+}$ but partial conversion of $[C_{60}@Pd_2\mathbf{L^1}_4]^{4+}$ into $[Pd_2\mathbf{L^1}_4]^{4+}$ in $d_6$-DMSO.

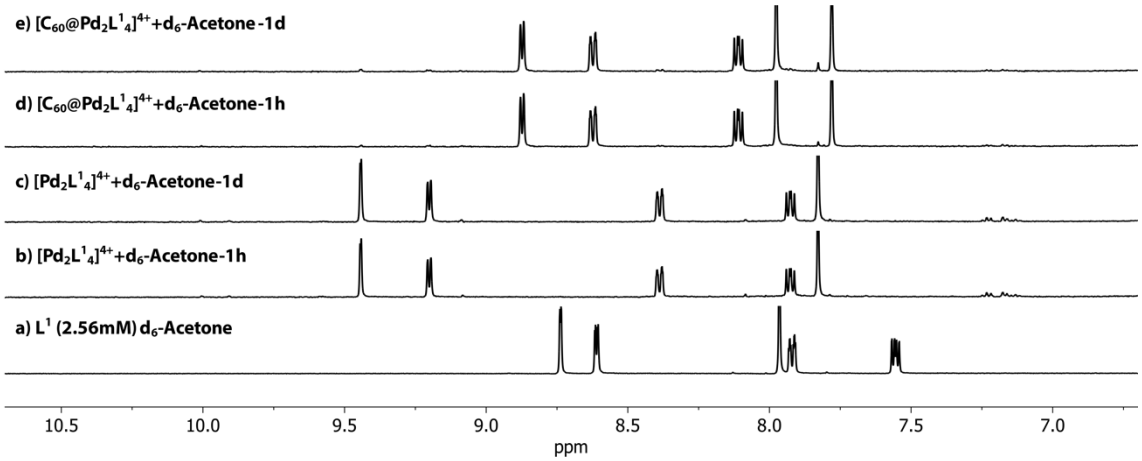


**Figure S86** $^1$H NMR spectra (500 MHz, 298 K, $d_6$-Acetone) of **L¹**, re-dissolved $[Pd_2\mathbf{L^1}_4]^{4+}$ and re-dissolved $[C_{60}@Pd_2\mathbf{L^1}_4]^{4+}$ in $d_6$-Acetone for 1 h or 1 d at room temperature, indicating good solubility and stability of $[Pd_2\mathbf{L^1}_4]^{4+}$ and $[C_{60}@Pd_2\mathbf{L^1}_4]^{4+}$ in $d_6$-Acetone.

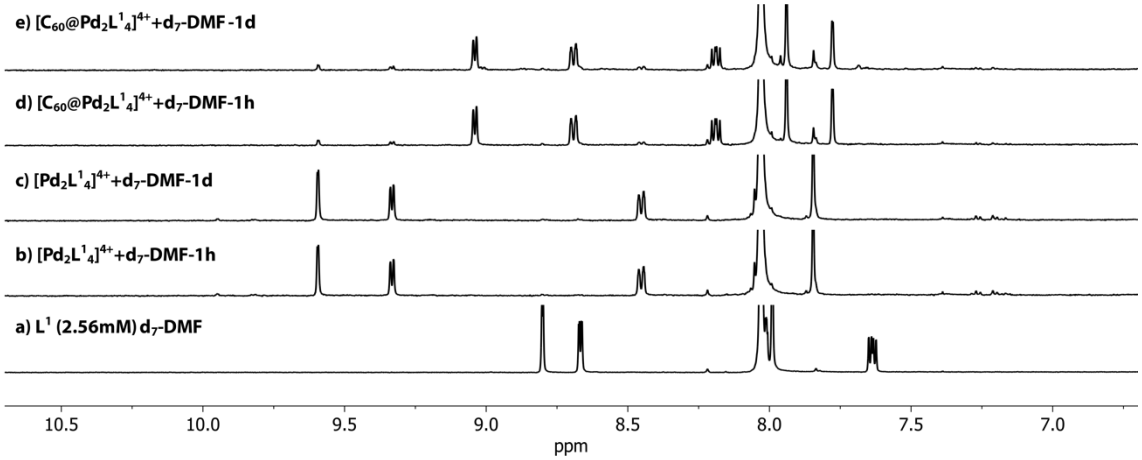


**Figure S87** $^1$H NMR spectra (500 MHz, 298 K, $d_7$-DMF) of **L¹**, re-dissolved $[Pd_2\mathbf{L^1}_4]^{4+}$ and re-dissolved $[C_{60}@Pd_2\mathbf{L^1}_4]^{4+}$ in $d_7$-DMF for 1 h or 1 d at room temperature, indicating good solubility and stability of $[Pd_2\mathbf{L^1}_4]^{4+}$ and $[C_{60}@Pd_2\mathbf{L^1}_4]^{4+}$ in $d_7$-DMF.

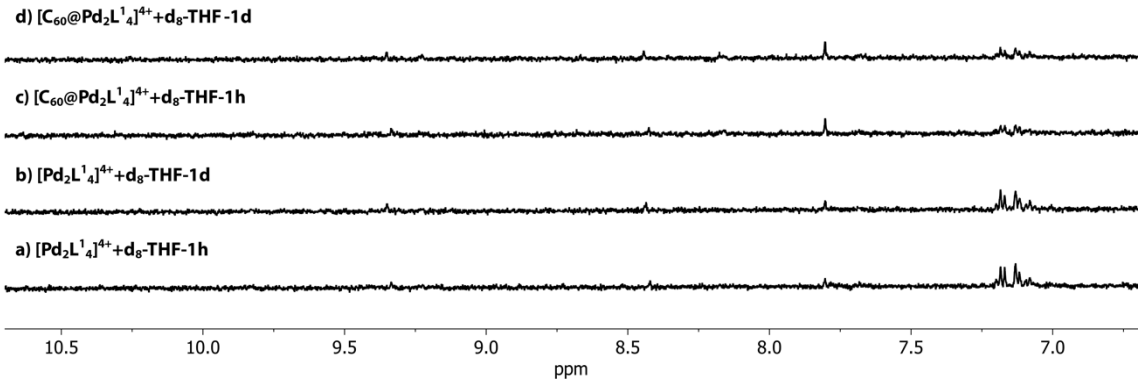


**Figure S88** $^1$H NMR spectra (500 MHz, 298 K, $d_8$-THF) of re-dissolved $[Pd_2\mathbf{L^1}_4]^{4+}$ and re-dissolved $[C_{60}@Pd_2\mathbf{L^1}_4]^{4+}$ in $d_8$-THF for 1 h or 1 d at room temperature, indicating insolubility of $[Pd_2\mathbf{L^1}_4]^{4+}$ and $[C_{60}@Pd_2\mathbf{L^1}_4]^{4+}$ in $d_8$-THF.

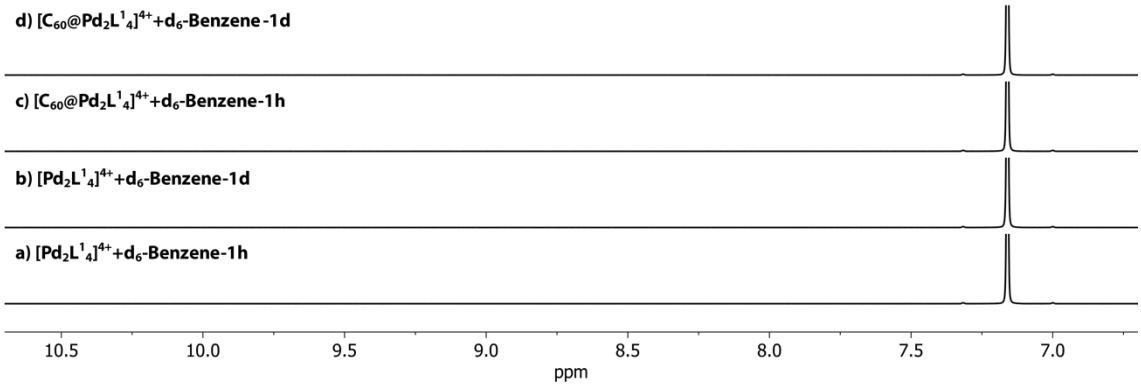


**Figure S89** $^1$H NMR spectra (500 MHz, 298 K, $d_6$-Benzene) of re-dissolved $[Pd_2\mathbf{L^1}_4]^{4+}$ and re-dissolved $[C_{60}@Pd_2\mathbf{L^1}_4]^{4+}$ in $d_6$-Benzene for 1 h or 1 d at room temperature, indicating insolubility of $[Pd_2\mathbf{L^1}_4]^{4+}$ and $[C_{60}@Pd_2\mathbf{L^1}_4]^{4+}$ in $d_6$-Benzene.

# 6 Diels-Alder reaction with bowl-protected $C_{60}$

## 6.1 Formation and characterization of $[C_{60}Ac@Pd_2\mathbf{L^2}_3Cl_2]^{2+}$

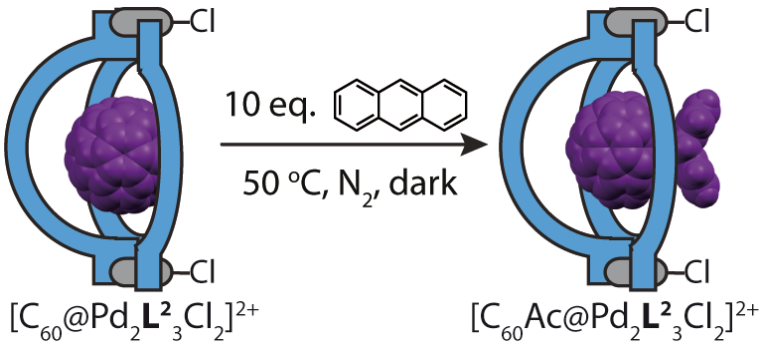


To the $CD_3CN$ solution of $[C_{60}@Pd_2\mathbf{L^2}_3Cl_2]^{2+}$ (500 µL, 0.56 mM, 0.28 µmol, 1 eq.) was added a concentrated $CD_3CN$ solution of anthracene (Ac) (280 µL, 10 mM, 2.80 µmol, 10 eq.) in an NMR tube under nitrogen protection. The NMR tube was wrapped with aluminium foil to avoid light irradiation and then heated at 50 °C in the dark overnight (*ca.* 14 h) to give a yellow solution.

**$^1$H NMR** (500 MHz, 298 K, $CD_3CN$): $\delta$ (ppm) = 10.65 (d, J = 9.2 Hz, 4H), 9.99 (d, J = 5.3 Hz, 2H), 9.49 (d, J = 5.3 Hz, 4H), 9.00 (d, J = 9.2 Hz, 2H), 8.52 (mixed with peaks of unreacted anthracene), 8.37 (d, J = 8.3 Hz, 2H), 8.24 (dd, J = 5.4, 3.3 Hz, 4H), 8.07 (mixed with peaks of unreacted anthracene), 7.95 (s, 4H), 7.89 – 7.77 (m, 14H), 7.73 (m, 6H), 7.67 (dd, J = 8.4, 5.3 Hz, 4H), 7.51 (peaks of unreacted anthracene), 6.95 – 6.83 (m, 2H), 6.28 (s, 2H). Peaks in the aliphatic region overlap with peaks of tetrabutylammonium cation and solvents.

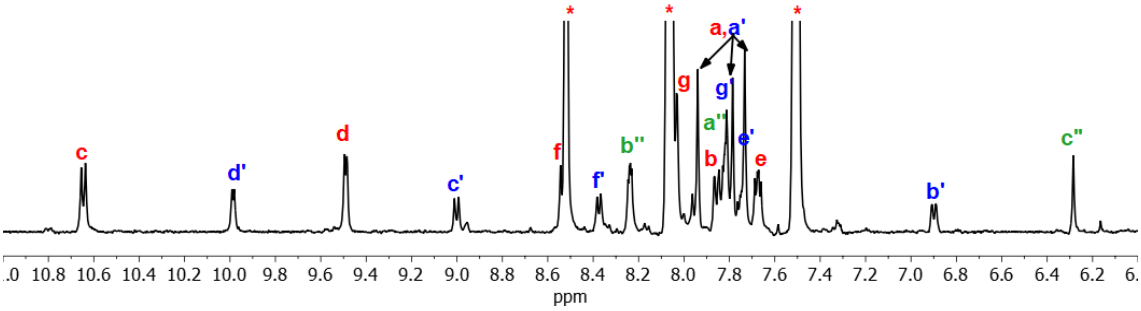


**Figure S90** $^1$H NMR spectrum (500 MHz, 298 K, $CD_3CN$) of $[C_{60}Ac@Pd_2\mathbf{L^2}_3Cl_2]^{2+}$. Relative positons of protons correspond to the case of $[C_{60}@Pd_2\mathbf{L^2}_3(MeCN)_2]^{4+}$. Red stars stand for the proton signals of unreacted anthracene.

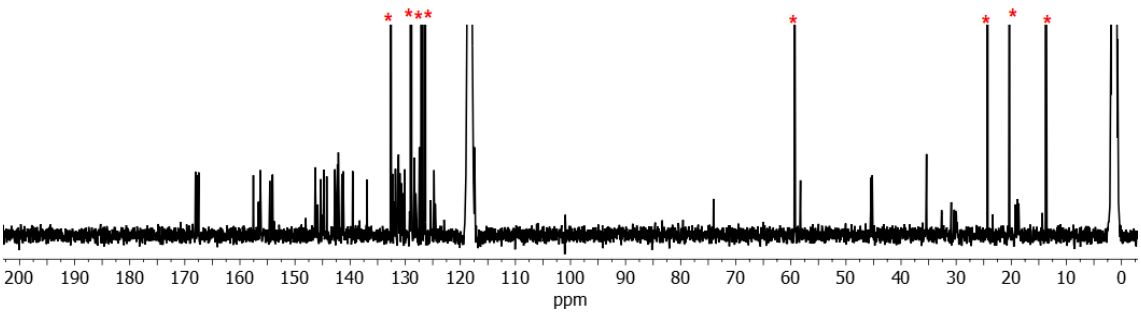


**Figure S91** $^{13}$C NMR spectrum (151 MHz, 298 K, $CD_3CN$) of $[C_{60}Ac@Pd_2\mathbf{L^2}_3Cl_2]^{2+}$. Red stars stand for the carbon signals of unreacted anthracene and tetrabutylammonium ions.

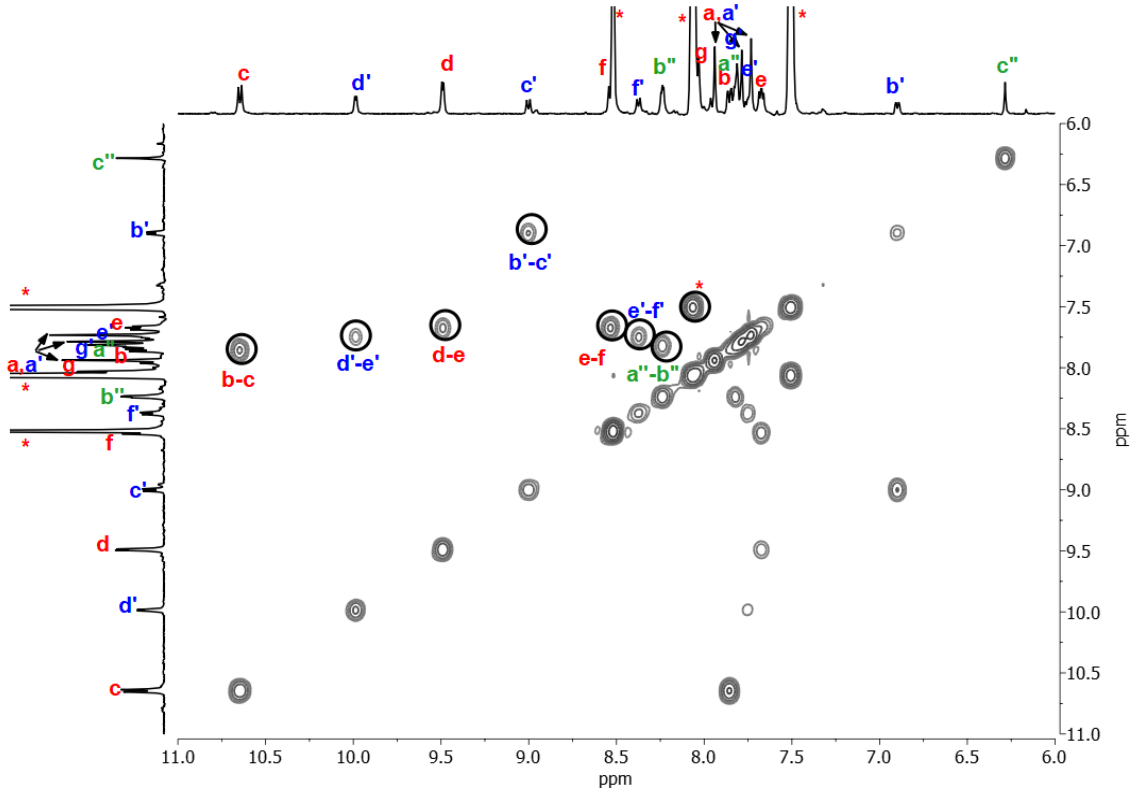


**Figure S92** Partial $^{1}H - {}^{1}H$ COSY spectrum (500 MHz, 298 K, $CD_3CN$) of $[C_{60}Ac@Pd_2\mathbf{L^2}_3Cl_2]^{2+}$. Red stars stand for the proton signals of unreacted anthracene.

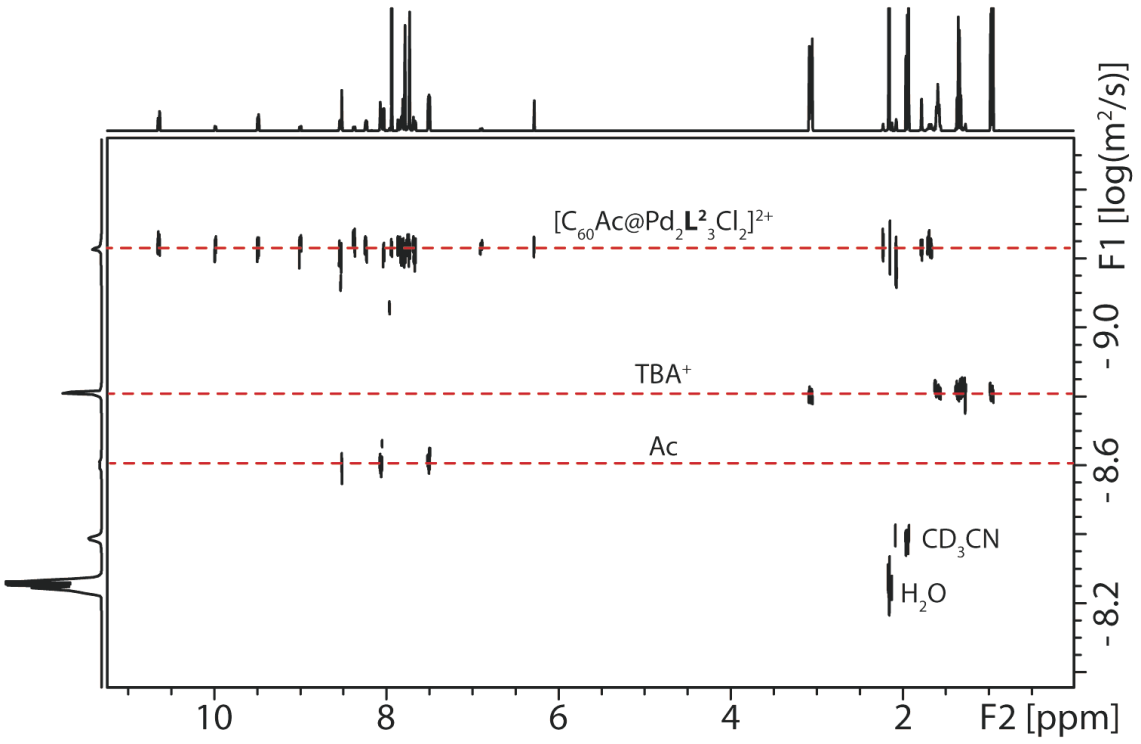


**Figure S93** DOSY spectrum (500 MHz, 298 K, $CD_3CN$) of $[C_{60}Ac@Pd_2\mathbf{L^2}_3Cl_2]^{2+}$ with the coexisting tetrabutylammonium ions ($TBA^+$) and unreacted anthracene. $[C_{60}Ac@Pd_2\mathbf{L^2}_3Cl_2]^{2+}$: diffusion coefficient = 5.9 x $10^{-10}$ $m^2s^{-1}$, log $D$ = −9.23, r = 10.7 Å; $TBA^+$ cation: diffusion coefficient = 1.5 x $10^{-9}$ $m^2s^{-1}$, log $D$ = −8.81, r = 4.1 Å; anthracene(Ac): diffusion coefficient = 2.5 x $10^{-9}$ $m^2s^{-1}$, log $D$ = −8.60, r = 2.5 Å.

**ESI HRMS** ($C_{194}H_{88}Cl_2N_{12}O_{12}Pd_2B_2F_8$): $[C_{60}Ac@Pd_2\mathbf{L^2}_3Cl_2]^{2+}$ calcd. for $C_{194}H_{88}Cl_2N_{12}O_{12}Pd_2$ 1531.2074; found 1531.2082.

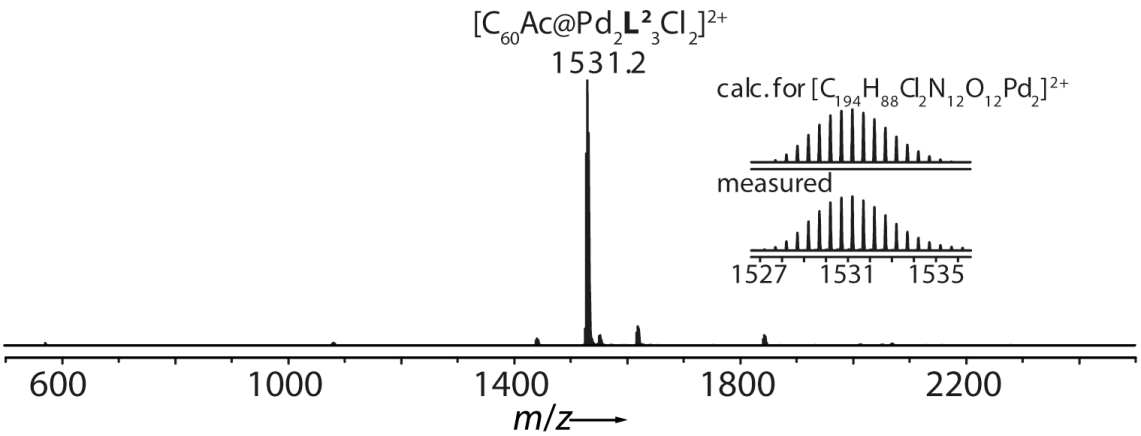


**Figure S94** ESI mass spectrum of $[C_{60}Ac@Pd_2\mathbf{L^2}_3Cl_2]^{2+}$.

## 6.2 Reaction between $[C_{60}@Pd_2\mathbf{L^2}_3Cl_2]^{2+}$ and anthracene in different ratios

**General procedure:** To the standard $CD_3CN$ solution of $[C_{60}@Pd_2\mathbf{L^2}_3Cl_2]^{2+}$ (500 µL, 0.56 mM, 0.28 µmol, 1 eq.) in the bottom of NMR tubes, different equivalents (1, 2, 5, 10 eq.) of the concentrated $CD_3CN$ solution of anthracene (10 mM) were added under nitrogen protection. All NMR tubes were wrapped with aluminium foil to avoid light irradiation and then heated at 50 °C in the dark. After a period of time, a $^1H$ NMR spectrum was recorded to monitor the partial conversion of $[C_{60}@Pd_2\mathbf{L^2}_3Cl_2]^{2+}$ and anthracene to $[C_{60}Ac@Pd_2\mathbf{L^2}_3Cl_2]^{2+}$.

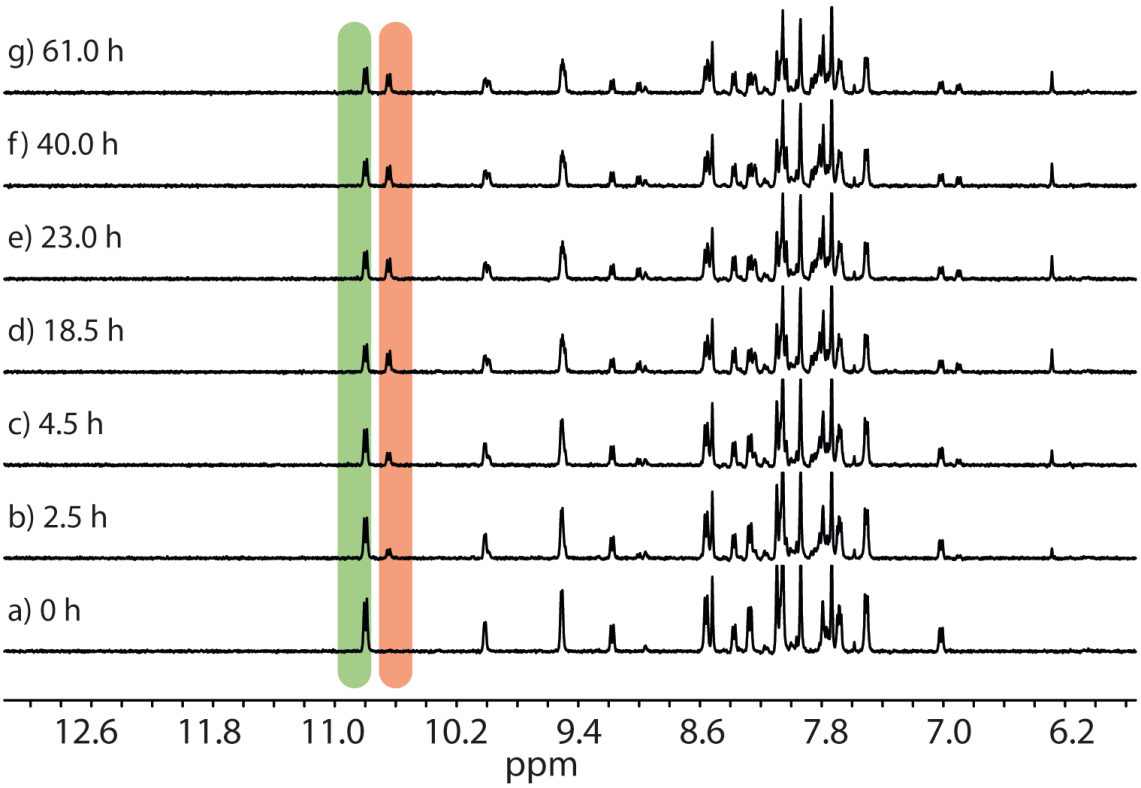


**Figure S95** $^1H$ NMR spectra (500 MHz, 298 K, $CD_3CN$) following the partial conversion of $[C_{60}@Pd_2\mathbf{L^2}_3Cl_2]^{2+}$ and 1 equivalent of Ac to $[C_{60}Ac@Pd_2\mathbf{L^2}_3Cl_2]^{2+}$ after heating at 50 °C. The quinoline proton c of $[C_{60}@Pd_2\mathbf{L^2}_3Cl_2]^{2+}$ and quinoline proton c of $[C_{60}Ac@Pd_2\mathbf{L^2}_3Cl_2]^{2+}$ are highlighted in green and red respectively.

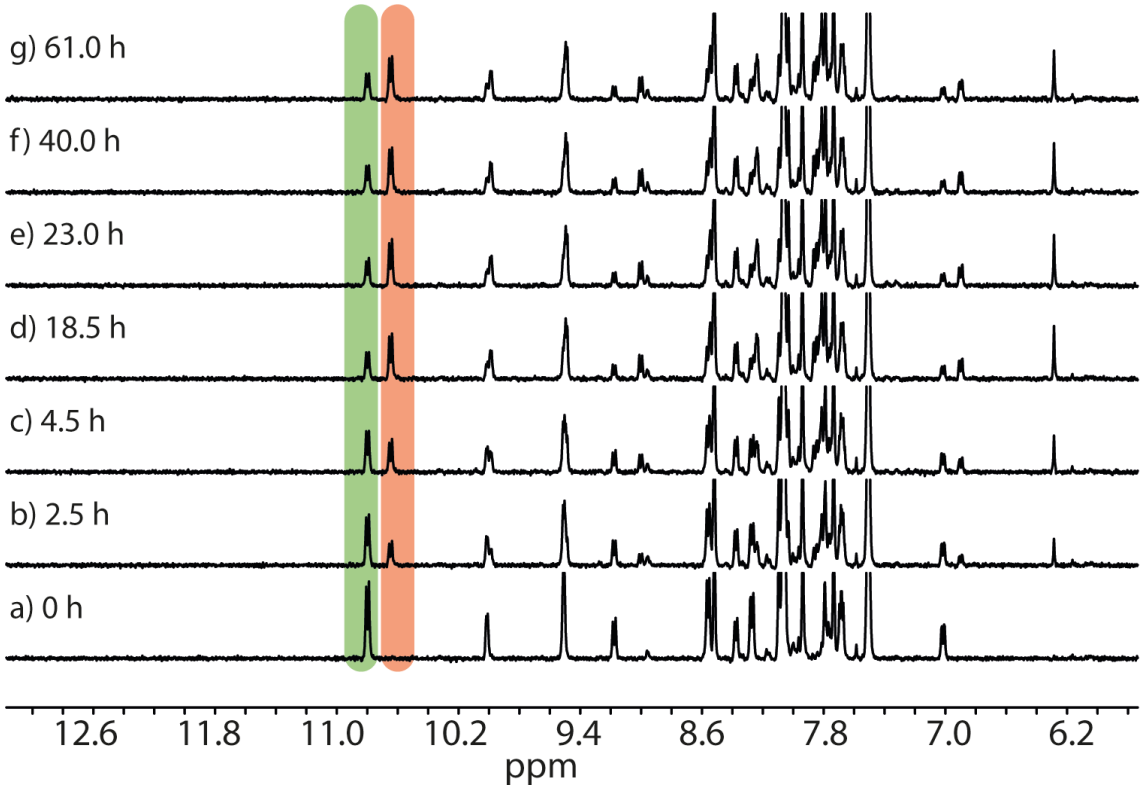


**Figure S96** $^1$H NMR spectra (500 MHz, 298 K, $CD_3CN$) following the partial conversion of $[C_{60}@Pd_2\mathbf{L^2}_3Cl_2]^{2+}$ and 2 equivalent of Ac to $[C_{60}Ac@Pd_2\mathbf{L^2}_3Cl_2]^{2+}$ after heating at 50 °C. The quinoline proton c of $[C_{60}@Pd_2\mathbf{L^2}_3Cl_2]^{2+}$ and quinoline proton c of $[C_{60}Ac@Pd_2\mathbf{L^2}_3Cl_2]^{2+}$ are highlighted in green and red respectively.

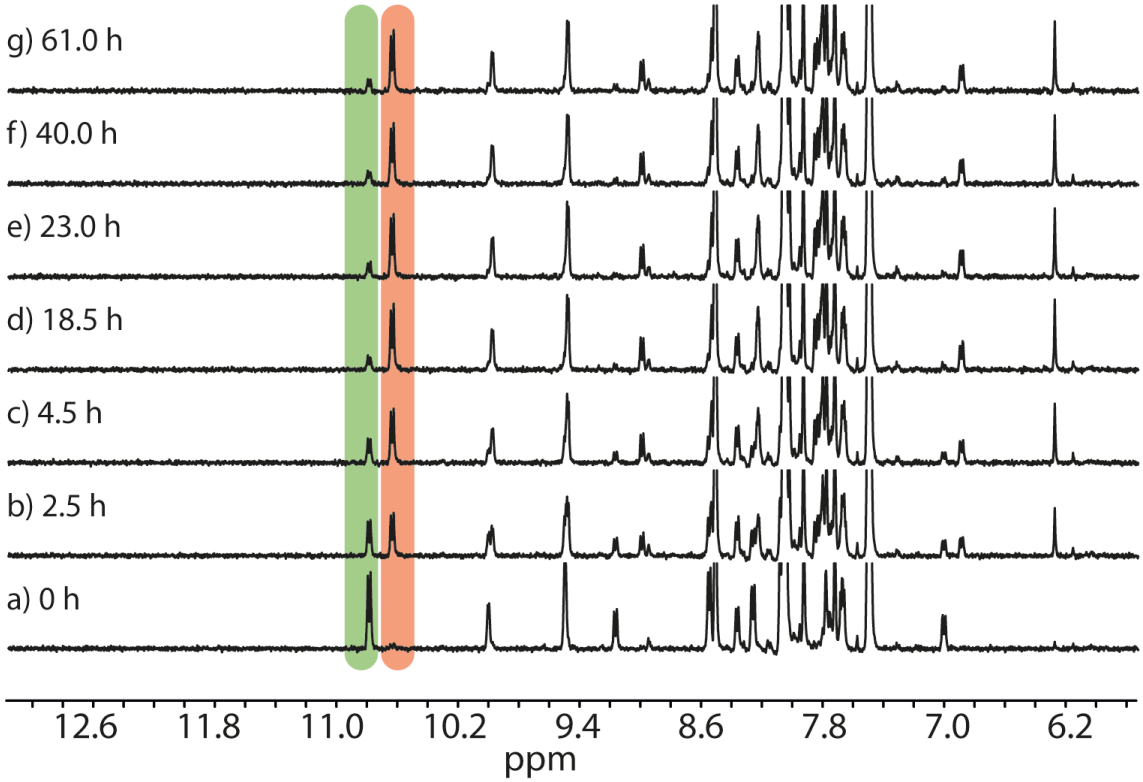


**Figure S97** $^1$H NMR spectra (500 MHz, 298 K, $CD_3CN$) following the partial conversion of $[C_{60}@Pd_2\mathbf{L^2}_3Cl_2]^{2+}$ and 5 equivalent of Ac to $[C_{60}Ac@Pd_2\mathbf{L^2}_3Cl_2]^{2+}$ after heating at 50 °C. The quinoline proton c of $[C_{60}@Pd_2\mathbf{L^2}_3Cl_2]^{2+}$ and quinoline proton c of $[C_{60}Ac@Pd_2\mathbf{L^2}_3Cl_2]^{2+}$ are highlighted in green and red respectively.

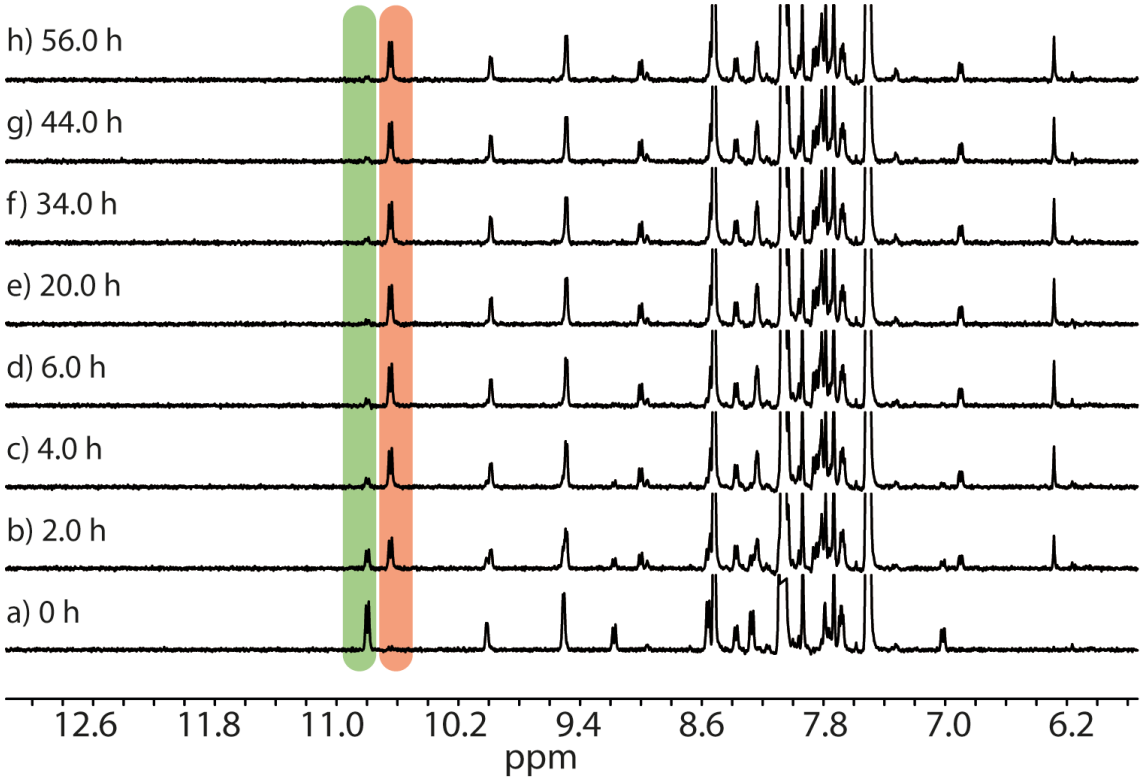


**Figure S98** $^{1}$H NMR spectra (500 MHz, 298 K, $CD_3CN$) following the partial conversion of $[C_{60}@Pd_2\mathbf{L^2}_3Cl_2]^{2+}$ and 10 equivalent of Ac to $[C_{60}Ac@Pd_2\mathbf{L^2}_3Cl_2]^{2+}$ after heating at 50 °C. The quinoline proton c of $[C_{60}@Pd_2\mathbf{L^2}_3Cl_2]^{2+}$ and quinoline proton c of $[C_{60}Ac@Pd_2\mathbf{L^2}_3Cl_2]^{2+}$ are highlighted in green and red respectively.

## 6.3 Conversion of $[C_{60}@Pd_2L^2{}_3Cl_2]^{2+}$ to $[C_{60}Ac@Pd_2L^2{}_3Cl_2]^{2+}$

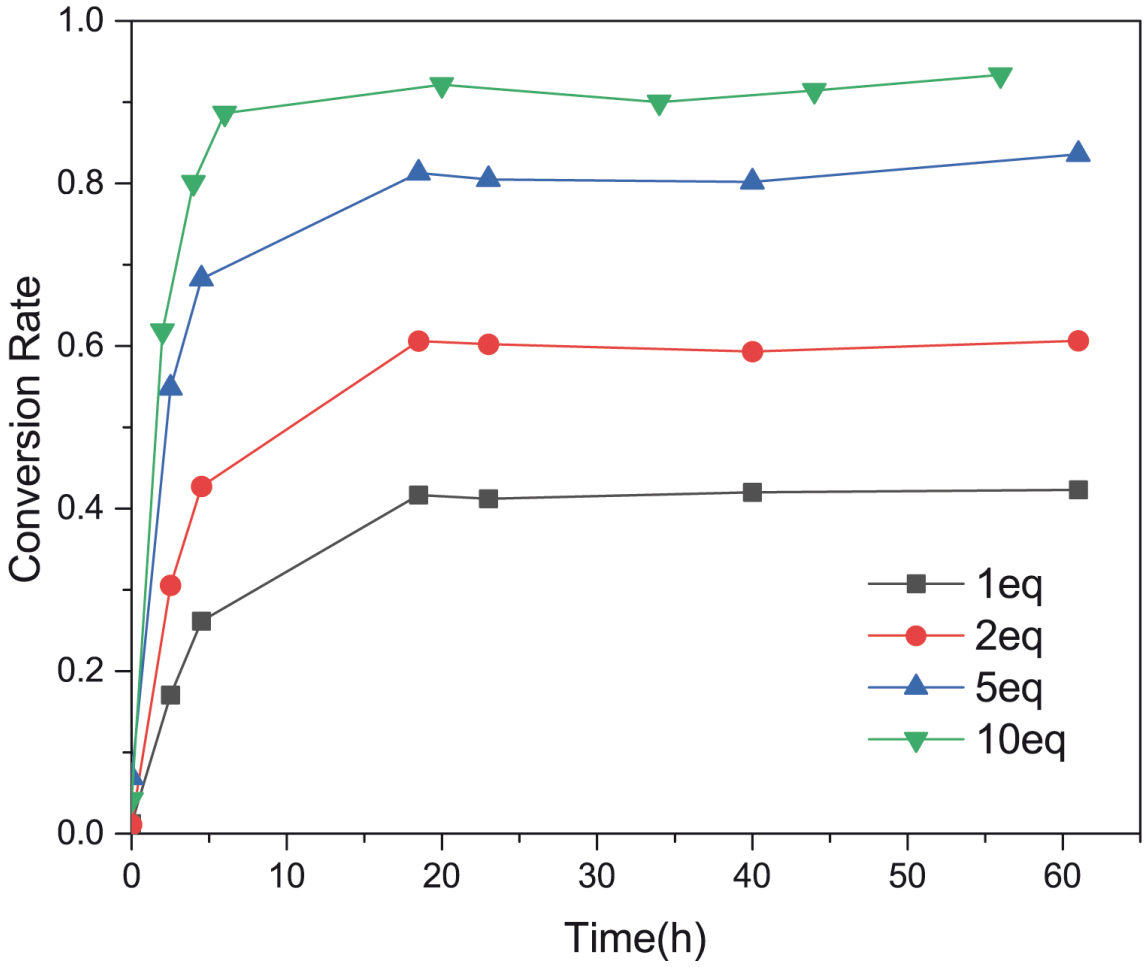


**Figure S99** Conversion of $[C_{60}@Pd_2\mathbf{L^2}_3Cl_2]^{2+}$ with different equivalents of anthracene to $[C_{60}Ac@Pd_2\mathbf{L^2}_3Cl_2]^{2+}$ after heating at 50 °C for a period of time, concluded from the calculation of integrals of protons in $^1$H NMR.

## 6.4 Determination of equilibrium constant $K_c$ for reaction between $[C_{60}@Pd_2L^2{}_3Cl_2]^{2+}$ and anthracene

$$[C_{60}@Pd_2\mathbf{L}^2{}_3Cl_2]^{2+} + Ac \rightleftharpoons [C_{60}Ac@Pd_2\mathbf{L}^2{}_3Cl_2]^{2+}$$

$$K_c = \frac{[C_{60}Ac@Bowl]}{[C_{60}@Bowl][Ac]}$$

where $[C_{60}Ac@Bowl]$, $[C_{60}@Bowl]$ and [Ac] stand for the equilibrium concentrations of $[C_{60}Ac@Pd_2\mathbf{L^2}_3Cl_2]^{2+}$, $[C_{60}@Pd_2\mathbf{L^2}_3Cl_2]^{2+}$ and anthracene at 323 K, respectively. These values are determined by the integration of the $H_c$ signals of $[C_{60}Ac@Pd_2\mathbf{L^2}_3Cl_2]^{2+}$ and $[C_{60}@Pd_2\mathbf{L^2}_3Cl_2]^{2+}$ in $^1$H NMR spectra. We assumed no change of the equilibrium position during the time required for recording the NMR spectra at 298 K (few minutes).

**Table S1** Calculation of the equilibrium constant $K_c$ with different amounts of added anthracene. Average value: 2210 L/mol.

| Amount of anthracene added | Percent of species in equilibrium | | Equilibrium constant $K_c$ (323 K) L/mol |
|---|---|---|---|
| | $[C_{60}@Pd_2\mathbf{L^2}_3Cl_2]^{2+}$ | $[C_{60}Ac@Pd_2\mathbf{L^2}_3Cl_2]^{2+}$ | |
| 1 eq. | 0.580 | 0.420 | 2360 |
| 2 eq. | 0.407 | 0.593 | 2061 |
| 5 eq. | 0.198 | 0.802 | 2210 |

## 6.5 One-pot formation of $C_{60}Ac$ inside $[Pd_2L^2_3Cl_2]^{2+}$

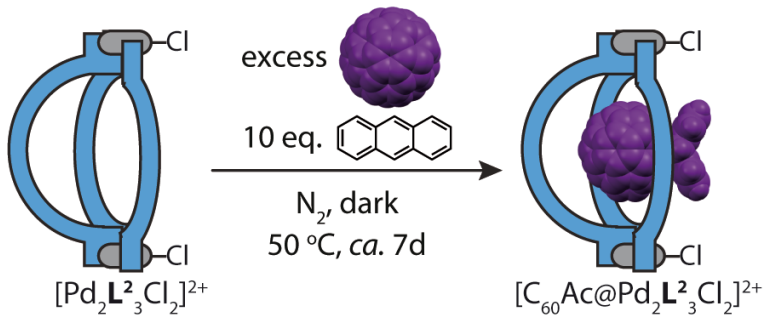


To an excess of $C_{60}$ solid (2.4 mg, 3.36 µmol), the standard $CD_3CN$ solution of $[Pd_2\mathbf{L^2}_3Cl_2]^{2+}$ (500 µL, 0.56 mM, 0.28 µmol, 1.0 eq.) and a concentrated $CD_3CN$ solution of anthracene (280 µL, 10 mM, 2.80 µmol, 10.0 eq.) were added under nitrogen protection. NMR tubes were wrapped with aluminium foil to avoid light irradiation and then heated at 50 °C in the dark. After a period of time, $^1H$ NMR spectra were recorded to monitor the partial conversion of $C_{60}$ to $C_{60}Ac$ inside the bowl $[Pd_2\mathbf{L^2}_3Cl_2]^{2+}$.

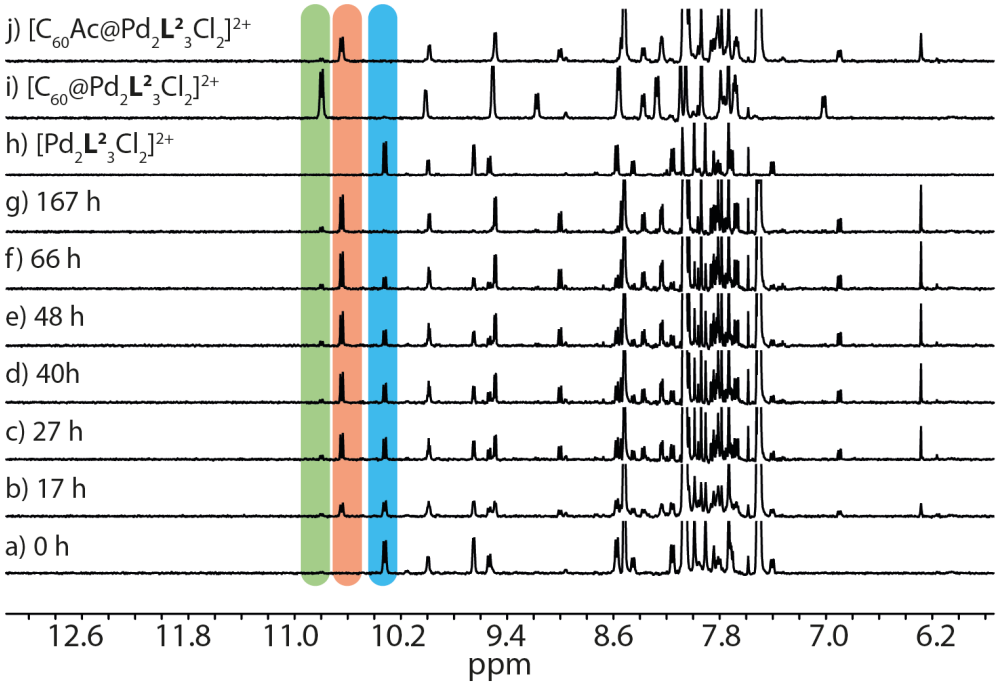


**Figure S100** $^1H$ NMR spectra (500 MHz, 298 K, $CD_3CN$) following the one-pot formation of $[C_{60}Ac@Pd_2\mathbf{L^2}_3Cl_2]^{2+}$ in the presence of 10 equivalent of anthracene and excess $C_{60}$ solid with $[C_{60}Ac@Pd_2\mathbf{L^2}_3Cl_2]^{2+}$ after heating at 50 °C. The quinoline proton c of $[C_{60}@Pd_2\mathbf{L^2}_3Cl_2]^{2+}$, proton c of $[C_{60}Ac@Pd_2\mathbf{L^2}_3Cl_2]^{2+}$ and proton c of $[Pd_2\mathbf{L^2}_3Cl_2]^{2+}$ are highlighted in green, red and blue respectively.

## 6.6 Control experiment

To excess $C_{60}$ solid (1.7 mg, 2.36 μmol), $CD_3CN$ (500 μL) and a concentrated $CD_3CN$ solution of anthracene (280 μL, 10 mM, 2.80 μmol) were added under nitrogen protection. NMR tubes were wrapped with aluminium foil to avoid light irradiation and then heated at 50 °C in the dark. After a period of time, $^1H$ NMR spectra were recorded.

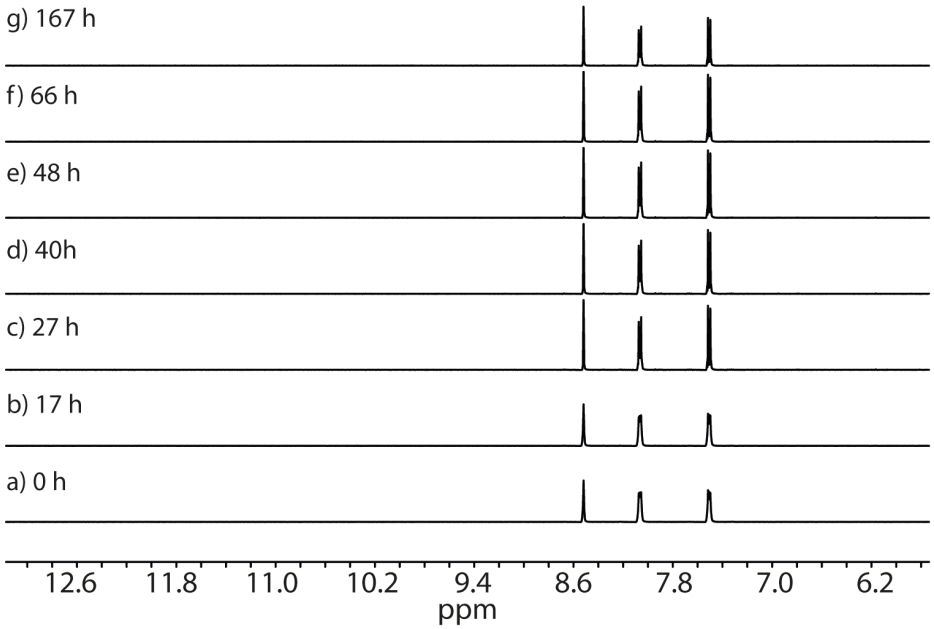


**Figure S101** $^1H$ NMR spectra (500 MHz, 298 K, $CD_3CN$) following the control experiment in the presence of 3.59 mM anthracene in $CD_3CN$ with $C_{60}$ solid after heating at 50°C.

To the $CD_3CN$ solution of $[C_{60}@Pd_2L^1_4]^{4+}$ (500 μL, 0.64 mM, 0.32 μmol), a concentrated $CD_3CN$ solution of anthracene (320 μL, 10 mM, 3.20 μmol) was added under nitrogen atmosphere. The NMR tube was wrapped in aluminium foil to avoid light irradiation and then heated at 50 °C in the dark. After the indicated period of time, $^1H$ NMR spectra were recorded.

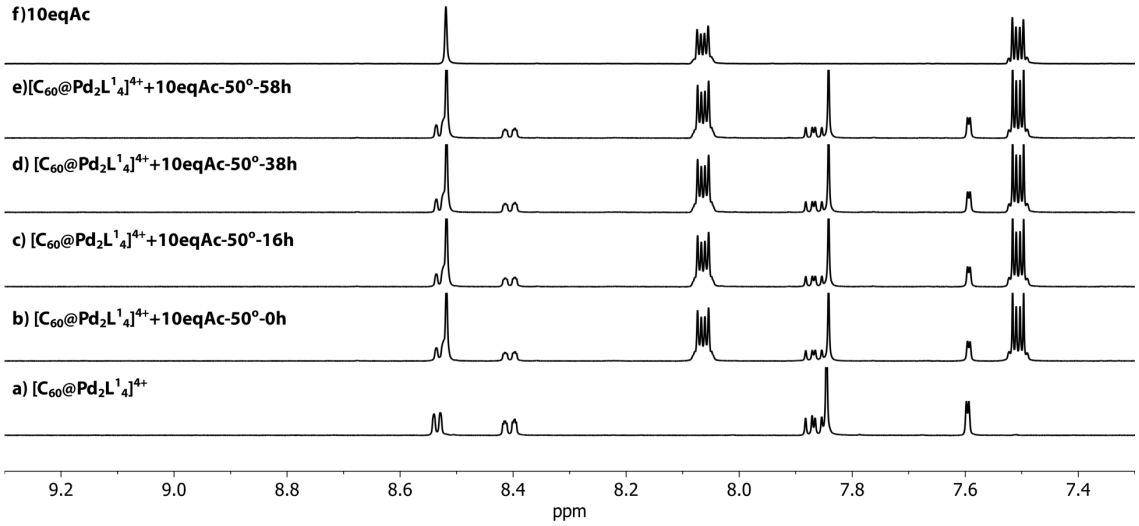


**Figure S102** $^1H$ NMR spectra (500 MHz, 298 K, $CD_3CN$) following the control experiment in the presence of $[C_{60}@Pd_2L^1_4]^{4+}$ and 10 eq. amount of anthracene in $CD_3CN$ after heating at 50 °C, suggesting that the entrapped $C_{60}$ in the cage $[C_{60}@Pd_2L^1_4]^{4+}$ cannot react with excess anthracene.

To the $CD_3CN$ solution of $[2C_{60}@Pd_4L^2{}_6(BDC)_2]^{4+}$ (600 µL, 0.31 mM, 0.18 µmol), a concentrated $CD_3CN$ solution of anthracene (184 µL, 10 mM, 1.84 µmol) was added under nitrogen atmosphere. The NMR tube was wrapped in aluminium foil to avoid light irradiation and then heated at 50 °C in the dark. After the indicated period of time, $^1H$ NMR spectra were recorded.

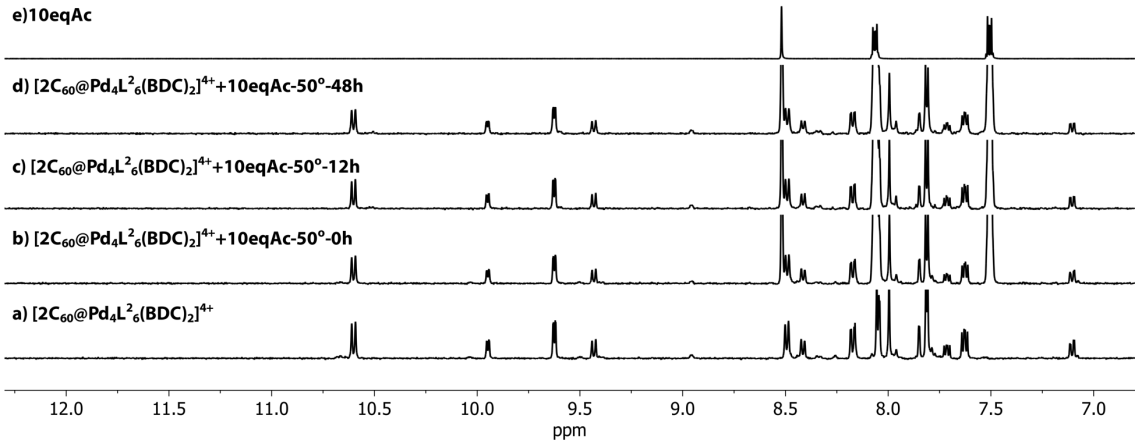


**Figure S103** $^1H$ NMR spectra (500 MHz, 298 K, $CD_3CN$) following the control experiment in the presence of $[2C_{60}@Pd_4L^2{}_6(BDC)_2]^{4+}$ and 10 eq. amount of anthracene in $CD_3CN$ after heating at 50 °C, suggesting that the entrapped $C_{60}$ in the dimer $[2C_{60}@Pd_4L^2{}_6(BDC)_2]^{4+}$ cannot react with excess anthracene.

# 7 UV-Vis spectra

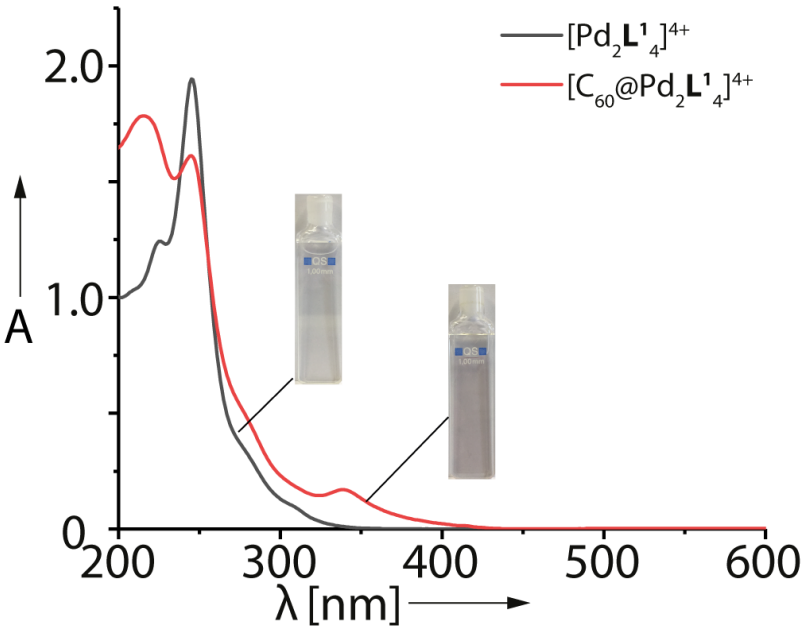


**Figure S104** UV-Vis spectra (0.064 mM, $CH_3CN$, 298 K) and photographs of solutions of $[Pd_2\mathbf{L^1}_4]^{4+}$ and $[C_{60}@Pd_2\mathbf{L^1}_4]^{4+}$.

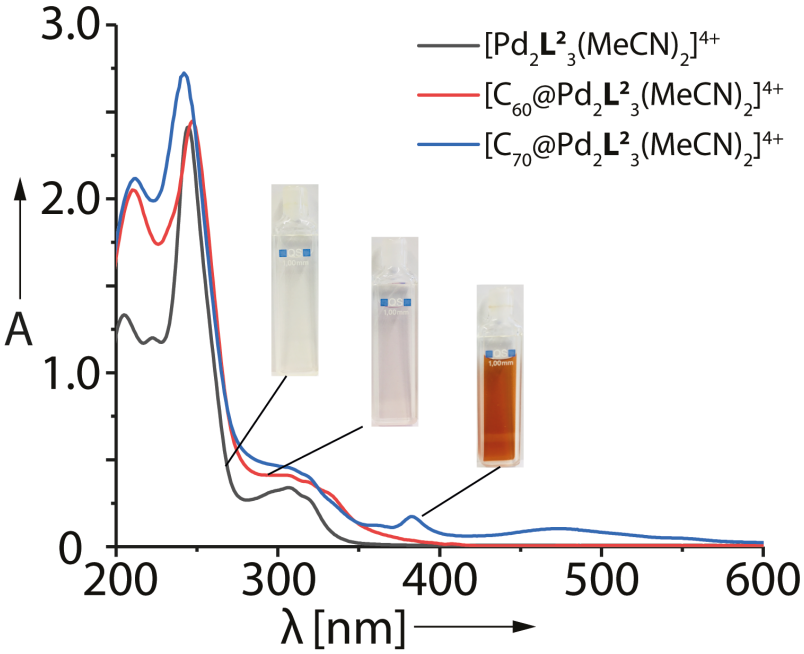


**Figure S105** UV-Vis spectra (0.064 mM, $CH_3CN$, 298 K) and photographs of solutions of $[Pd_2\mathbf{L^2}_3(MeCN)_2]^{4+}$, $[C_{60}@Pd_2\mathbf{L^2}_3(MeCN)_2]^{4+}$ and $[C_{70}@Pd_2\mathbf{L^2}_3(MeCN)_2]^{4+}$.

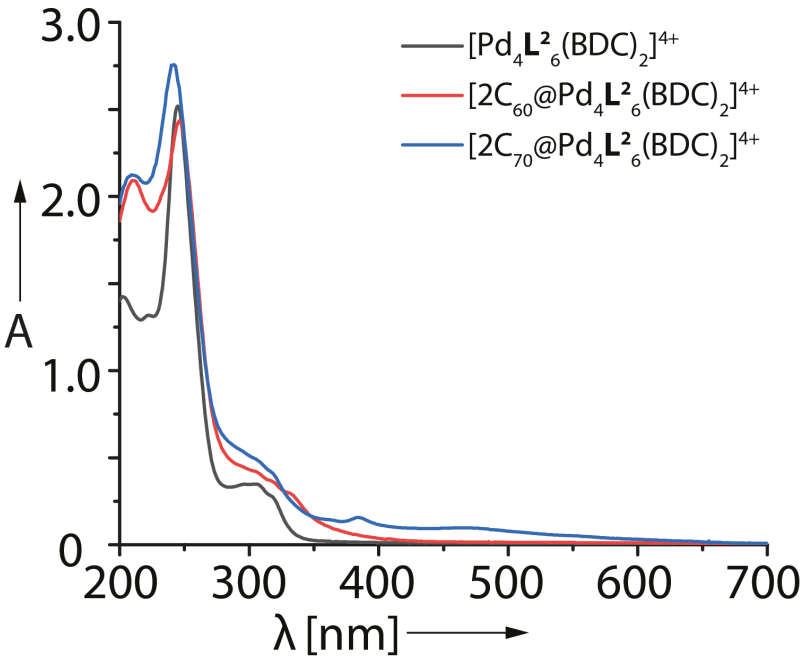


**Figure S106** UV-Vis spectra (0.031 mM, $CH_3CN$, 298 K) of solutions of $[Pd_4\mathbf{L^2}_6(BDC)_2]^{4+}$, $[2C_{60}@Pd_4\mathbf{L^2}_6(BDC)_2]^{4+}$ and $[2C_{70}@Pd_4\mathbf{L^2}_6(BDC)_2]^{4+}$.

# 8 X-ray Crystallography

## 8.1 General Methods

Five different supramolecular assemblies $[Pd_2\mathbf{L^1}_4](BF_4)_4$, $[C_{60}@Pd_2\mathbf{L^1}_4](BF_4)_4$ $[Pd_2\mathbf{L^2}_4](BF_4)_4$, $[C_{60}@Pd_2\mathbf{L^2}_3(MeCN)_2](BF_4)_4$, $[C_{60}Ac@Pd_2\mathbf{L^2}_3Cl_2](BF_4)_2$ and one ligand system ($\mathbf{L^2}$) were studied using single crystal X-ray crystallography. The small

molecule ligand system (**L²**) could easily be studied on our in-house diffractometer using microfocussed MoK$\alpha$ radiation. In contrast, crystals of supramolecular assemblies were extremely sensitive to loss of organic solvent. Due to very thin (5 – 20 ym) plate like crystals the analysis was further hampered by the limited scattering power of the samples not allowing to reach the desired (sub-)atomic resolution using our a modern microfocussed X-ray in-house CuK$\alpha$ source. Gaining detailed structural insight thus required cryogenic crystal handling and highly brilliant synchrotron radiation. Hence, diffraction data of most of supramolecular assemblies was collected during three beamtime shifts at macromolecular synchrotron beamline P11, PETRA III, DESY.[1] Modelling of $C_{60}$ disorder as well as counterion and solvent flexibility required carefully adapted macromolecular refinement protocols employing geometrical restraint dictionaries, similarity restraints and restraints for anisotropic displacement parameters (ADPs). Analyzing morphologies and detailed geometries of metallo-supramolecular fullerene receptors greatly enhanced the in-depth understanding of how they adapt to changes of external conditions and their pronounced tendency to co-crystallize with one or more different fullerene species as guests. Especially the $[Pd_2\mathbf{L^2}_3X_2]$ bowl is well suited as supramolecular protection group and to facilitate the structural characterization of new light- and oxygen-sensitive fullerene derivatives by X-ray diffraction methods.

**Table S2** Crystallographic data of $[Pd_2\mathbf{L^1}_4](BF_4)_4$, $[C_{60}@Pd_2\mathbf{L^1}_4](BF_4)_4$ and **L²**.

| Compound | $\mathbf{[Pd_2L^1_4](BF_4)_4}$ | $\mathbf{[C_{60}@Pd_2L^1_4](BF_4)_4}$ | $\mathbf{L^2}$ |
|---|---|---|---|
| CCDC number | 1850358 | 1850359 | 1850360 |
| Identification code | bc7a_sq | bc16a_sq | bc12d |
| Empirical formula | $C_{128}H_{88}N_{16}O_{16}Pd_2B_4F_{16}$ | $C_{188}H_{88}N_{16}O_{16}Pd_2B_2F_8$ | $C_{40}H_{26}N_4O_4$ |
| Formula weight | 2666.18 | 3213.16 | 626.65 |
| Temperature (K) | 80(2) | 80(2) | 100(2) |
| Crystal system | Triclinic | Triclinic | Monoclinic |
| Space group | P-1 | P-1 | $P2_1$ |
| *a* (Å) | 15.689(3) | 29.482(6) | 7.3461(2) |
| *b* (Å) | 17.074(3) | 30.095(6) | 8.2067(3) |
| *c* (Å) | 17.522(4) | 33.669(7) | 23.9093(8) |
| $\alpha$ (º) | 112.90(3) | 97.35(3) | 90 |
| $\beta$ (º) | 113.54(3) | 93.16(3) | 93.499(2) |
| $\gamma$ (º) | 90.59(3) | 112.74(3) | 90 |
| Volume (Å$^3$) | 3886.8(18) | 27145(11) | 1438.74(8) |
| *Z* | 1 | 6 | 2 |
| Density (calc.) (g/cm$^3$) | 1.139 | 1.179 | 1.447 |
| Absorption coefficient (mm$^{-1}$) | 0.279 | 0.246 | 0.767 |
| F(000) | 1352 | 9780 | 652 |
| Crystal size (mm$^3$) | 0.200 x 0.020 x 0.020 | 0.300 x 0.050 x 0.020 | 0.200 x 0.100 x 0.020 |
| $\theta$ range for data collection (º) | 1.280 to 26.202 | 0.595 to 21.512 | 3.704 to 80.342 |
| Reflections collected | 53426 | 226990 | 24133 |

| | | | |
|---|---|---|---|
| Observed reflections [R(int)] | 15802 [0.0413] | 64579 [0.0527] | 6093 [0.0470] |
| Goodness-of-fit on $F^2$ | 1.049 | 1.165 | 1.053 |
| $R_1$ [I>2σ(I)] | 0.0801 | 0.0887 | 0.0290 |
| $wR_2$ (all data) | 0.2626 | 0.3067 | 0.0717 |
| Largest diff. peak and hole (e.Å$^{-3}$) | 1.537 and -1.238 | 0.942 and -0.819 | 0.172 and -0.148 |
| Data / restraints / parameters | 15802 / 2120 / 824 | 64579 / 423903 / 7958 | 6093 / 1 / 435 |

**Table S3** Crystallographic data of $[Pd_2\mathbf{L^2}_4](BF_4)_4$, $[C_{60}@Pd_2\mathbf{L^2}_3(MeCN)_2](BF_4)_4$ and $[C_{60}Ac@Pd_2\mathbf{L^2}_3Cl_2](BF_4)_2$.

| Compound | **$[Pd_2L^2_4](BF_4)_4$** | **$[C_{60}@Pd_2L^2_3(MeCN)_2](BF_4)_4$·4MeCN** | **$[C_{60}Ac@Pd_2L^2_3Cl_2](BF_4)_2$·2MeCN·4THF** |
|---|---|---|---|
| CCDC number | 1850361 | 1850362 | 1858158 |
| Identification code | bc11c_sq | bc-bg8c_sq | bc20a_plate_sq |
| Empirical formula | $C_{160}H_{104}N_{16}O_{16}Pd_2B_4F_{16}$ | $C_{192}H_{96}N_{18}O_{12}Pd_2B_4F_{16}$ | $C_{214}H_{126}N_{14}O_{16}Pd_2B_2F_8Cl_2$ |
| Formula weight | 3066.63 | 3406.90 | 3606.60 |
| Temperature (K) | 80(2) | 100(2) | 80(2) |
| Crystal system | Monoclinic | Triclinic | Monoclinic |
| Space group | $P2_1/n$ | P-1 | $P2_1/n$ |
| *a* (Å) | 16.884(3) | 18.9931(18) | 18.628(4) |
| *b* (Å) | 19.386(4) | 20.6975(19) | 37.428(8) |
| *c* (Å) | 32.974(7) | 24.287(2) | 25.814(5) |
| α (º) | 90 | 69.678(6) | 90 |
| β (º) | 103.27(3) | 72.978(6) | 92.11(3) |
| γ (º) | 90 | 69.473(6) | 90 |
| Volume (Å$^3$) | 10505(4) | 8224.2(14) | 17986(6) |
| *Z* | 2 | 2 | 4 |
| Density (calc.) (g/cm$^3$) | 0.970 | 1.376 | 1.332 |
| Absorption coefficient (mm$^{-1}$) | 0.213 | 2.496 | 0.283 |
| F(000) | 3120 | 3452 | 7376 |
| Crystal size (mm$^3$) | 0.220 x 0.100 x 0.005 | 0.300 x 0.200 x 0.100 | 0.080 x 0.080 x 0.020 |
| θ range for data collection (º) | 1.189 to 22.790 | 1.978 to 41.209 | 0.929 to 23.606 |
| Reflections collected | 102108 | 56017 | 187883 |
| Observed reflections [R(int)] | 15328 [0.0590] | 10167 [0.1148] | 29314 [0.0589] |
| Goodness-of-fit on $F^2$ | 1.074 | 1.063 | 1.474 |
| $R_1$ [I>2σ(I)] | 0.0791 | 0.0994 | 0.1230 |
| $wR_2$ (all data) | 0.2696 | 0.2675 | 0.3816 |
| Largest diff. peak and hole (e.Å$^{-3}$) | 1.300 and -0.710 | 1.282 and -0.934 | 3.312 and -0.683 |
| Data / restraints / parameters | 15328 / 2208 / 964 | 10167 / 52795 / 2738 | 29314 / 5529 / 2461 |

## 8.2 Crystal structure of $[Pd_2L^1_4](BF_4)_4$

Colorless, needle-shaped crystals of $[Pd_2\mathbf{L^1}_4](BF_4)_4$ were grown over a period of 2 months by slow vapor diffusion of THF into a 0.64 mM $CD_3CN$ solution of $[C_{60}@Pd_2\mathbf{L^1}_4](BF_4)_4$. A single crystal of $[Pd_2\mathbf{L^1}_4](BF_4)_4$ in mother liquor was pipetted onto a glass slide containing NVH oil. To avoid collapse of the crystal lattice, the crystal was quickly mounted onto a 0.3 mm nylon loop and immediately flash cooled in liquid nitrogen. Crystals were stored at cryogenic temperature in dry shippers, in which they were safely transported to macromolecular beamline P11 at Petra III[1], DESY, Germany.

A wavelength of $\lambda$ = 0.6888 Å was chosen using a liquid $N_2$ cooled double crystal monochromator. Single crystal X-ray diffraction data was collected at 80(2) K on a single axis goniometer, equipped with an Oxford Cryostream 800 a Pilatus 6M. 1800 diffraction images were collected in a 360° ϕ sweep at a detector distance of 156 mm, 30% filter transmission, 0.2° step width and 0.2 seconds exposure time per image. Data integration and reduction were undertaken using XDS.[2] The structure was solved by intrinsic phasing/direct methods using SHELXT[3] and refined with SHELXL[4] using 22 cpu cores for full-matrix least-squares routines on $F^2$ and ShelXle[5] as a graphical user interface and the DSR program plugin was employed for modeling.[6]

### 8.2.1 Specific refinement details of $[Pd_2L^1_4](BF_4)_4$

Stereochemical restraints for the EAP ligands (**L¹**) were generated by the GRADE program using the GRADE Web Server (http://grade.globalphasing.org) and applied in the refinement. A GRADE dictionary for SHELXL contains target values and standard deviations for 1,2-distances (DFIX) and 1,3-distances (DANG), as well as restraints for planar groups (FLAT). All displacements for non-hydrogen atoms were refined anisotropically. The refinement of ADP's for carbon, nitrogen and oxygen atoms was enabled by a combination of similarity restraints (SIMU) and rigid bond restraints (RIGU).[7] The contribution of the electron density from disordered counterions and solvent molecules, which could not be modeled with discrete atomic positions were handled using the SQUEEZE[8] routine in PLATON.[9] The solvent mask file (.fab) computed by PLATON were included in the SHELXL refinement via the ABIN instruction leaving the measured intensities untouched.

**Table S4** Definition of residues involved in $[Pd_2\mathbf{L^1}_4](BF_4)_4$.

| Fragment | Residue class | Occurrence | Residue numbers |
|---|---|---|---|
| Ligand **L¹** | EAP | 2 | 2,3 |
| $BF_4^-$ | BF4 | 2 | 10,11 |

### 8.2.2 Description of the structure of $[Pd_2L^1_4](BF_4)_4$

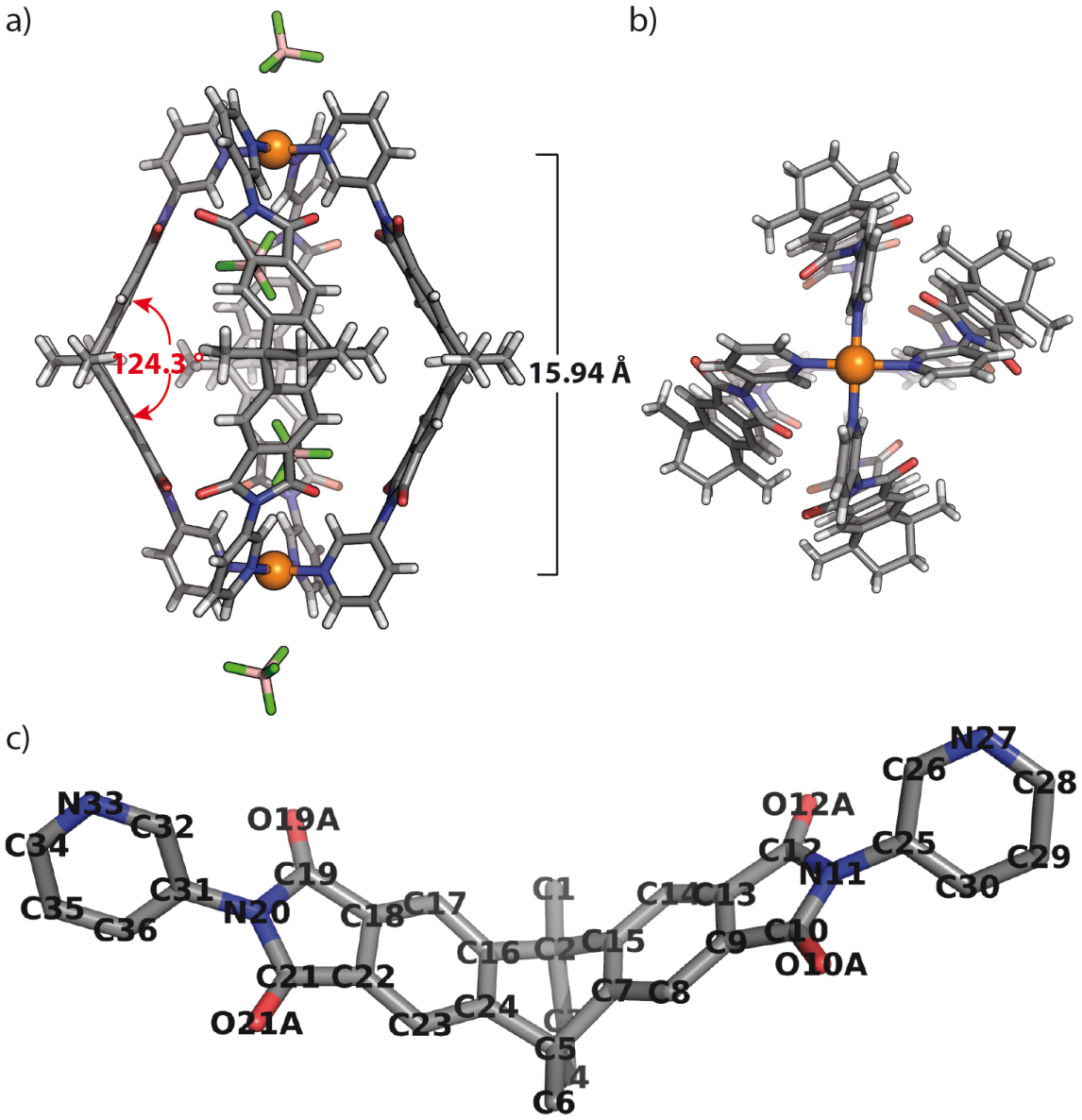


**Figure S107** X-ray structure of $[Pd_2L^1_4](BF_4)_4$: (a) the structure showing the occupation of the cavity by two $BF_4^-$ counterions; (b) top view of the structure; (c) atomic naming scheme of ligand $L^1$ ( residue class EAP). The same atom labels are used in all other $L^1$ containing structures. Color scheme: H, light grey; B, pink; C, dark grey; N, blue; O, red; F, green; Pd, orange.

**Table S5** Structural details involved in $[Pd_2L^1_4](BF_4)_4$.

| Residues No. | Dihedral angle (°) between the backbone's benzene planes C16_C17_C18_C22_C23_C24 and C7_C8_C9_C13_C14_C15 | Esd | Dihedral angle (°) between planes N27_Pd1_Pd2 and N33_Pd1_Pd2 | Esd |
|---|---|---|---|---|
| 2 | 56.060 | 0.158 | 0.715 | 0.162 |
| 3 | 55.333 | 0.234 | 1.264 | 0.201 |
| Average | 55.7 | | 1.0 | |

## 8.3 Crystal structure of $[C_{60}@Pd_2L^1_4](BF_4)_4$

Red plate crystals of $[C_{60}@Pd_2\mathbf{L^1}_4](BF_4)_4$ were obtained by slow vapor diffusion of isopropyl ether into a 0.64 mM $CD_3CN$ solution of $[C_{60}@Pd_2\mathbf{L^1}_4](BF_4)_4$. A single crystal in mother liquor was pipetted onto a glass slide containing NVH oil. To avoid collapse of the crystal lattice, the crystal was quickly mounted onto a 0.2 mm nylon loop and immediately flash cooled in liquid nitrogen. Crystals were stored at cryogenic temperature in dry shippers, in which they were safely transported to macromolecular beamline P11 at Petra III[1], DESY, Germany.

A wavelength of $\lambda$ = 0.6888 Å was chosen using a liquid $N_2$ cooled double crystal monochromator. Single crystal X-ray diffraction data was collected at 80(2) K on a single axis goniometer, equipped with an Oxford Cryostream 800 a Pilatus 6M. 1800 diffraction images were collected in a 360° ϕ sweep at a detector distance of 155 mm, 100% filter transmission, 0.2° step width and 0.1 seconds exposure time per image. Data integration and reduction were undertaken using XDS.[2] The structure was solved by intrinsic phasing/direct methods using SHELXT[3] and refined with SHELXL[4] using 22 cpu cores for full-matrix least-squares routines on $F^2$ and ShelXle[5] as a graphical user interface and the DSR program plugin was employed for modeling.[6]

### 8.3.1 Specific refinement details of $[C_{60}@Pd_2L^1_4](BF_4)_4$

The unit cell contained three crystallographically independent cages. Stereochemical restraints for the EAP ligands ($\mathbf{L^1}$) were generated by the GRADE program using the GRADE Web Server (http://grade.globalphasing.org) and applied in the refinement. A GRADE dictionary for SHELXL contains target values and standard deviations for 1,2-distances (DFIX) and 1,3-distances (DANG), as well as restraints for planar groups (FLAT). All displacements for non-hydrogen atoms were refined anisotropically. The refinement of ADP's for carbon, nitrogen and oxygen atoms was enabled by a combination of similarity restraints (SIMU) and rigid bond restraints (RIGU).[7] Disorder of all three $C_{60}$ guests was modelled with two discrete positions each using the DSR program GUI and its SADI restraints for 1,2-distances and 1,3-distances for $C_{60}$.[6, 10] The contribution of the electron density from disordered counterions and solvent molecules, which could not be modeled with discrete atomic positions were handled using the SQUEEZE[8] routine in PLATON.[9] The solvent mask file (.fab) computed by PLATON were included in the SHELXL refinement via the ABIN instruction leaving the measured intensities untouched.

**Table S6** Definition of residues involved in $[C_{60}@Pd_2\mathbf{L^1}_4](BF_4)_4$.

| Fragment | Residue class | Occurrence | Residue numbers |
|---|---|---|---|
| $Pd^{2+}$ | PD | 3 | 60,61,62 |
| Ligand $\mathbf{L^1}$ | EAP | 12 | 1,2,3,4,5,6,7,8,9,10,11,12 |
| $C_{60}$ | C60 | 6 | 13,14,15,16,17,18 (Three $C_{60}$ with disorder) |
| $BF_4^-$ | BF4 | 7 | 21,22,23,24,25,26,27(One $BF_4^-$ with disorder) |

### 8.3.2 Description of the structure of $[C_{60}@Pd_2L^1_4](BF_4)_4$

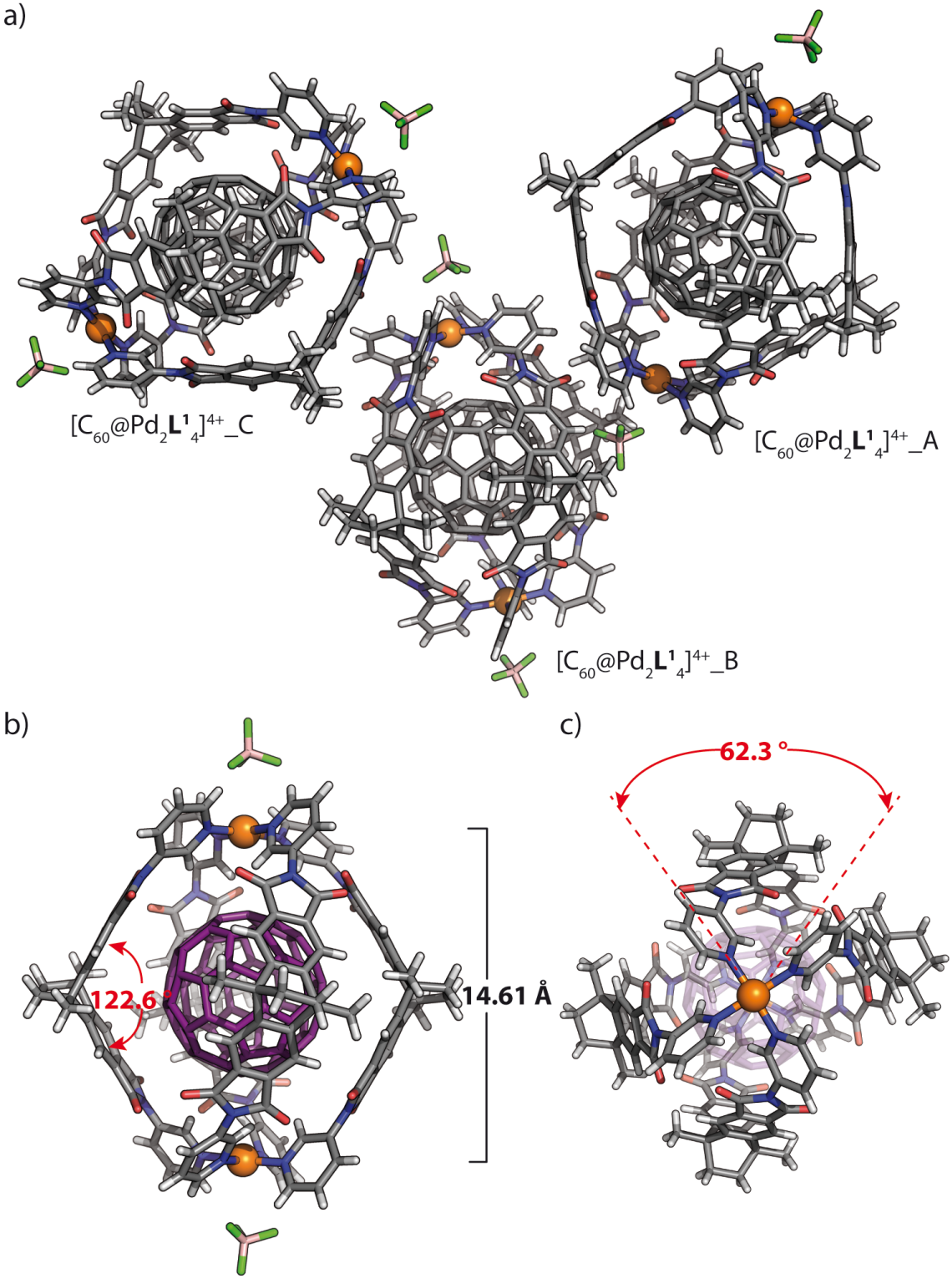


**Figure S108** X-ray structure of $[C_{60}@Pd_2L^1_4](BF_4)_4$: (a) The asymmetric unit of three crystallographically independent cages; (b) the structure of $[C_{60}@Pd_2L^1_4]^{4+}$_C with the Pd–Pd distance of 14.61 Å; (c) top view of the structure of $[C_{60}@Pd_2L^1_4]^{4+}$_C depicting a dihedral angle of 62.3° in between two pyridine arms of the same ligand. Color scheme: H, light grey; B, pink; C, dark grey; N, blue; O, red; F, green; Pd, orange. Minor disordered position of C60 guests was omitted for clarity.

**Table S7** Structural details involved in $[C_{60}@Pd_2\mathbf{L^1}_4](BF_4)_4$.

| Residues No. | Dihedral angle (°) between the backbone's benzene planes C16_C17_C18_C22_C23_C24 and C7_C8_C9_C13_C14_C15 | Esd (°) | Dihedral angle (°) between planes N27_Pd1_Pd2 and N33_Pd1_Pd2 | Esd (°) |
|---|---|---|---|---|
| 1 | 58.798 | 0.174 | 61.443 | 0.244 |
| 2 | 56.727 | 0.252 | 61.550 | 0.219 |
| 3 | 56.932 | 0.219 | 62.943 | 0.24 |
| 4 | 56.962 | 0.250 | 63.640 | 0.241 |
| Average | 57.4 | | 62.4 | |
| 5 | 60.993 | 0.239 | 63.990 | 0.254 |
| 6 | 59.238 | 0.228 | 64.740 | 0.268 |
| 7 | 58.638 | 0.292 | 64.570 | 0.244 |
| 8 | 57.046 | 0.203 | 61.829 | 0.261 |
| Average | 59.0 | | 63.8 | |
| 9 | 58.207 | 0.282 | 62.001 | 0.133 |
| 10 | 59.225 | 0.343 | 62.604 | 0.167 |
| 11 | 55.518 | 0.273 | 61.422 | 0.139 |
| 12 | 56.530 | 0.264 | 63.021 | 0.132 |
| Average | 57.4 | | 62.3 | |

### 8.3.3 Analysis of the host–guest interaction

Method of distance measurement: At first, the main position of all disordered $C_{60}$ guest (Part 1) was used to create a PDB file for further analysis in the Olex2 program.[11] The 'CENT' and 'MPLN' commands were used to create the centroid of $C_{60}$ and the mean planes of interest situated on the ligands and fullerene surfaces. The corresponding distances in between centroids of the ligands benzene rings, hydrogen atoms, $C_{60}$ centroids and centroids of $C_{60}$ rings were analyzed by using the 'Distances and angles' function.

**Table S8** Distances associated with the host–guest interaction in $[C_{60}@Pd_2\mathbf{L^1}_4](BF_4)_4$.

| Residues No. | Planes | Centroid of plane to centroid of $C_{60}$ (Å) | Centroid of plane to the five or six membered ring centroid of $C_{60}$ (Å) | Hydrogen atoms | Hydrogen atoms to centroid of $C_{60}$ (Å) | Shortest distance to the rings of $C_{60}$ (Å) |
|---|---|---|---|---|---|---|
| 1 | C7_C8_C9_C13_C14_C15 | 6.75 | 3.60 | H26 | 6.07 | 2.85 |
| 1 | C16_C17_C18_C22_C23_C24 | 6.74 | 3.67 | H32 | 5.96 | 2.76 |
| 2 | C7_C8_C9_C13_C14_C15 | 6.71 | 3.88 | H26 | 6.22 | 3.29 |
| 2 | C16_C17_C18_C22_C23_C24 | 6.67 | 3.64 | H32 | 6.06 | 2.80 |
| 3 | C7_C8_C9_C13_C14_C15 | 6.72 | 3.61 | H26 | 6.25 | 3.11 |
| 3 | C16_C17_C18_C22_C23_C24 | 6.65 | 3.63 | H32 | 6.04 | 2.86 |
| 4 | C7_C8_C9_C13_C14_C15 | 6.69 | 3.75 | H26 | 6.14 | 2.88 |
| 4 | C16_C17_C18_C22_C23_C24 | 6.80 | 3.62 | H32 | 6.18 | 3.15 |
| 5 | C7_C8_C9_C13_C14_C15 | 6.77 | 3.78 | H26 | 6.03 | 3.06 |
| 5 | C16_C17_C18_C22_C23_C24 | 6.71 | 3.77 | H32 | 6.01 | 2.81 |
| 6 | C7_C8_C9_C13_C14_C15 | 6.72 | 3.79 | H26 | 6.04 | 2.81 |
| 6 | C16_C17_C18_C22_C23_C24 | 6.74 | 3.68 | H32 | 6.20 | 3.16 |
| 7 | C7_C8_C9_C13_C14_C15 | 6.78 | 3.59 | H26 | 6.26 | 3.08 |
| 7 | C16_C17_C18_C22_C23_C24 | 6.73 | 3.85 | H32 | 6.13 | 3.23 |
| 8 | C7_C8_C9_C13_C14_C15 | 6.73 | 3.78 | H26 | 6.12 | 3.24 |
| 8 | C16_C17_C18_C22_C23_C24 | 6.75 | 3.74 | H32 | 6.01 | 2.78 |
| 9 | C7_C8_C9_C13_C14_C15 | 6.72 | 3.81 | H26 | 6.13 | 3.17 |
| 9 | C16_C17_C18_C22_C23_C24 | 6.72 | 3.83 | H32 | 6.10 | 2.91 |
| 10 | C7_C8_C9_C13_C14_C15 | 6.72 | 3.84 | H26 | 6.05 | 3.18 |
| 10 | C16_C17_C18_C22_C23_C24 | 6.78 | 3.62 | H32 | 6.12 | 2.97 |
| 11 | C7_C8_C9_C13_C14_C15 | 6.69 | 3.56 | H26 | 6.10 | 2.99 |
| 11 | C16_C17_C18_C22_C23_C24 | 6.66 | 3.77 | H32 | 6.12 | 3.24 |
| 12 | C7_C8_C9_C13_C14_C15 | 6.65 | 3.69 | H26 | 6.17 | 2.99 |
| 12 | C16_C17_C18_C22_C23_C24 | 6.69 | 3.72 | H32 | 6.20 | 3.20 |
| Average | | 6.72 | 3.72 | | 6.11 | 3.02 |

## 8.4 Crystal structure of $L^2$

Colorless block crystals of **$L^2$** were obtained by slow evaporation of a 0.67 mM $CHCl_3$/MeCN (v/v: 1/2) solution of **$L^2$**. A single crystal in mother liquor was mounted onto a 0.2 mm nylon loop using NVH oil. Single crystal X-ray diffraction data was collected on a Bruker D8 venture equipped with an Incoatec microfocus source (Iμs 2.0) using Cukα radiation on a four axis κ-goniometer, equipped with an Oxford Cryostream 800 and a Photon 100 detector. Data integration was done with SAINT. Data scaling and absorption correction were performed with SADABS. The space group was determined using XPREP.[12] The structure was solved by intrinsic phasing/direct methods using SHELXT[3] and refined with SHELXL[4] for full-matrix least-squares routines on $F^2$ and ShelXle[5] as a graphical user interface.

### 8.4.1 Specific refinement details of ligand $L^2$

The chiral space group $P2_1$ originated from chiral packing of the achiral EAQ ligand (**$L^2$**). All displacements for non-hydrogen atoms were refined anisotropically.

### 8.4.2 Description of the structure of ligand $L^2$

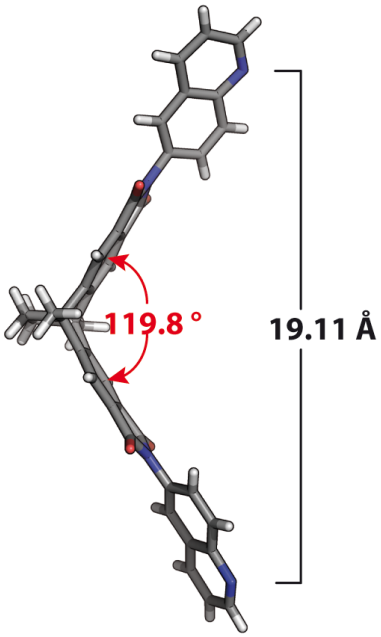


**Figure S109** X-ray structure of **$L^2$** with the N–N distance of 19.11 Å. Color scheme: H, light grey; C, dark grey; N, blue; O, red.

**Table S9** Structural details involved in **$L^2$**.

| Residues No. | Dihedral angle (°) between the backbone's benzene planes C16_C17_C18_C22_C23_C24 and C7_C8_C9_C13_C14_C15 | Esd (°) |
|---|---|---|
| - | 60.2 | 0.1 |

### 8.4.3 Thermal ellipsoid plots

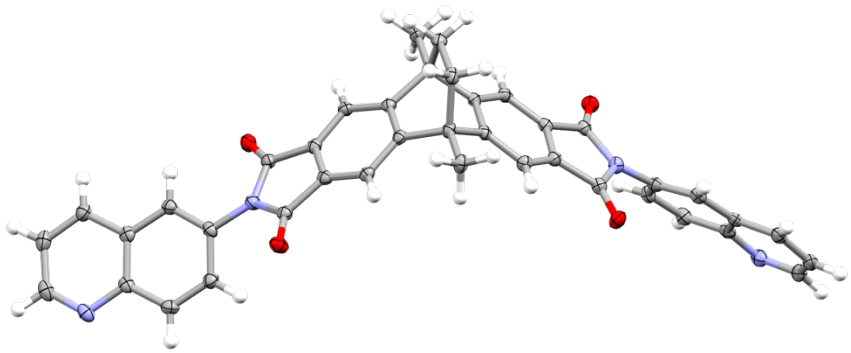

**Figure S110** The asymmetric unit of the X-ray structure of **L²**, with all non-hydrogen atoms shown as ellipsoids at the 50% probability level. Color scheme: H, white; C, dark grey; N, pale blue; O, red.

## 8.5 Crystal structure of $[Pd_2L^2_4](BF_4)_4$

Colorless plate crystals of $[Pd_2\mathbf{L}^2_4](BF_4)_4$ were obtained by slow vapor diffusion of isopropyl ether into a 0.64 mM $CD_3CN$ solution of $[Pd_2\mathbf{L}^2_3(MeCN)_2](BF_4)_4$. A single crystal in mother liquor was pipetted onto a glass slide containing NVH oil. To avoid collapse of the crystal lattice, the crystal was quickly mounted onto a 0.2 mm nylon loop and immediately flash cooled in liquid nitrogen. Crystals were stored at cryogenic temperature in dry shippers, in which they were safely transported to macromolecular beamline P11 at Petra III[1], DESY, Germany.

A wavelength of $\lambda$ = 0.6888 Å was chosen using a liquid $N_2$ cooled double crystal monochromator. Single crystal X-ray diffraction data was collected at 80(2) K on a single axis goniometer, equipped with an Oxford Cryostream 800 a Pilatus 6M. 1800 diffraction images were collected in a 360° ϕ sweep at a detector distance of 200 mm, 100% filter transmission, 0.2° step width and 0.2 second exposure time per image. Data integration and reduction were undertaken using XDS.[2] The structure was solved by intrinsic phasing/direct methods using SHELXT[3] and refined with SHELXL[4] using 22 cpu cores for full-matrix least-squares routines on $F^2$ and ShelXle[5] as a graphical user interface and the DSR program plugin was employed for modeling.[6]

### 8.5.1 Specific refinement details of $[Pd_2L^2_4](BF_4)_4$

Stereochemical restraints for the EAQ ligands (**L²**) were generated by the GRADE program using the GRADE Web Server (http://grade.globalphasing.org) and applied in the refinement. A GRADE dictionary for SHELXL contains target values and standard deviations for 1,2-distances (DFIX) and 1,3-distances (DANG), as well as restraints for planar groups (FLAT). All displacements for non-hydrogen atoms were refined anisotropically. The refinement of ADP's for carbon, nitrogen and oxygen atoms was enabled by a combination of similarity restraints (SIMU) and rigid bond restraints (RIGU).[7] The contribution of the electron density from disordered counterions and solvent molecules, which could not be modeled with discrete atomic positions were handled using the SQUEEZE[8] routine in PLATON.[9] The solvent mask file (.fab) computed by PLATON were included in the SHELXL refinement via the ABIN instruction leaving the measured intensities untouched.

**Table S10** Definition of residues involved in this structure.

| Fragment | Residue class | Occurrence | Residue numbers |
|---|---|---|---|
| Ligand **L²** | EAQ | 2 | 2,3 |
| $BF_4^-$ | BF4 | 2 | 4,5 |

### 8.5.2 Description of the structure of $[Pd_2L^2_4](BF_4)_4$

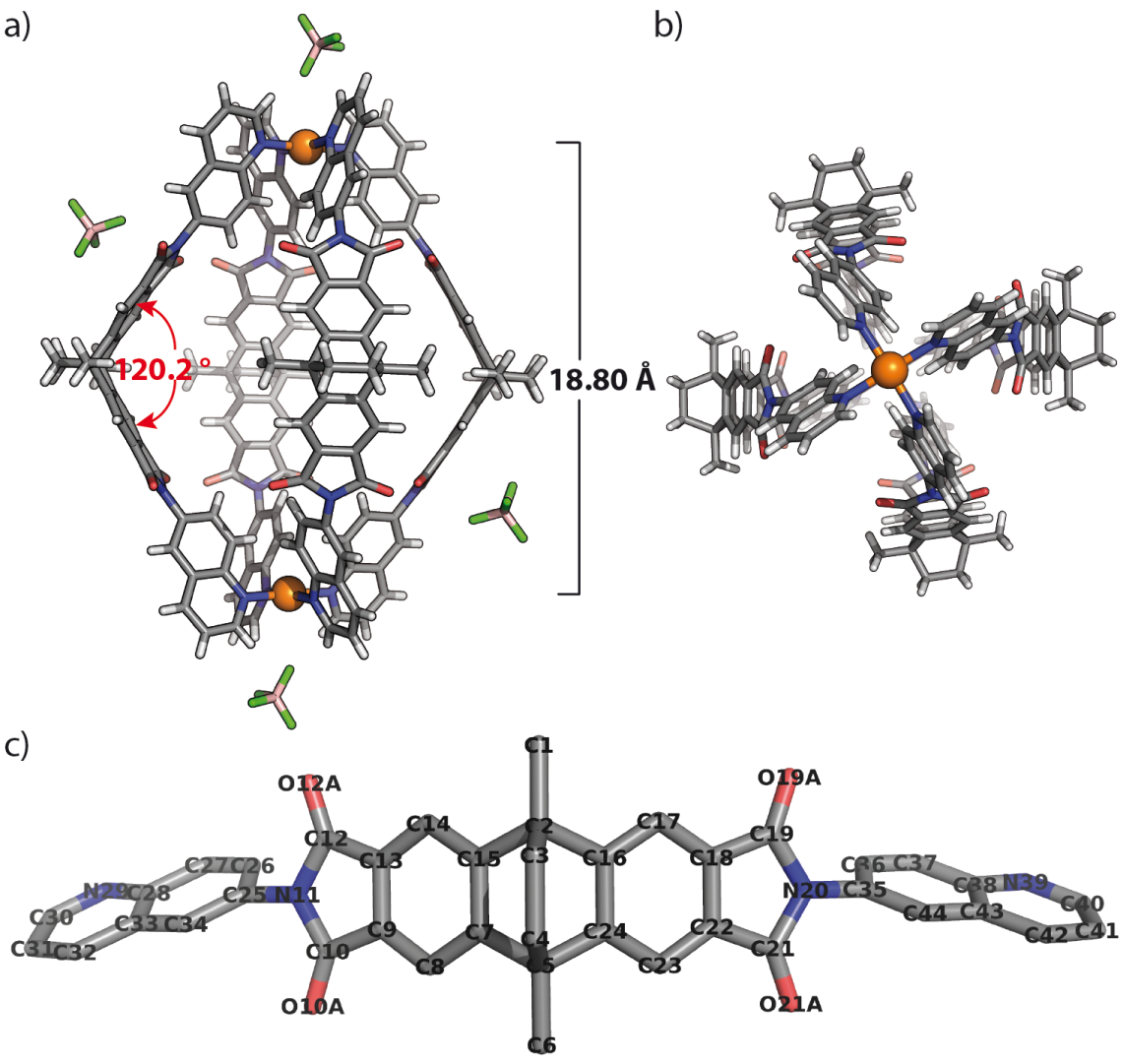


**Figure S111** X-ray structure of $[Pd_2L^2_4](BF_4)_4$: (a) the structure showing the Pd–Pd distance of 18.80 Å; (b) top view of the structure; (c) Atomic naming scheme of ligand **L²** ( residue class EAQ). The same atom labels are used in all other **L²** containing structures. Color scheme: H, light grey; B, pink; C, dark grey; N, blue; O, red; F, green; Pd, orange.

**Table S11** Structural details involved in $[Pd_2\mathbf{L^2}_4](BF_4)_4$.

| Residues No. | Dihedral angle (°) between the backbone's benzene planes C16_C17_C18_C22_C23_C24 and C7_C8_C9_C13_C14_C15 | Esd (°) | Dihedral angle (°) between planes N29_Pd1_Pd2 and N39_Pd1_Pd2 | Esd (°) |
|---|---|---|---|---|
| 2 | 59.298 | 0.229 | 1.711 | 0.255 |
| 3 | 60.300 | 0.157 | 0.757 | 0.181 |
| Average | 59.8 | | 1.2 | |

## 8.6 Crystal structure of $[C_{60}@Pd_2\mathbf{L^2}_3(MeCN)_2](BF_4)_4$

Pale red block crystals of $[C_{60}@Pd_2\mathbf{L^2}_3(MeCN)_2](BF_4)_4$ were obtained by slow vapor diffusion of isopropyl ether into a 0.64 mM $CD_3CN$ solution of $[C_{60}@Pd_2\mathbf{L^2}_3(MeCN)_2](BF_4)_4$. A single crystal in mother liquor was pipetted onto a glass slide containing NVH oil. To avoid collapse of the crystal lattice, the crystal was quickly mounted onto a 0.2 mm nylon loop and immediately flash cooled in liquid nitrogen.

Single crystal X-ray diffraction data was collected on a Bruker D8 venture equipped with an Incoatec microfocus source (Iμs 2.0) using Cukα radiation on a four axis κ-goniometer, equipped with an Oxford Cryostream 800 and a Photon 100 detector. The data were integrated with XDS.[2] The structure was solved by intrinsic phasing/direct methods using SHELXT[3] and refined with SHELXL[4] using 22 cpu cores for full-matrix least-squares routines on $F^2$ and ShelXle[5] as a graphical user interface and the DSR program plugin was employed for modelling.[6]

### 8.6.1 Specific refinement details of $[C_{60}@Pd_2\mathbf{L^2}_3(MeCN)_2](BF_4)_4$

Stereochemical restraints for the EAQ ligands ($\mathbf{L^2}$) were generated by the GRADE program using the GRADE Web Server (http://grade.globalphasing.org) and applied in the refinement. A GRADE dictionary for SHELXL contains target values and standard deviations for 1,2-distances (DFIX) and 1,3-distances (DANG), as well as restraints for planar groups (FLAT). All displacements for non-hydrogen atoms were refined anisotropically. The refinement of ADP's for carbon, nitrogen and oxygen atoms was enabled by a combination of similarity restraints (SIMU) and rigid bond restraints (RIGU).[7] The contribution of the electron density from disordered counterions and solvent molecules, which could not be modeled with discrete atomic positions were handled using the SQUEEZE[8] routine in PLATON.[9] The solvent mask file (.fab) computed by PLATON were included in the SHELXL refinement via the ABIN instruction leaving the measured intensities untouched.

**Table S12** Definition of residues involved in $[C_{60}@Pd_2\mathbf{L^2}_3(MeCN)_2](BF_4)_4$.

| **Fragment** | **Residue class** | **Occurrence** | **Residue numbers** |
|---|---|---|---|
| $Pd^{2+}$ | | 1 | 1 |
| Ligand $\mathbf{L^2}$ | EAQ | 3 | 2,3,4 |
| $C_{60}$ | C60 | 2 | 5,6 (One $C_{60}$ with disorder) |
| $BF_4^-$ | BF4 | 4 | 7,8,9,10 |
| MeCN | ACN | 6 | 11,12,13,14,15,16 |

### 8.6.2 Description of the structure of $[C_{60}@Pd_2L^2{}_3(MeCN)_2](BF_4)_4$

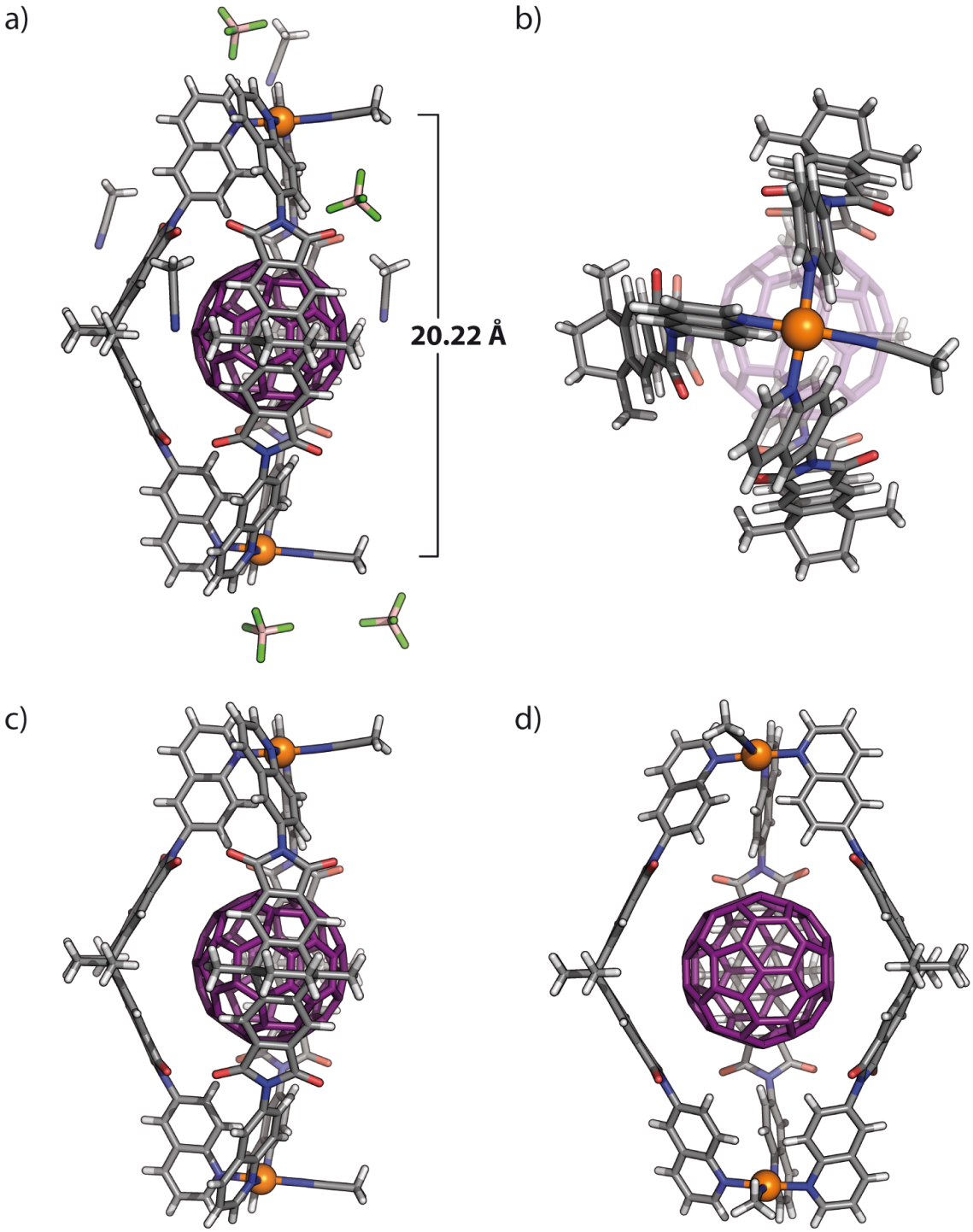


**Figure S112** X-ray structure of $[C_{60}@Pd_2\mathbf{L^2}_3(MeCN)_2](BF_4)_4$: (a) The asymmetric unit showing the entrapped $C_{60}$ by bowl geometry and the peripheral $BF_4^-$ counterions and acetonitrile; (b) top view of the structure of $[C_{60}@Pd_2\mathbf{L^2}_3(MeCN)_2](BF_4)_4$; (c) and (d) two equatorial views of the structure of $[C_{60}@Pd_2\mathbf{L^2}_3(MeCN)_2](BF_4)_4$. Color scheme: H, light grey; B, pink; C, dark grey; N, blue; O, red; F, green; Pd, orange.

**Table S13** Structural details involved in $[C_{60}@Pd_2\mathbf{L^2}_3(MeCN)_2](BF_4)_4$.

| Residues No. | Dihedral angle (°) between the backbone's benzene planes C16_C17_C18_C22_C23_C24 and C7_C8_C9_C13_C14_C15 | Esd (°) | Dihedral angle (°) between planes N29_Pd1_Pd2 and N39_Pd1_Pd2 | Esd (°) |
|---|---|---|---|---|
| 2 | 56.011 | 0.395 | 1.098 | 0.345 |
| 3 | 55.070 | 0.537 | 0.165 | 0.166 |
| 4 | 57.249 | 0.410 | 0.446 | 0.403 |
| Average | 56.1 | | 0.6 | |

### 8.6.3 Analysis of the host–guest interaction

Method of distance measurement: At first, the main position of all disordered $C_{60}$ guest (Part 1) was used to create a PDB file for further analysis in the Olex2 program.[11] The 'CENT' and 'MPLN' commands were used to create the centroid of $C_{60}$ and the mean planes of interest situated on the ligands and fullerene surfaces. The corresponding distances in between centroids of the ligands benzene rings, hydrogen atoms, $C_{60}$ centroids and centroids of $C_{60}$ rings were analyzed by using the 'Distances and angles' function.

**Table S14** Distances associated with the host–guest interaction in $[C_{60}@Pd_2\mathbf{L^2}_3(MeCN)_2](BF_4)_4$.

| Residues No. | Planes | Centroid of plane to centroid of $C_{60}$ (Å) | Centroid of plane to the five or six membered ring centroid of $C_{60}$ (Å) | Hydrogen atoms | Hydrogen atoms to centroid of $C_{60}$ (Å) | Shortest distance to the rings of $C_{60}$ (Å) |
|---|---|---|---|---|---|---|
| 2 | C7_C8_C9_C13_C14_C15 | 6.76 | 3.88 | H26 | 6.49 | 3.53 |
| 2 | C16_C17_C18_C22_C23_C24 | 6.81 | 3.93 | H36 | 6.43 | 3.43 |
| 3 | C7_C8_C9_C13_C14_C15 | 6.82 | 3.76 | H26 | 6.16 | 3.00 |
| 3 | C16_C17_C18_C22_C23_C24 | 6.80 | 3.74 | H36 | 6.12 | 2.92 |
| 4 | C7_C8_C9_C13_C14_C15 | 6.84 | 3.77 | H26 | 6.71 | 3.50 |
| 4 | C16_C17_C18_C22_C23_C24 | 6.71 | 3.67 | H36 | 6.42 | 3.21 |
| Average | | 6.79 | 3.79 | | 6.39 | 3.27 |

## 8.7 Crystal structure of $[C_{60}Ac@Pd_2\mathbf{L^2}_3Cl_2](BF_4)_2$

Red thin plate crystals of $[C_{60}Ac@Pd_2\mathbf{L^2}_3Cl_2](BF_4)_2$ were obtained by fast vapor diffusion of THF into a 0.44 mM $CD_3CN$ solution of $[C_{60}Ac@Pd_2\mathbf{L^2}_3Cl_2](BF_4)_2$. A single crystal in mother liquor was pipetted onto a glass slide containing NVH oil. To avoid collapse of the crystal lattice, the crystal was quickly mounted onto a 0.1 mm nylon loop and immediately flash

cooled in liquid nitrogen. Crystals were stored at cryogenic temperature in dry shippers, in which they were safely transported to macromolecular beamline P11 at Petra III, DESY, Germany.[1]

A wavelength of $\lambda$ = 0.6888 Å was chosen using a liquid $N_2$ cooled double crystal monochromator. Single crystal X-ray diffraction data was collected at 80(2) K on a single axis goniometer, equipped with an Oxford Cryostream 800 a Pilatus 6M. 3600 diffraction images were collected in a 360° ϕ sweep at a detector distance of 155 mm, 100% filter transmission, 0.1° step width and 0.06 seconds exposure time per image. Data integration and reduction were undertaken using XDS.[2] The structure was solved by intrinsic phasing/direct methods using SHELXT[3] and refined with SHELXL[4] using 22 cpu cores for full-matrix least-squares routines on $F^2$ and ShelXle[5] as a graphical user interface and the DSR program plugin was employed for modeling.[6]

### 8.7.1 Specific refinement details of $[C_{60}Ac@Pd_2L^2{}_3Cl_2](BF_4)_2$

Stereochemical restraints for the EAQ ligands (**L²**) were generated by the GRADE program using the GRADE Web Server (http://grade.globalphasing.org) and applied in the refinement. A GRADE dictionary for SHELXL contains target values and standard deviations for 1,2-distances (DFIX) and 1,3-distances (DANG), as well as restraints for planar groups (FLAT). All displacements for non-hydrogen atoms were refined anisotropically. The refinement of ADP's for carbon, nitrogen and oxygen atoms was enabled by a combination of similarity restraints (SIMU) and rigid bond restraints (RIGU).[7] The $C_{60}Ac$ Diels-Alder adduct was not disordered and all atomic positions of non-hydrogen atoms were freely refined without the help of any geometrical restraints. The contribution of the electron density from disordered counterions and solvent molecules, which could not be modeled with discrete atomic positions were handled using the SQUEEZE[8] routine in PLATON.[9] The solvent mask file (.fab) computed by PLATON were included in the SHELXL refinement via the ABIN instruction leaving the measured intensities untouched.

**Table S15** Definition of residues involved in $[C_{60}Ac@Pd_2L^2{}_3Cl_2](BF_4)_2$.

| Fragment | Residue class | Occurrence | Residue numbers |
|---|---|---|---|
| $Pd^{2+}$ | PD | 1 | 1 |
| Ligand **L²** | EAQ | 3 | 2,3,4 |
| $Cl^-$ | CL | 1 | 5 |
| $C_{60}Ac$ | FAC | 1 | 6 |
| $BF_4^-$ | BF4 | 2 | 7,8,9,10 (Two $BF_4^-$ with disorder) |
| MeCN | ACN | 2 | 11,12 |
| THF | THF | 4 | 13,14,15,16 |

### 8.7.2 Description of the structure of $[C_{60}Ac@Pd_2L^2{}_3Cl_2](BF_4)_2$

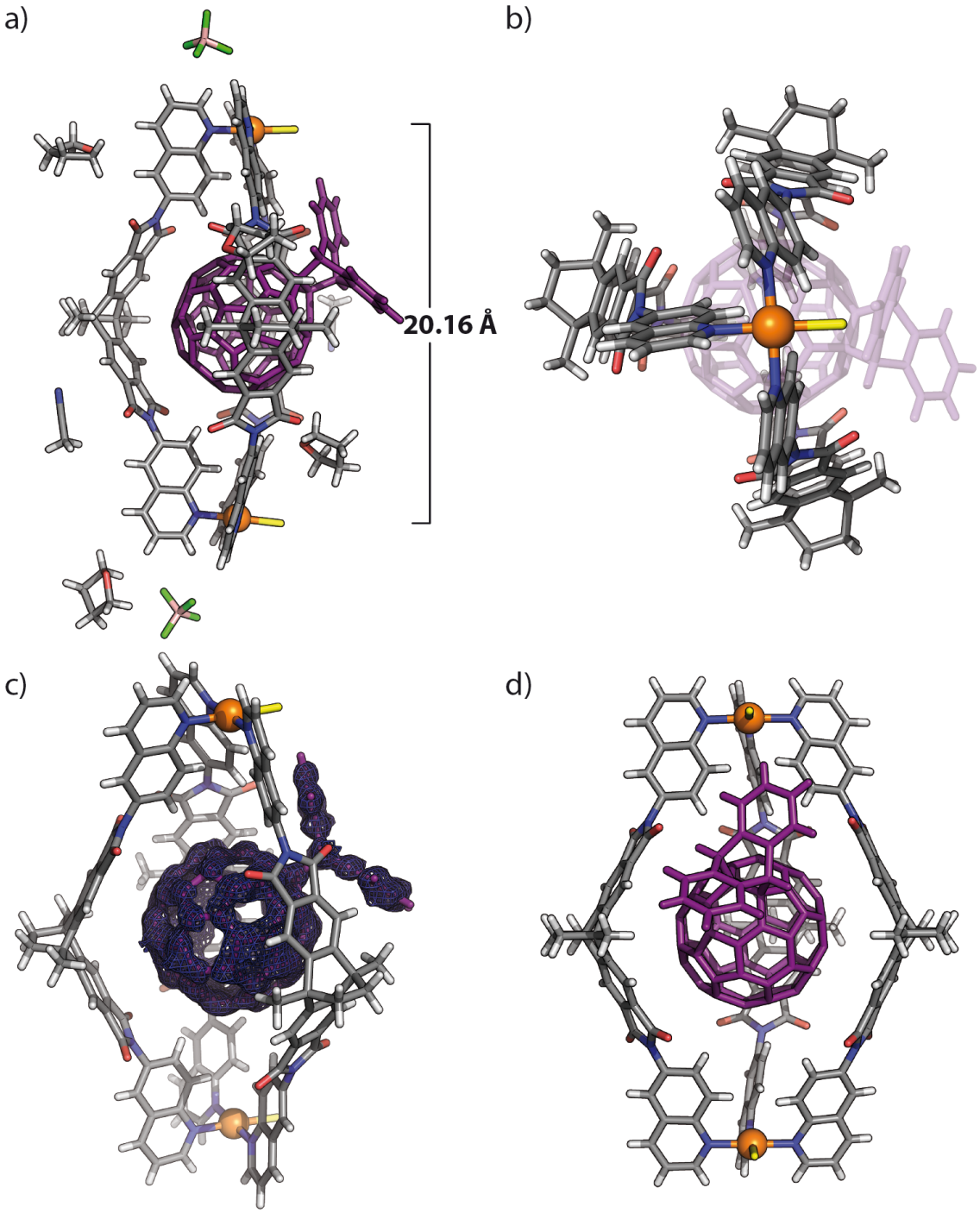


**Figure S113** X-ray structure of $[C_{60}Ac@Pd_2\mathbf{L^2}_3Cl_2](BF_4)_2$: (a) The asymmetric unit showing the entrapped $C_{60}Ac$ by bowl geometry and the peripheral $BF_4^-$ counterions, acetonitrile and tetrahydrofuran; (b) top view of the structure of $[C_{60}Ac@Pd_2\mathbf{L^2}_3Cl_2](BF_4)_2$; (c) and (d) two orientation views of the structure of $[C_{60}Ac@Pd_2\mathbf{L^2}_3Cl_2](BF_4)_2$, wherein electron density map of $C_{60}Ac$ is represented in blue mesh in (c). Color scheme: H, light grey; B, pink; C, dark grey; N, blue; O, red; F, green; Pd, orange; Cl, yellow; $C_{60}Ac$, purple.

**Table S16** Structural details involved in $[C_{60}Ac@Pd_2\mathbf{L^2}_3Cl_2](BF_4)_2$.

| Residues No. | Dihedral angle (°) between the backbone's benzene planes C16_C17_C18_C22_C23_C24 and C7_C8_C9_C13_C14_C15 | Esd (°) | Dihedral angle (°) between planes N29_Pd1_Pd2 and N39_Pd1_Pd2 | Esd (°) |
|---|---|---|---|---|
| 2 | 56.205 | 0.179 | 2.165 | 0.259 |
| 3 | 55.250 | 0.206 | 1.577 | 0.221 |
| 4 | 49.120 | 0.284 | 0.911 | 0.251 |
| Average | 53.5 | | 1.6 | |

## 8.8 Calculation of the cavity volumes

Crystallographically determined structures of $[Pd_2\mathbf{L^1}_4]^{4+}$ and $[Pd_2\mathbf{L^2}_4]^{4+}$ were symmetry expanded and $BF_4^-$ counter ions were removed. Resulting inner cavities were calculated with VOIDOO[13] using a primary grid and plot grid spacing of 0.1 Å and 10 cycles of volume refinement with the size probe radius of 3.2 Å, the minimum radius such that it would not exit the cavity of the structures. Molecular visualization was done using PyMol.[14]

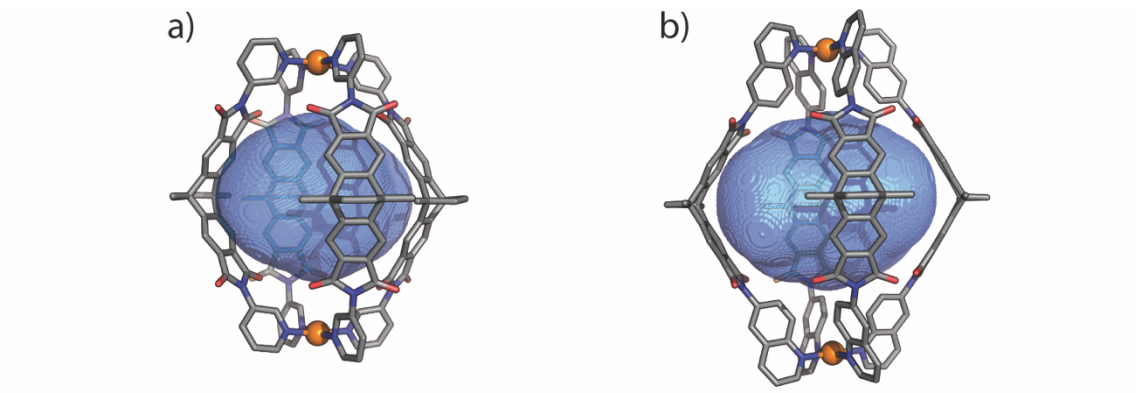


**Figure S114** The VOIDOO-calculated void space as shown (blue mesh) within the corresponding crystal structures for (a) cage $[Pd_2\mathbf{L^1}_4]^{4+}$ (572 Å$^3$) and (b) cage $[Pd_2\mathbf{L^2}_4]^{4+}$ (1099 Å$^3$). Color scheme: C, dark grey; N, blue; O, red; Pd, orange.

## 8.9 Comparison of structural information

**Table S17** Comparison of averaged structural details of all six structures.

| Compounds | Pd-Pd distance (Å) | Dihedral Angle of N-Pd-Pd-N (°) | Dihedral Angle[a] (°) | 180 – Dihedral Angle (°) |
|---|---|---|---|---|
| $[Pd_2\mathbf{L^1}_4](BF_4)_4$ | 15.94 | 1.0[b] | 55.7 | 124.3 |
| $[C_{60}@Pd_2\mathbf{L^1}_4](BF_4)_4$_A | 14.66 | 62.4[b] | 57.4 | 122.6 |
| $[C_{60}@Pd_2\mathbf{L^1}_4](BF_4)_4$_C | 14.61 | 62.3[b] | 57.4 | 122.6 |
| $[C_{60}@Pd_2\mathbf{L^1}_4](BF_4)_4$_B | 14.55 | 63.8[b] | 59.0 | 121.0 |

| cont. | | | | |
|---|---|---|---|---|
| $\mathbf{L^2}$ | 19.11[d] | - | 60.2 | 119.8 |
| $[Pd_2\mathbf{L^2}_4](BF_4)_4$ | 18.80 | 1.2[c] | 59.8 | 120.2 |
| $[C_{60}@Pd_2\mathbf{L^2}_3(MeCN)_2](BF_4)_4$ | 20.22 | 0.6[c] | 56.1 | 123.9 |
| $[C_{60}Ac@Pd_2\mathbf{L^2}_3Cl_2](BF_4)_2$ | 20.16 | 1.6[c] | 53.5 | 126.5 |

[a] The angle between two planes constructed by two benzene rings of the bridged ethanoanthracene backbone

[b] between two pyridine arms of the same ligand

[c] between two quinoline arms of the same ligand

[d] Distance between quinoline nitrogen atoms

## 8.10 Comparison of photos of $[Pd_2L^1_4](BF_4)_4$ and $[C_{60}@Pd_2L^1_4](BF_4)_4$ crystals

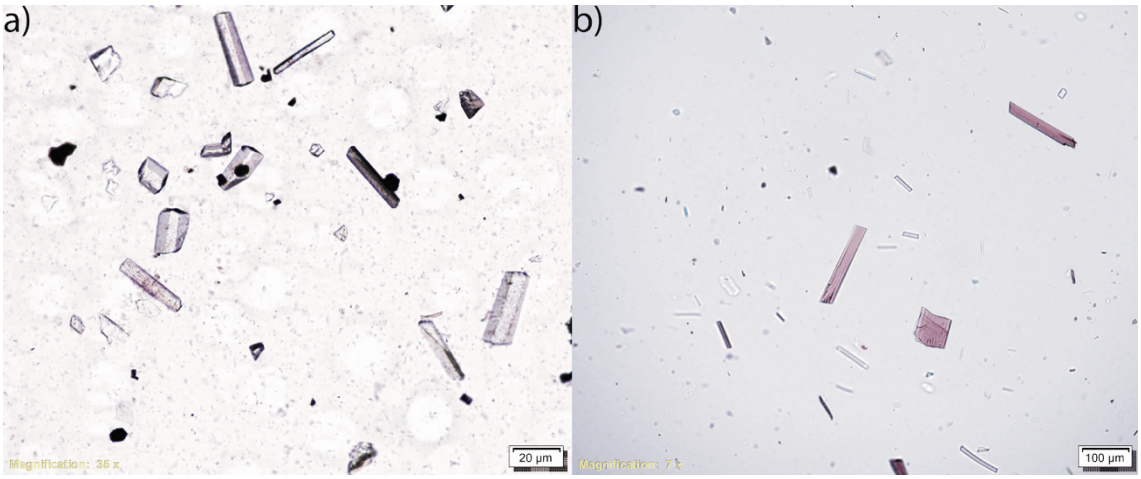


**Figure S115** Comparison of crystals of $[Pd_2\mathbf{L^1}_4](BF_4)_4$ and $[C_{60}@Pd_2\mathbf{L^1}_4](BF_4)_4$: (a) colourless block crystals of $[Pd_2\mathbf{L^1}_4](BF_4)_4$ (Magnification: 35X); (b) red thin plate crystals of $[C_{60}@Pd_2\mathbf{L^1}_4](BF_4)_4$ (Magnification: 7X).

# 9 Computational studies

In order to design a suitable backbone for the coordination cage fullerene receptors, models shown below were constructed using Wavefunction SPARTAN '14[15] and first optimized on semiempiric PM6 level of theory without constraints. The resulting structures were then further refined by DFT structure optimization (B3LYP/C, H, N, O = 6-31g(d)/Pd LANL2DZ) using GAUSSIAN 09.[16] Distances within the individually optimized fragments shown in Figure S109 c) and d) refer to the same carbon atom position in the final cage-based receptor and the center of $C_{60}$ and the Pd position, respectively, thus indicating that coordinative tethering of four backbones, equipped with *meta*-pyridyl donors, to square-planar Pd(II) should create a $C_4$-symmetric hollow structure perfectly dimensioned to encapsulate one Buckminster fullerene.

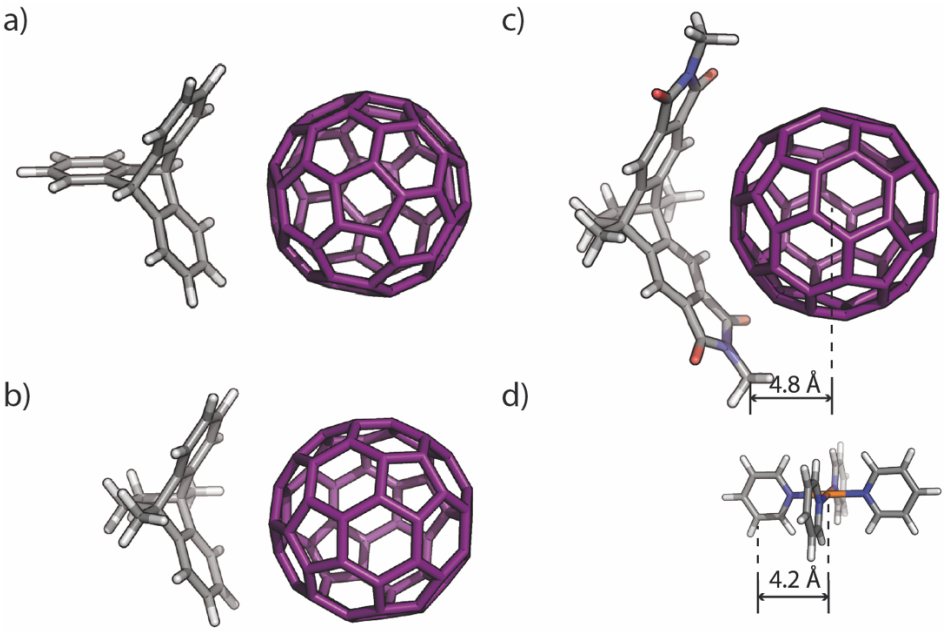


**Figure S116** DFT optimized structures supporting the host design process.

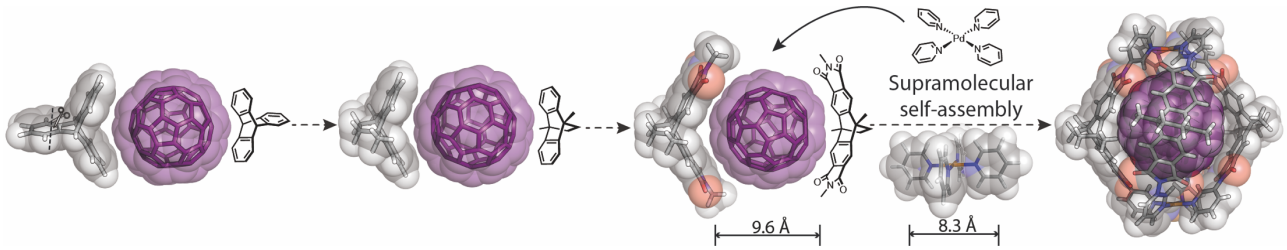


**Figure S117** Design of a self-assembled, minimal-size metallo-supramolecular fullerene receptor.

# 10 References

[1] A. Burkhardt, T. Pakendorf, B. Reime, J. Meyer, P. Fischer, N. Stube, S. Panneerselvam, O. Lorbeer, K. Stachnik, M. Warmer, P. Rodig, D. Gories, A. Meents, *Eur. Phys. J. Plus* **2016**, *131*, 1-9.
[2] W. Kabsch, *Acta Crystallogr. Sect. D* **2010**, *66*, 125-132.
[3] G. Sheldrick, *Acta Crystallogr. Sect. A* **2015**, *71*, 3-8.
[4] G. Sheldrick, *Acta Crystallogr. Sect. C* **2015**, *71*, 3-8.
[5] C. B. Hubschle, G. M. Sheldrick, B. Dittrich, *J. Appl. Crystallogr.* **2011**, *44*, 1281-1284.
[6] D. Kratzert, J. J. Holstein, I. Krossing, *J. Appl. Crystallogr.* **2015**, *48*, 933-938.
[7] A. Thorn, B. Dittrich, G. M. Sheldrick, *Acta Crystallogr. Sect. A* **2012**, *68*, 448-451.
[8] A. Spek, *Acta Crystallogr. Sect. C* **2015**, *71*, 9-18.
[9] A. Spek, *Acta Crystallogr. Sect. D* **2009**, *65*, 148-155.
[10]D. Kratzert, I. Krossing, *J. Appl. Crystallogr.* **2018**, *51*, 928-934.
[11]O. V. Dolomanov, L. J. Bourhis, R. J. Gildea, J. A. K. Howard, H. Puschmann, *J. Appl. Crystallogr.* **2009**, *42*, 339-341.
[12]Bruker-Nonius, APEX, SAINT, SADABS and XPREP, Bruker AXS Inc., Madison (USA), **2013**.
[13]G. J. Kleywegt, T. A. Jones, *Acta Crystallogr. Sect. D* **1994**, *50*, 178-185.
[14]W. L. DeLano, DeLano Scientific LLC, San Carlos (USA).
[15]Spartan '08 Version 1.2.0, Wavefunction, Inc., Irvine (USA), **2009**.
[16]M. J. Frisch, et al., Gaussian09, Gaussian Inc., Wallingford (USA), **2009**.